2016

Characterization of Thermoplastic Fusion Bonding of Microchannels using Pressure Assisted Boiling Point Control System

Kavya Dathathreya
Louisiana State University and Agricultural and Mechanical College

CHARACTERIZATION OF THERMOPLASTIC FUSION BONDING OF MICROCHANNELS USING PRESSURE ASSISTED BOILING POINT CONTROL SYSTEM

A Thesis

Submitted to the Graduate Faculty of the
Louisiana State University and
Agricultural and Mechanical College
in partial fulfillment of the
requirements for the degree of
Masters of Science

in

The Department of Mechanical Engineering

by

Kavya Dathathreya
B.E., Peoples Education Society's Institute of Technology, 2009
December 2016

Acknowledgements

I would like to thank my advisor Dr. Michael C. Murphy for his invaluable insight, support and guidance throughout my research. I would also like to express my gratitude to Dr. Daniel Park for all his help, advice and support. I would like to acknowledge my committee members Dr. Sunggook Park and Dr. Ingmar Schoegl for agreeing to be in my committee and for all the scientific advice. I thank my lab mates for their help and assistance in this venture. I am thankful to Mr. J. Guy at the Advanced Manufacturing and Machining Facility (AMFF) at LSU for micromilling of the brass mold insert and the Centre for Advanced Microstructures and Devices (CAMD) at LSU for microfabrication support.

I would like to thank my husband Pratap Rao and my family for their love, patience and encouragement which has been vital in completion of this research.

This work was supported by funding from the National Institute of Biomedical Imaging and Bioengineering grant NIBIB,1-P41-EB020594-01.

Table of Contents

Abstract

An innovative method of thermoplastic fusion bonding using a pressure assisted boiling point control (PABP) system was characterized to determine the optimum parameters for bonding polymethyl methacrylate (PMMA) components containing microchannels and thin, 250 µm cover sheets. The PABP system enables precise control of the temperature boundary condition and the applied pressure by immersing the components being bonded in boiling water and varying the vapor pressure. Test structure geometries containing microchannels of two depths and four different aspect ratios were designed: 1:10 (Depth: 10µm, Width: 100 µm and Depth: 5µm, Width: 50 µm), 1:50 (Depth: 10µm, Width: 500µm and Depth: 5µm, Width: 250 µm), 1:100 (Depth: 10µm, Width: 1000µm and Depth: 5µm, Width: 500µm) and 1:200 (Depth: 10µm, Width: 2000µm and Depth: 5µm, Width: 1000µm). Microchannels were hot embossed using micro-milled brass mold inserts. Bonding conditions were optimized by observing microchannel deformation under a microscope. The quality of the bonded samples were rupture and leak tested to determine the integrity and strength of the bonds. Mean rupture pressures for channels of AR of 1:10, 1:50 and 1:100 were 851.02 kPa, 780.14 kPa and 706.09 kPa repectively for shallower channels and 831.93 kPa, 739.3 kPa and 524.38 kPa respectively for deeper channels bonded using open loop system. Rupture pressure decreased with decreasing AR and was higher for shallower channels. A closed loop control system was developed for the automatic temperature control. Results of bonding with both open loop and closed loop systems were compared. Mean rupture pressure for channels of AR 1:10, 1:50 and 1:100 for 5 µm depth were 977.54 kPa, 930.93 kPa and 751.39 kPa respectively and 912.11 kPa, 800.07 kPa and 550.96 kPa respectively for 10 µm depth. It was found that the rupture test

results were more consistent and repeatable with closed loop system because of better control of the bonding temperature.

CHAPTER 1: INTRODUCTION

1.1 Motivation

Microfluidics is one of the rapidly progressing areas of research with new innovations and numerous applications in the biomedical field. Microfluidic systems process very small (10^{-9} to 10^{-18} liters) quantities of fluids using microchannels [1]. Among its numerous applications, Lab-on-a-Chip (LOC) technology has attracted increasing interest over past few years. LOCs are microdevices which assist in rapid and precise diagnoses for several diseases, such as stroke and cancer, much faster than traditional labs potentially leading to more precise medical treatments tailored for each individual. Figure 1.1 shows a LOC which analyzes whole blood by using 5 µL of sample at the inlet port which is very helpful for point of care diagnostics. [3] These microdevices contain enclosed microchannels formed by bonding a substrate and a cover. Bonding is a critical step in the fabrication process and can be broadly classified into two types: indirect and direct bonding [2].

Indirect bonding uses an adhesive layer like a glue or laminate sheet, to bond two polymers. Although this method of bonding is very simple, it has many disadvantages

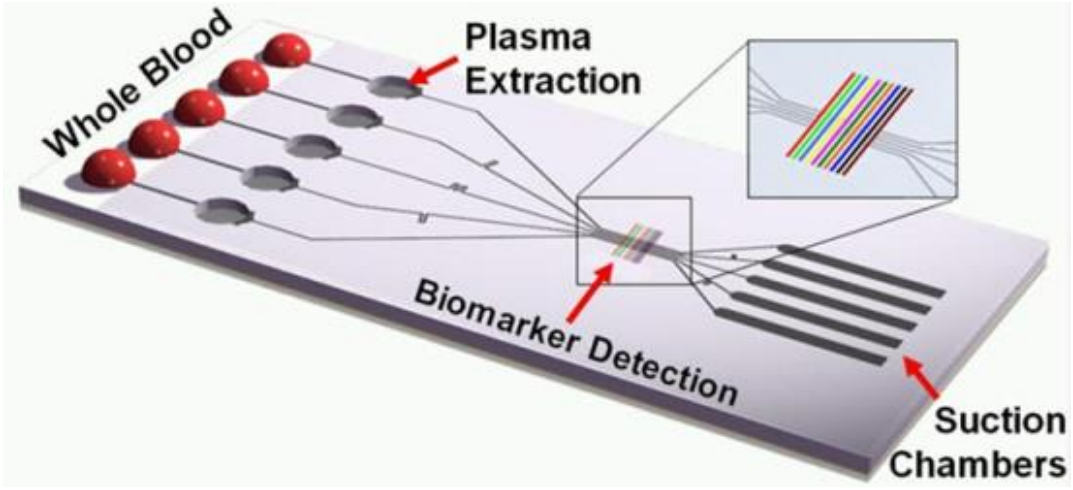

Figure 1.1 Self-powered Integrated Microfluidic Blood Analysis System (SIMBAS) [3]

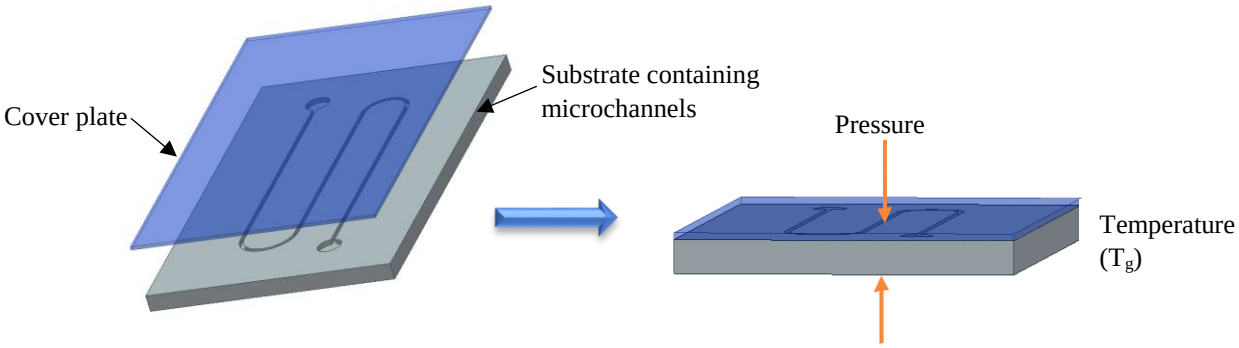

Figure 1.2 Schematic of thermal fusion bonding of two polymers.

like clogging of the channels, creating dead volumes and contamination of biological samples because of deposition of excessive adhesive. Also, as the adhesive is usually of a different material from the two polymer sheets that must be bonded, it can introduce different surface properties, affecting the overall function of the microdevice.

In direct bonding, no external material is used to bond the two polymers and results in homogeneous surface properties and reduced contamination [2]. Among different direct bonding methods like localized welding [15, 16], thermoplastic fusion bonding (TFB) is most widely used because of high bond strength and its simplicity. [2] In this method, polymers to be bonded are heated close to or above the glass transition temperature (T_g) under pressure which results in the diffusion of polymer chains at the surface creating a bond [2]. Figure 1.2 shows a schematic of TFB. It is very important to have controlled temperature and pressure to achieve good bonding without any channel deformation. Several groups have studied various methods of TFB by using conventional ovens, heated weights, hot presses, boiling water and other novel methods. However, in these methods there is usually an uneven pressure distribution and precise temperature control is difficult. Each chip design requires optimization of different boundary conditions. Park, et al. developed a novel pressure assisted boiling point (PABP) TFB system to ensure uniform pressure and precise control of temperature [4]. A polymer substrate containing microchannels and the cover plate are

brought together and inserted in a sealing bag. The entire assembly is then immersed in a pressure vessel containing water and heated to the boiling point. The vapor pressure ensures an even pressure distribution over the entire surface of the polymer and the boiling water produces constant surface temperatures during bonding. Park demonstrated the technique but did not fully characterize it.

1.2 Goals of this research

To characterize the process, microchannels of different aspect ratios (height: width) were designed and fabricated. Specific objectives were:

1. Optimize conditions for different aspect ratios;
2. Evaluate the effect of channel dimensions on bond performance;
3. Characterize bond performance using leak and rupture tests;
4. Implement a closed loop temperature control system

To conduct bonding at different conditions and to determine optimum temperature and pressure for each channel design with minimum channel deformation using PABP bonding system. To study the effect of channel dimension, pressure and temperature on the bonding performance. To check for leakage of the bonded samples by passing fluorescent dye through the channels and to determine the bond strength for each channel by conducting the rupture test. To study the effect of aspect ratio on the bond strength. To develop a closed loop system to maintain constant temperature throughout the bonding process eliminating human intervention and to compare the bond strengths of open loop and closed loop systems.

1.3 Thesis organization

The chapters are organized in sequence. The second chapter provides a literature review about the different bonding methods followed by the details about the design and fabrication of the polymer samples in the third chapter. The fourth chapter includes the details about the experimental apparatus, procedures and results. A summary of the conclusions from this research and the scope for future work is discussed in the fifth chapter. The references used in the entire thesis are included in the reference section. Additional details and explanations about the topics presented in the chapters are added in the appendices.

CHAPTER 2: LITERATURE REVIEW

2.1 Introduction

The history of microfluidics dates to the 70's when the first miniature device was fabricated to separate mixture of gases in a very short time. [6] Later, these microdevices were used in numerous applications like detection and analysis of cells, clinical diagnosis of various biological samples, DNA analysis and to serve as detectors for chemical or biological threats. [7] This area is receiving enormous attention because of the many advantages it offers such as low cost, reduced size of the operating system, portability, speed of analysis, and decreased requirements for power, sample and reagents.

Much of the earlier work in this field was done using silicon and glass as materials for fabrication. [8, 9] They were the dominant materials because of the well-established fabrication methods and favorable optical properties. However, the cost of producing the devices was high and lead to the increased attention towards polymer substrates mainly for their low production cost which enabled to use the microdevices as disposable devices. [10] The popularity of polymer material has grown significantly because of the various fabrication methods available.

Irrespective of the fabrication method used to create microfluidic patterns, sealing the open microchannels to produce enclosed fluidic paths is a critical step for the device to function satisfactorily. This literature review primarily focuses on the different bonding techniques used for affixing the covers to polymer substrates to form enclosed devices.

2.2 Polymers as substrate materials

Polymers are increasingly being used as an alternative material in making of microfluidic devices because of several attractive material properties like

machinability, optical properties, molecular adsorption, electroosmotic flow, mobility, surface charge, auto-fluorescence, permeability, chemical resistance and many others. [10] The cost of the devices are reduced because of the simpler and inexpensive methods of fabrication that enable disposable devices and eliminate the problem of contamination due to reusing instruments. An additional benefit is the availability of a wide variety of materials with a range of different properties, which allows the selection of the right material for any given application. Based on the behavior of the polymer, they can be broadly classified as thermoset, thermoplastic, and elastomer. [11] Thermoset polymers harden because of cross-linking of polymer chains (curing) on heating and become inflexible. Once hardened, the polymers do not soften with additional heating and cannot be reshaped. This includes epoxy-based resist materials for lithography like SU-8. [11] Thermoplastic polymers soften when the temperature is close to the glass transition temperature (T_g) of the material and harden when cooled below that. Since no curing occurs in these materials, they can be reshaped upon additional heating. This property enables a wide variety of fabrication methods for thermoplastic polymers. Based on the molecular arrangement, thermoplastics can be further classified into amorphous, semi-crystalline, or crystalline. Amorphous thermoplastics include most commonly used materials like poly methyl methacrylate (PMMA) and polycarbonate (PC). [11] Polypropylene is semi-crystalline and used in cell culture platforms. In elastomers, the polymer chains are longer and more entangled. On applying external forces, the polymer expands elastically and returns to its original state on removing external force. The most commonly used material is poly dimethyl siloxane (PDMS). [11]

Table 1.1 Summary of physical properties for common thermoplastic materials [2]

Polymer	Acronym	T_g (ºC)	T_m (ºC)	CTE (10^{-6}ºC^{-1})	Water absorption	Solvent resistance	Acid/base resistance	Optical transmissivity	
								Visible	UV
Cyclic Olefin (co) polymer	COC	70-155	190-320	60-80	0.01	Excellent	Good	Excellent	Excellent
Polymethylmethacrylate	PMMA	100-122	250-260	70-150	03-0.6	Good	Good	Excellent	Good
Polycarbonate	PC	145-148	260-270	60-70	0.12-0.34	Good	Good	Excellent	Poor
Polystyrene	PS	92-100	240-260	10-150	0.02-0.15	Poor	Good	Excellent	Poor
Polypropylene	PP	-20	160	18-185	0.1	Good	Good	Good	Fair
Polyetheretherketone	PEEK	147-158	340-350	47-54	0.1-0.5	Excellent	Good	Poor	Poor
Polyethylene terephthalate	PET	69-78	248-260	48-78	0.1-0.3	Excellent	Excellent	Good	Good
Polyethylene	PE	-30	120-130	180-230	0.01	Excellent	Excellent	Fair	Fair
Polyvinylidene chloride	PVDC	0	76	190	0.1	Good	Good	Good	Poor
Polyvinyl chloride	PVC	80	180-210	50	0.04-0.4	Good	Excellent	Good	Poor
Polysulfone	PSU	170-187	180-190	55-60	0.3-0.4	Fair	Good	Fair	Poor

T_m – melting point, CTE – Co-efficient of thermal expansion

2.3 Bonding methods

Capping of the open microchannels is a very important step in the fabrication process of microdevices. Some of the functional requirements for the final microdevices are good bond strength, no channel deformation, no leaks, no clogging or dead volume, and no contamination of the fluid used. Based on the application, an appropriate bonding method should be selected and applied. Bonding methods can be broadly classified into adhesive bonding and non-adhesive bonding techniques. [2]

2.3.1 Adhesive bonding methods

Adhesive bonding also known as indirect bonding and uses a different material like glue, laminate sheets or a solvent to bond two polymer sheets. Liquid adhesive is the most commonly used which forms a bond on exposure to UV light radiation. Dang et al. achieved bonding of a PMMA chip with PMMA film using an adhesive printing process that enabled control of the thickness of the adhesive layer with sacrificial channels to remove air bubbles and excessive adhesive to achieve good sealing. [12] The chip was used for electrophoretic separation containing an array of microchannels (50µm deep and 50 µm wide) as shown in Fig. 2.1.

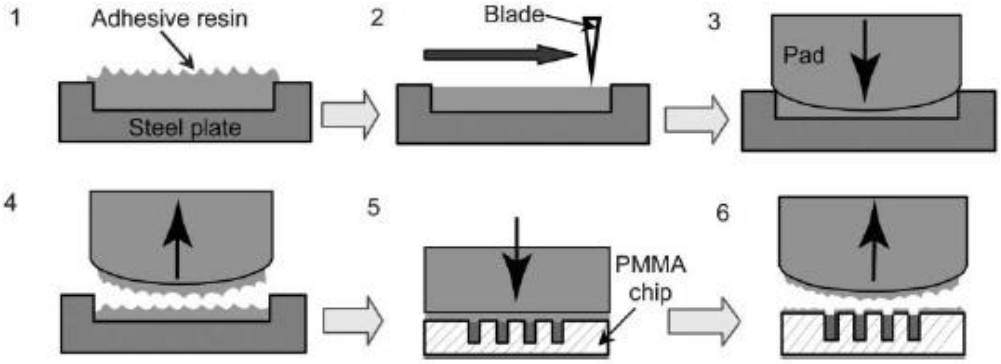

Figure 2.1 Schematic of Adhesive printing bonding method developed by Dang et al. [12]

Chow et al. developed a new technique of bonding PMMA substrates using PDMS as the adhesive. Channels of AR 3:1 (Width: 100 µm, Depth: 300 µm) were hot embossed in PMMA and was bonded using PDMS which was spin coated on blank PMMA cover sheets and partially cured for 20hrs and bonded at 90 °C for 3 hrs. Bond strength was evaluated using the tensile strength tester and was found to be 0.015 MPa. [13] Fig. 2.2 shows the bonding process and cross-sectional images of the bonded sample.

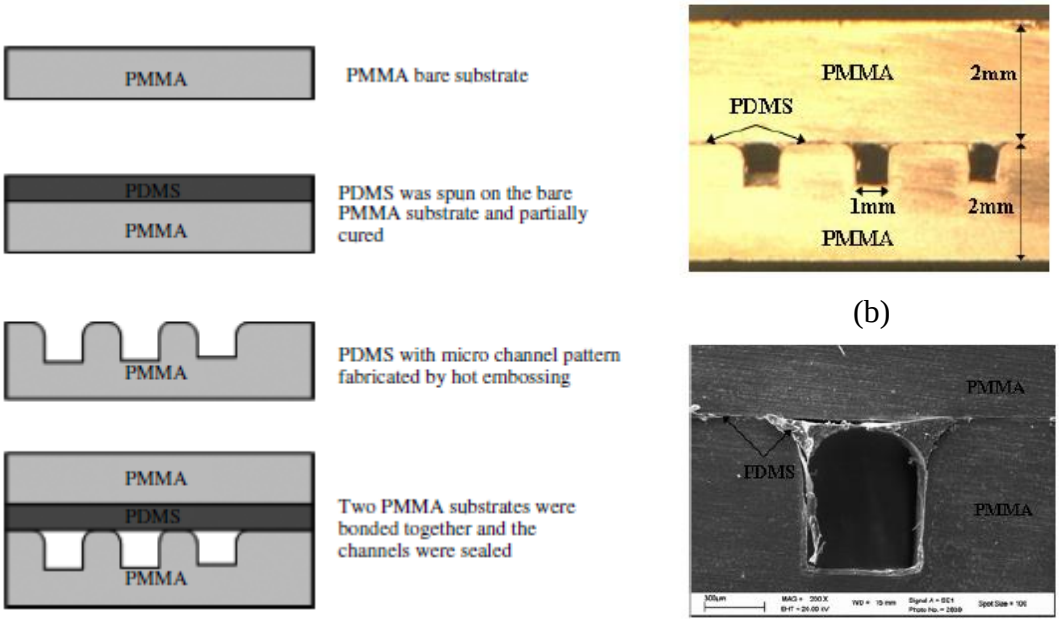

(a) (b) (c)

Figure 2.2 Chow et al. developed a method of bonding as shown in (a) Schematic of the process of bonding (b) Microscopic image of cross-sectional view of the bonded sample (c) SEM image of the cross section of bonding interface [13]

Although adhesive bonding techniques are simple, it poses several risks like clogging of the channel with extra adhesive, creating dead volumes and contamination of biological samples. In addition, as the adhesive is of different material, it may exhibit different performance characteristics at the interface than the other channel walls, which will affect the overall functionality of the device. [14]

2.3.2 Nonadhesive bonding methods

Unlike adhesive bonding nonadhesive or direct bonding, does not use an external material to bond the polymers and has homogenous surface properties for all the walls and eliminates the problem of contamination. This includes different methods of bonding like localized welding using ultrasound, lasers or microwave, thermoplastic fusion bonding and other novel methods.

In 2006, Truckenmüller et al. bonded a PMMA microdevices of AR 1:1 (Depth: 500µm, Width: 500µm) using ultrasonic (US) welding. In this method, parts are joined by local melting using the sound waves in the ultrasonic region in the form of oscillating compressive stress on the joint area through temporary structures known as energy directors. A schematic of the US welding process is shown in Fig. 2.3 (a). The polymer samples to be bonded were clamped on the anvil of the machine and bonded using US at 35 kHz and a power of 1000W. The devices bonded were pressure-resistant up to minimum 0.4MPa. [15] Although the results are good, this method is commonly used on macroscale and requires special chip designs to effectively focus and direct energy to the bonding parts, making mold design more complex.

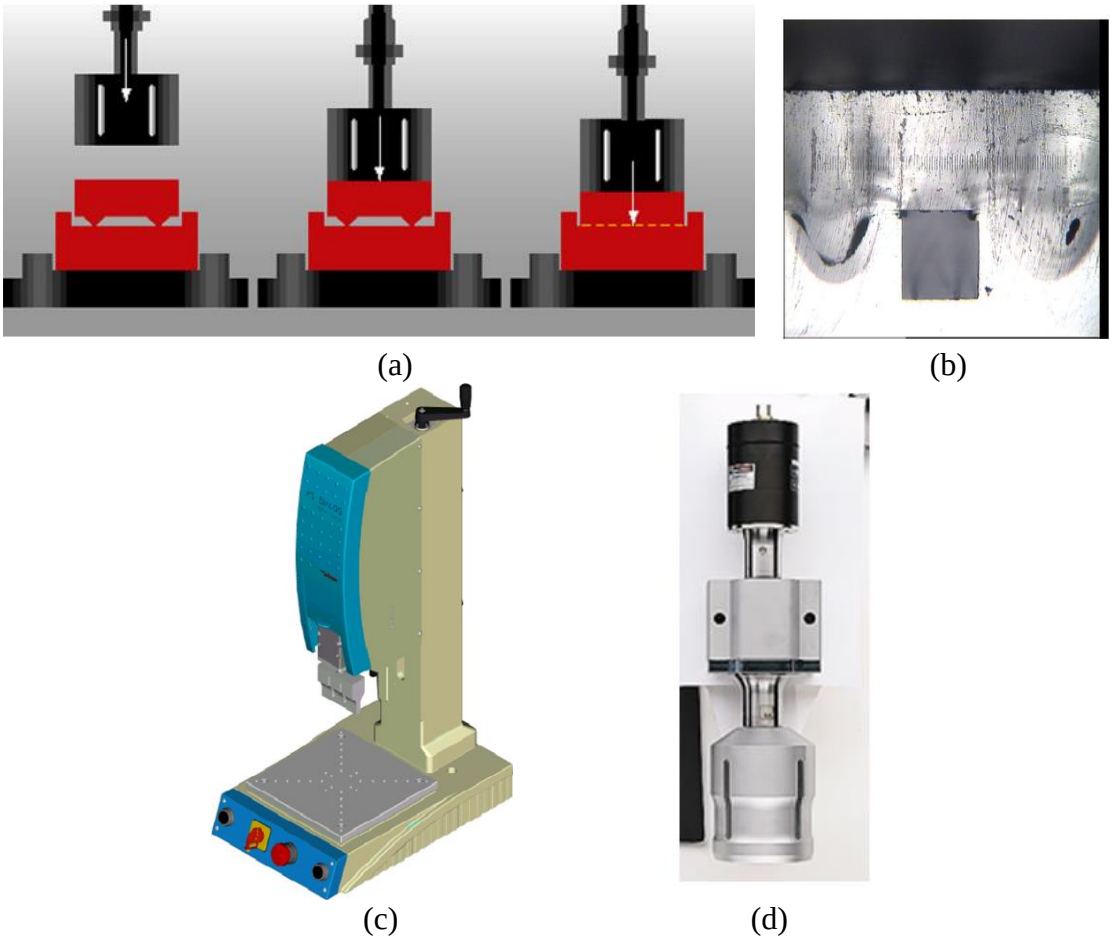

Figure 2.3 (a) Schematic of US welding process (b) Microscopic image of cross sectional view of the bonded microchannel (c) Standard US welding machine (courtesy of Hermann Ultraschalltechnik GmbH and Co., Germany) (d) Resonance stack comprising of piezo US convertor, booster and sonotrade [15]

In 2003, Kim and Xu bonded polyethyleneterephthalate (PET) polymer by localized welding using a laser. The parts to be bonded consist of one transparent and one opaque polymer. The laser beam passes through the transparent polymers and was absorbed by the opaque polymer. Heat conducted into the transparent polymer aids in bonding the polymers at the interface due to melting and resolidification. Fig. 2.4(a) shows a schematic of the process. The experimental apparatus consisted of a laser (λ=1100 nm), lens, aperture and specimen holder. The size of the bonding area depended on the laser beam diameter, exposure time and intensity. [16] This is a local bonding method and the sample must be moved to bond along a line or any other shape. Good bonding

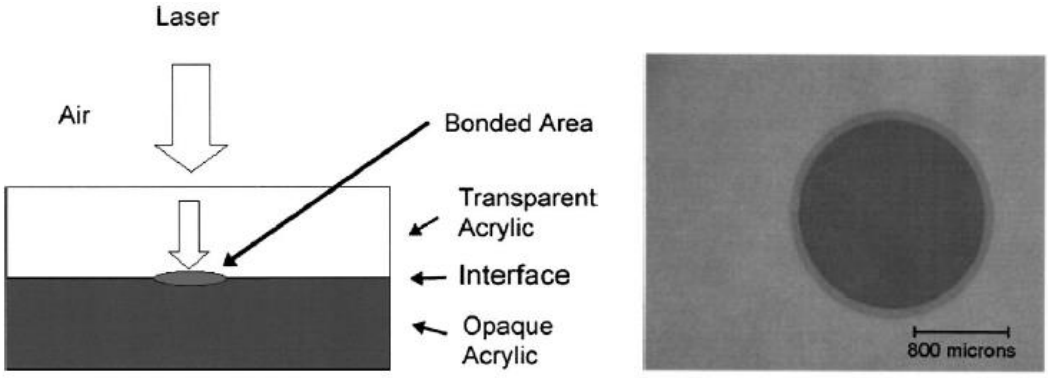

(a) (b)

Figure 2.4 (a) Schematic diagram of laser bonding process (b) Top view of bonded spot of sample [16]

depends on the absorption characteristics of the material, intensity, exposure time and focusing of the beam which makes this process challenging.

Among the various available bonding techniques, thermoplastic fusion bonding is widely used for bonding of thermoplastics because of its simplicity and strong bonds produced at low cost. In TFB, the two polymers are brought together with the application of heat and pressure for sufficient time.

In 1997, Martynova et al. conducted TFB of PMMA with microchannels imprinted using wire on both the substrate and coverslip using a conventional oven. The two PMMA devices were clamped between two microscope slides, placed in an oven and bonded at 108℃ for 10 mins. [17]

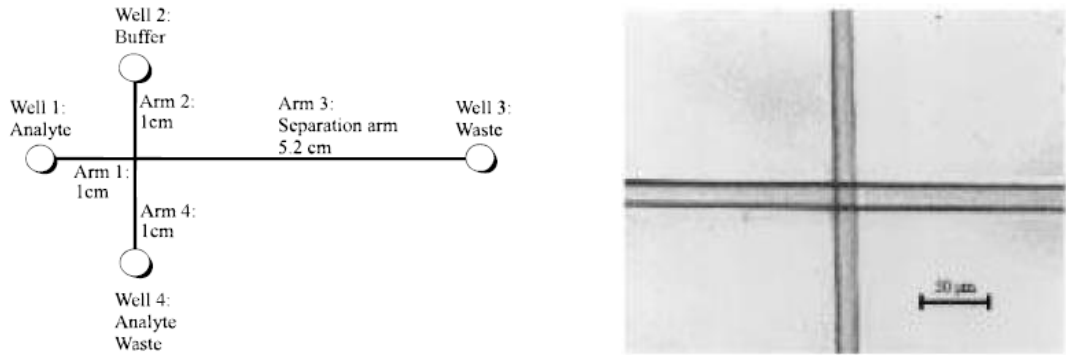

(a) (b)

Figure 2.5 (a) Schematic of prototype wire imprinted device (b) Photograph of typical 25µm wire imprinted device by Martynova et al. [17]

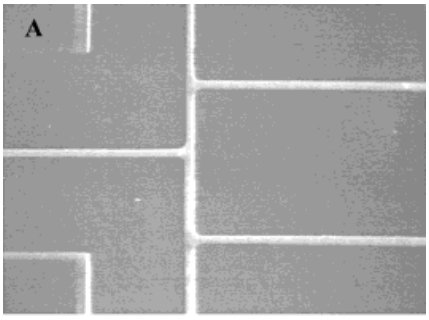

Figure 2.6 Optical micrograph of the PMMA microdevice after thermal bonding [18]

In 1998, Ford et al. bonded PMMA devices using a hot plate and copper weights. The substrate and cover slip were heated to 150℃ for 5-10 mins and then placed in the jig with 50-lb copper weight placed on the entire assembly. The jig with the samples were placed in a programmable oven and slowly cooled to room temperature for about 2hrs. [18] Microscopic image of bonded sample is shown in Fig. 2.6.

In 2004, Chen et al. bonded PMMA using vacuum assisted thermal bonding procedure. Imprinted PMMA pieces 5mm thick were bonded with 5mm thick blank PMMA cover by placing the assembly in vacuum heating oven for 60 mins at 120℃ under vacuum pressure of 10 mbar which lead to bonding at the interface of the PMMA pieces. [19] The bond strength of the device was determined using a tensile testing system and was found to be about 153 kPa for channels of depth 16 µm and width 156 µm. [19] Figure 2.7 shows the bonded microdevice and its microscopic image.

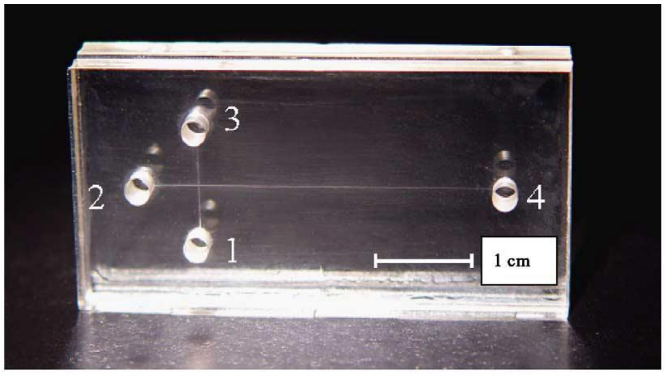

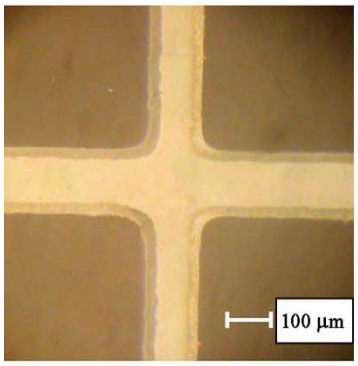

(a) (b)

Figure 2.7 (a) Photograph of entire PMMA microdevice (b) Microscopic image of bonded sample [19]

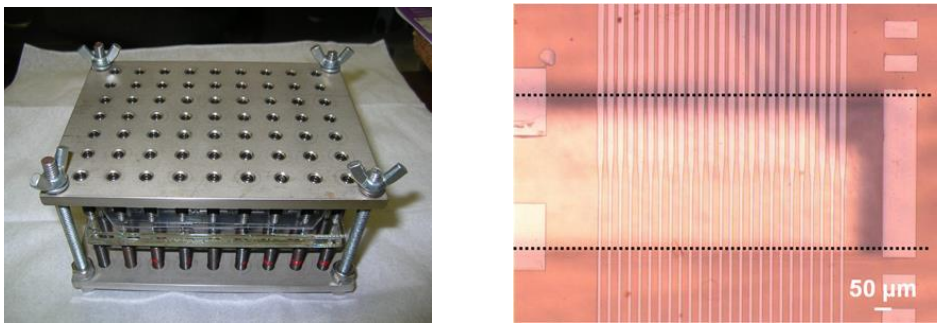

(a) (b)

Figure 2.7 (a) Custom-made TFB apparatus after assembly (b) Close-up image of sealed chip [20]

Park et al. developed a microtiter plate formatted array of continuous flow polymerase chain reaction (CFPCR) devices for DNA amplification by bonding 2.3 mm thick PC sheet with 250 µm thick PC cover slip using a custom made TFB apparatus with an array of spring loaded plungers that was subsequently placed in a convection oven. Channels with AR 2 and width of 20 µm were bonded at a temperature of 154℃ and pressure of 37.9 kPa for 2 hrs. [20]

There are several methods of TFB using different heating sources like conventional ovens, hot plates or hot presses. However, the temperature variation in commercial ovens is large (>1℃) and distribution varies with the location and number of parts to be bonded. Precise control of bonding temperature at the device level is difficult with local heating being a frequent problem.

Kelly et al. demonstrated a new method of bonding PMMA devices in 2003 using boiling water. Imprinted microchannels on PMMA sheet of 1/8” thickness was bonded with cover slip of 1/16” thickness by clamping it together using C clamps and was sandwiched between glass slides and aluminum blocks. The entire assembly was immersed in boiling water for 1 hour to bond the two PMMA pieces together. [21] The bond strength of the microdevices were evaluated by loading the bonded device with

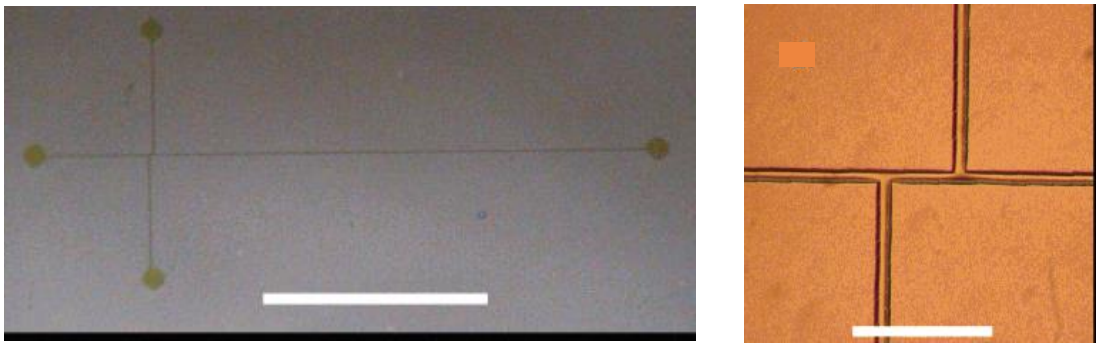

(a) (b)

Figure 2.8 (a) Silicon template with imprinted trapezoidal microchannels with 22 µm height, top and base widths of 20 and 48 µm. [21]

weights until it ruptured. The maximum pressure recorded was 130kPa. However, there was no control of the boiling point and samples were exposed to water directly.

Park et al. bonded PMMA substrates 3 mm thick and cover slips of 250 µm thick using a novel TFB method using a modified pressure cooker to ensure uniform temperature and pressure distribution. Channels up to 1:100 AR (Depth: 10 µm, Depth: 1000 µm) were bonded at temperature of 105℃ and pressure of 21.2 kPa for 15 mins without any deformation. Bond strength was tested using rupture test and a rupture pressure of 496 kPa was measured using nitrogen gas. [4] Fig. 2.9 (a) shows the microscopic image of a bonded sample. Bonding of curved samples were also demonstrated. The method was open loop with the operator manually controlling the valve for pressure relief. The bonding results were better than that using a forced convection oven to control the temperature and pressure applied using paper clips. [27] It was observed that the temperature inside the oven varied based on the location of the samples and the temperature sensor. Fig. 2.9 (b) shows the inhomogeneity of the collapsed deformation indicators on the four corners of the chip that indicate uneven pressure distribution on the entire surface.

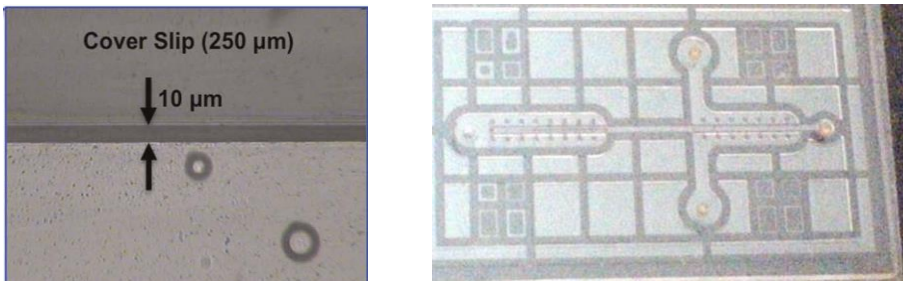

Figure 2.9 (a) Microscopic image of bonded sample of AR 1:100 [4] (b) Rectangular chambers (1 mm or 1.5 mm length and 10 µm or 15 µm depth) were collapsed – bonded in an oven. (105°C with paper clips)

2.4 Conclusions

Bonding is a critical step in the fabrication of microdevices. Different bonding approaches and their limitations are available. Thermal fusion bonding is a simple and widely used method. Even distribution and precise control of the temperature and pressure are the two major challenges in TFB for maximum strength and minimum deformation. Current methods of TFB use hot plates, conventional ovens and hot presses for heat input and cannot ensure even temperature distribution over the entire polymer surface. Poorly calibrated load applicators like weights and paper clips are used to apply pressure and even pressure distribution remains a challenge. A new cost-effective, repeatable and simple approach to overcome the limitations of the current bonding methods and to obtain even temperature and pressure distribution is required.

CHAPTER 3: DESIGN AND FABRICATION

3.1 Introduction

PMMA samples were fabricated for bonding experiments. A brass mold insert containing microchannels of four different aspect ratios was micromilled. PMMA substrates were hot embossed using the brass mold insert. This method was used because of its simplicity, high volume production, less time and cost-effectiveness. Dimensions of samples obtained were verified for accuracy optical profilometry. Sample dimensions were compared with those of the mold insert.

3.2 AutoCAD drawing and machining of the mold insert

Microchannels were laid out using AutoCAD v2014 and v2015 (Autodesk Inc., CA, USA). The mold was designed with eight serpentine microchannels of four different aspect ratios 1:10, 1:50, 1:100 and 1:200 for two different depths 5µm and 10 µm as shown in Table 3.1. The top row channels have a depth of 10µm while the bottom row channels are 5µm deep. In order to study the effects of channel dimensions and aspect ratio on bonding conditions and bond strength a set of test patterns were selected.

Table 3.1 Channel descriptions

TOP ROW (µm)	1:10 Depth: 10 Width:100	1:50 Depth: 10 Width:500	1:100 Depth: 10 Width:1000	1:200 Depth: 10 Width:2000
BOTTOM ROW (µm)	1:10 Depth: 5 Width:50	1:50 Depth: 5 Width:250	1:100 Depth: 5 Width:500	1:200 Depth: 5 Width:1000

Two brass (Alloy 353) mold inserts were made. A representative solid model of the mold for Version 1 is shown in Fig. 3.1 (a). Each channel is surrounded by rectangular structures of 100µm tall which act as a guide while cutting the channels after hot embossing. Each channel has an inlet and outlet reservoir to pass the fluid into the channels. Reservoirs have two different diameters, 1.5mm and 0.5mm with 100µm and 200µm high respectively from the base plane. The smaller diameter structures

shown in Fig. 3.1(b) help in locating the center by naked eye and to guide drilling the hole accurately for connecting the capillary. [22] Every channel was numbered on the left side for easy identification. This version of the mold did not have any dummy structures (additional rectangular structures around the main channel).

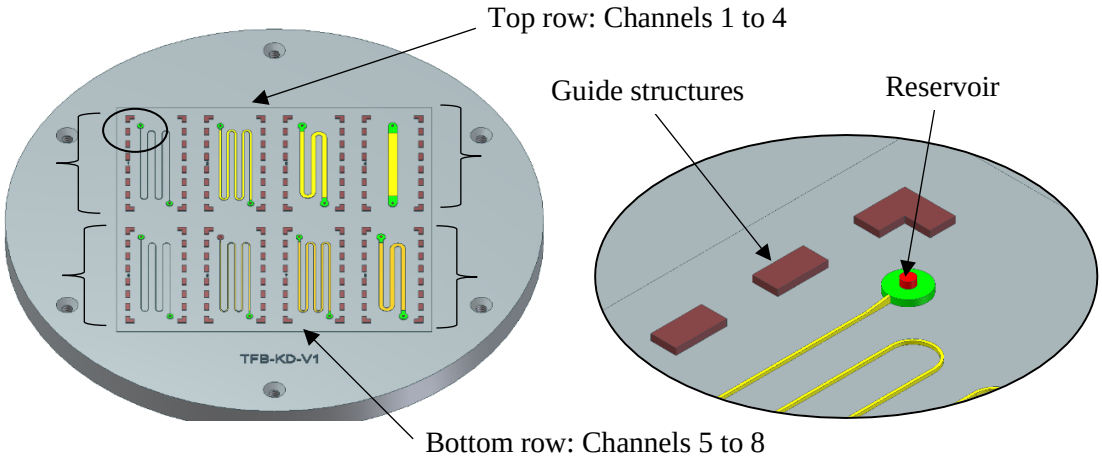

Figure 3.1(a) Representative model of mold insert Version 1 (b) Enlarged picture of reservoir design

Rectangular 100µm dummy structures were added around the main channels occupying the empty area as shown in Fig. 3.2(b). These additional structures help in achieving local homogeneous pressure distribution during hot embossing and helps in reducing demolding forces. [23] It is also thought that these structures help in removing the trapped air during the bonding process. [22] Addition of dummy structures reduces the bonding area and for the same pressure, force applied during bonding will be less.

Each mold insert was named at the bottom for easy identification in “Process-Name-Version” format. For example, TFB-KD-V1, ‘TFB’ for Thermal fusion bonding process, ‘KD’ for Kavya Dathathreya’s mold, ‘V1’ means Version 1.

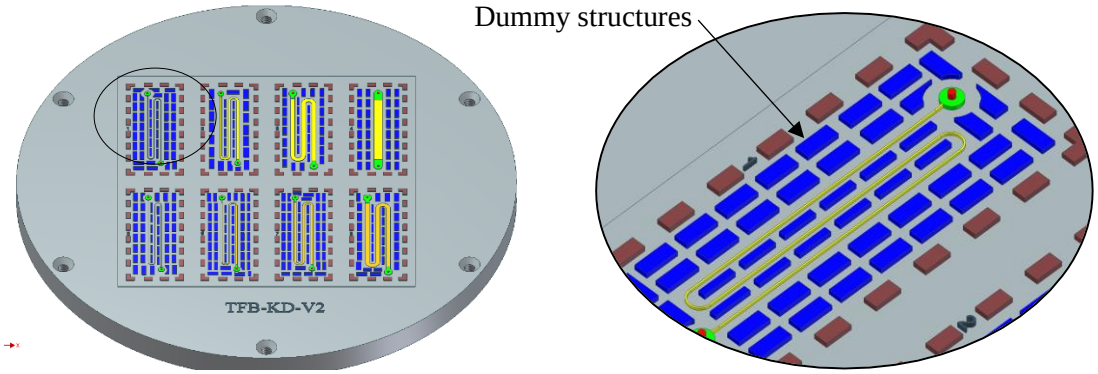

(a) (b)

Figure 3.2(a) Model of mold insert Version 2 (b) Detailed view of channel 1

Mold inserts were micromilled (MMP, KERN Micro- und Feinwerktechnik GmbH and Co. KG, Eschenlohe, Germany) from 4.75” diameter and 0.25” thick brass discs at LSU. Micromilling was done using the AutoCAD drawing compatible with the GibbsCAM (3D Systems, CA, USA) software. Surface finishing was done at 40000 rpm at a feed rate of 150mm/min. Additional details are given in Appendix 2.

After machining, the mold was scanned using an optical profilometer (Nanovea ST400, Irvine, CA, USA) to ensure the correctness of the channel dimensions. Fig. 3.2 (a) shows the entire scan of the channel 3 from the Surface Map software. Once scanned, heights of the channels were measured by taking horizontal sections using Mountain Map software as shown in Fig. 3.2(b).

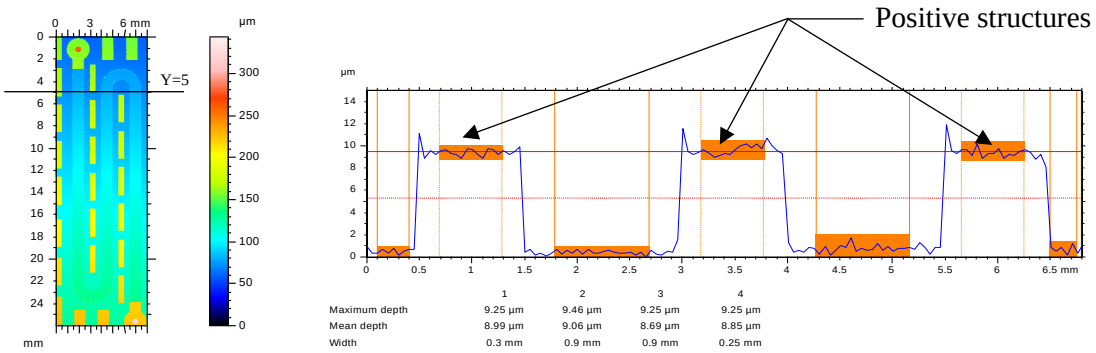

(a) (b)

Figure 3.2(a) Scanned image of channel 3 (b) Cross sectional view at y=5mm

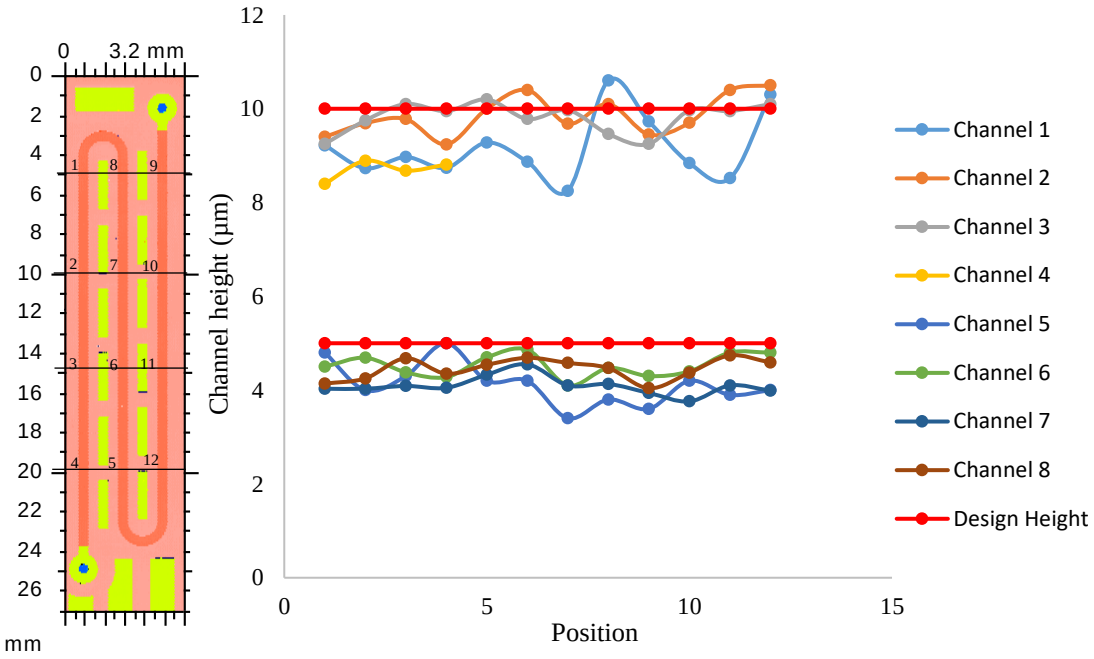

Figure 3.3 (a) Position of the height measured (b) Variation of height of all eight channels along the length

Profiles were extracted at four different locations 5, 10, 15 and 20mm along the length of the channels. A representative cross sectional profile is shown in Fig. 3.2 (b). Height of the channel was measured at 12 different positions along the channel and the variation of heights for all channels are shown in Fig. 3.3. The difference in height is maximum for the low AR 1:10 (Channel 1 and 5) with narrow channels as it is challenging to achieve the designed dimension. The difference in the heights of the channels to the designed dimension might be due to the temperature variation in the micromilling facility and use of more than one milling bit.

3.3 Fabrication of PMMA samples

Lower material and manufacturing cost has made polymers a very attractive material for microdevices. [10] Compared to the traditional materials like glass and silicon, polymers can be fabricated using various methods like photodefinable polymer technology (ex. Photolithography, Stereolithography, laser ablation) and replication methods (ex. Injection molding, hot embossing, casting, and thermoforming). [11]. In this research, PMMA MC Grade thermoplastic was used as the substrate material for

the manufacture of the microdevices because of its well-established molding parameters, good optical properties and more importantly range of T_g, which is suitable and feasible for the bonding process employed. Refer to Appendix 1 for more details about the physical properties from the manufacturer.

PMMA MC Grade polymer (Altuglas International, PA, USA) 3mm thickness were hot embossed using a Jenoptik HEX 02 (Jena, Germany) at the Center for Advanced Microstructures and Devices (CAMD) at LSU and at UNC using Jenoptik HEX 03 (Jena, Germany) as shown in Fig. 3.4 (a). The brass mold insert is fixed to the top plate and a 152 mm X 152 mm (6" X 6") PMMA sheet is placed on the bottom plate. Both the plates are heated in vacuum to 170℃ and a force of 15kN is applied for 120s. The temperature is reduced to 80℃ and the sample is demolded at a velocity of 1mm/min. Fig. 3.4(b) shows a typical hot embossed PMMA sample.

3.4 Verification of sample dimensions

The hot embossed PMMA samples were scanned using the optical profilometer (Nanovea ST400, Irvine, CA, USA) to measure the depths of the channels before bonding. For every sample, all eight channels were scanned and profiles were taken at four different locations along the length of the channel (y=5, 10, 15 and 20mm). A representative scan of channel 3 and its profile extractions are shown in Fig. 3.5 (a) and (b) respectively.

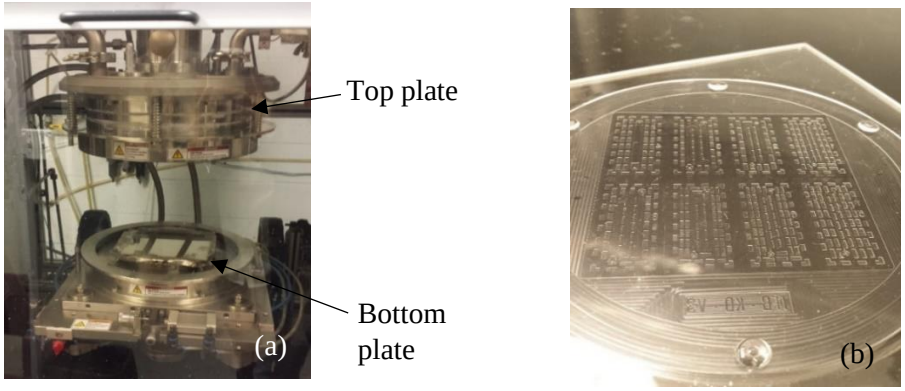

Figure 3.4 (a) Jenoptix HEX 02 hot embossing machine and (b) Hot embossed PMMA sample

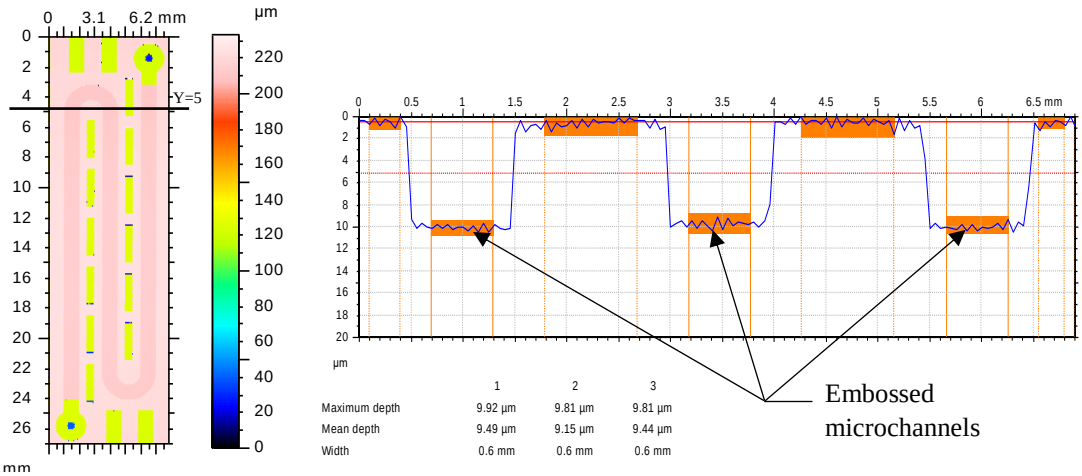

(a) (b)

Figure 3.5(a) Scanned image of channel 3 of PMMA sample (b) Cross sectional view at y=5mm

Using the scanned images, channel depths were extracted at 12 different locations along all the channels. Channel 4 is a straight channel and 4 measurements were taken along the length. Figs. 3.6 (a) to (d) shows the variation of the depths along the channels. Error bars indicate the 95% confidence interval for the mean depth for 15 samples using Student's t distribution. [24] Details regarding the calculations are given in Appendix 3.

Results of the replication were compared to the mean depths of the samples to the height of the mold insert. From Fig. 3.7, it can be seen that the PMMA samples are very close to the mold. Replication error (RE) percentage was calculated from the mean of channel depth to the mold height using the equation 1 [25]

$$\%RE = \frac{mold\ height - channel\ depth}{mold\ height} \times 100 \qquad \text{(Equation 1)}$$

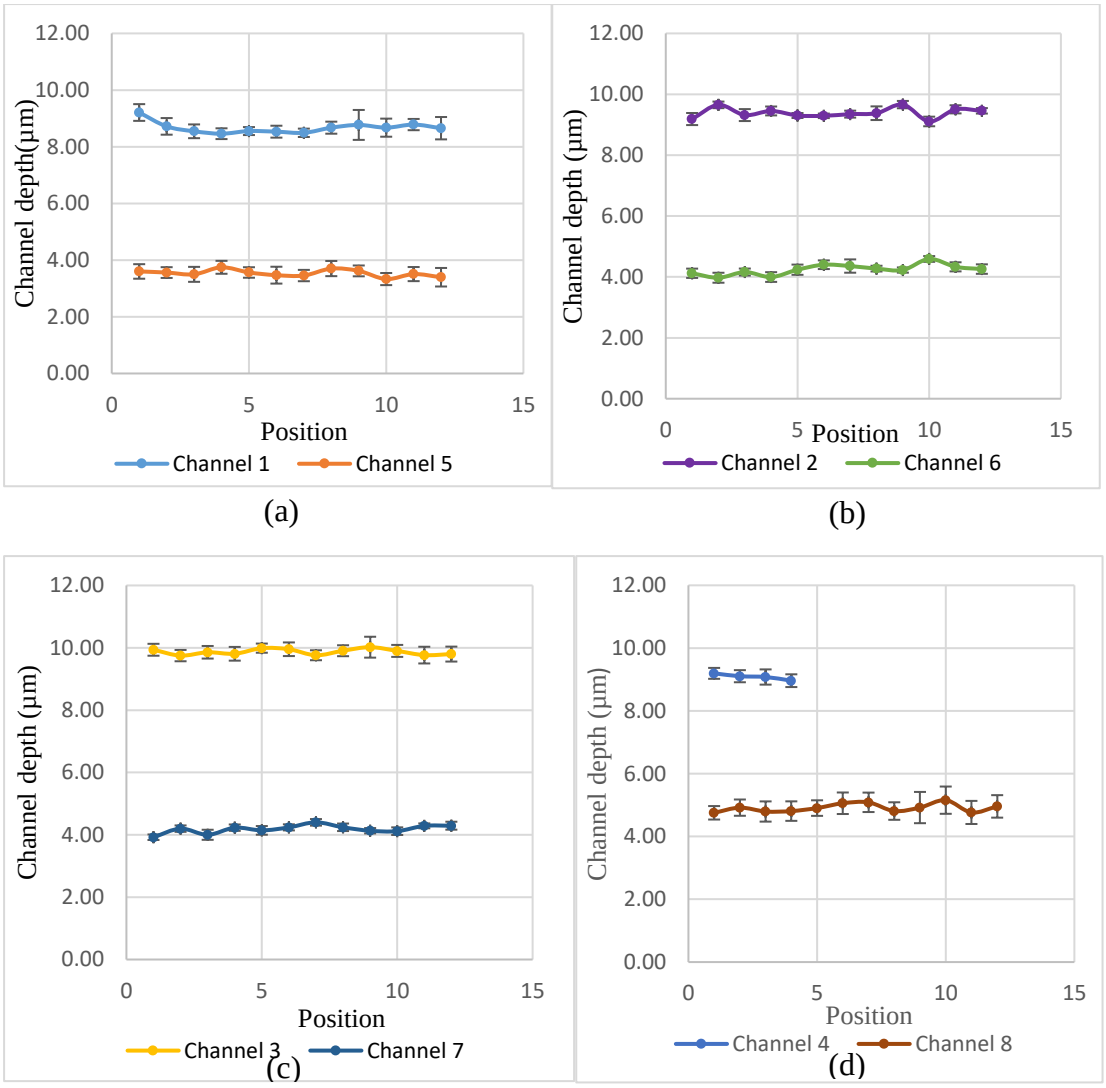

Figure 3.6 (a) Depth variation along the length of channels for AR 1:10 (b) Depth variation along the length of channels for AR 1:50 (c) Depth variation along the length of channels for AR 1:100 (d) Depth variation along the length of channels for AR 1:200

The replication error was <6% for AR 1:50, 1:100 and 1:200. For Channel 1 and Channel 5, RE was 10% and 14% respectively because of the channel dimensions (width: 50 µm and depth: 5 µm) which were challenging for hot embossing. RE for hot embossed PMMA channels with depth of 81.2±1.1 µm was measured to be 4.5%. [25] No literature discusses the replication error for similar depths to make a comparison. Figs. 3.8 (a) to (d) shows the comparison of the variation of the samples to that of the mold.

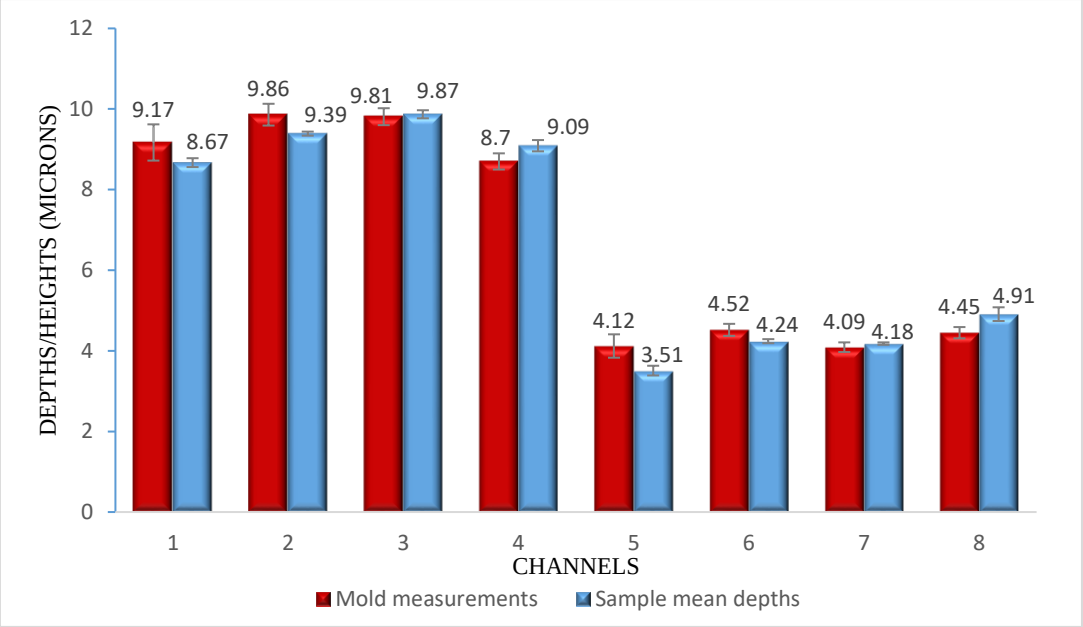

Figure 3.7 Comparison of depths of samples to the mold heights for all channels

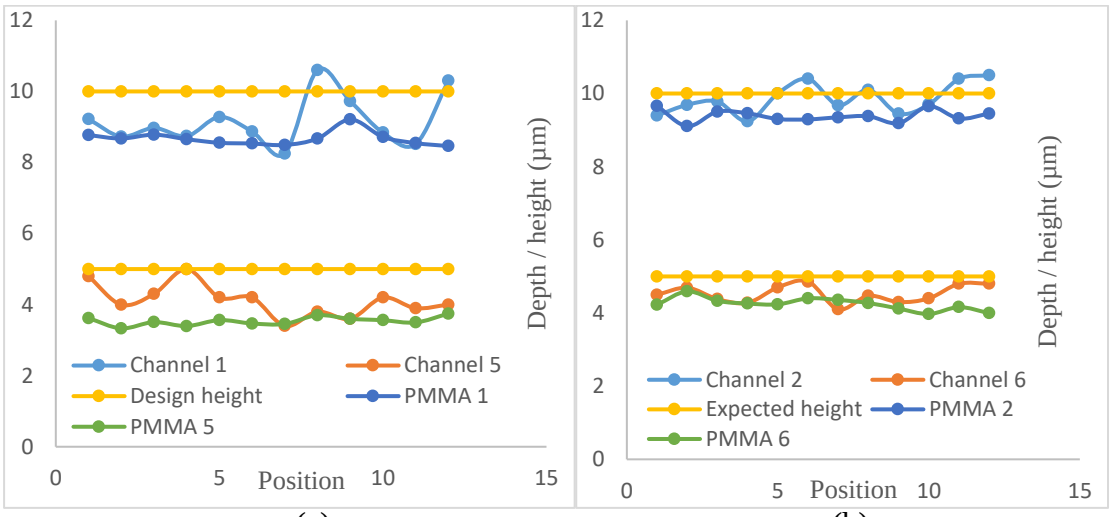

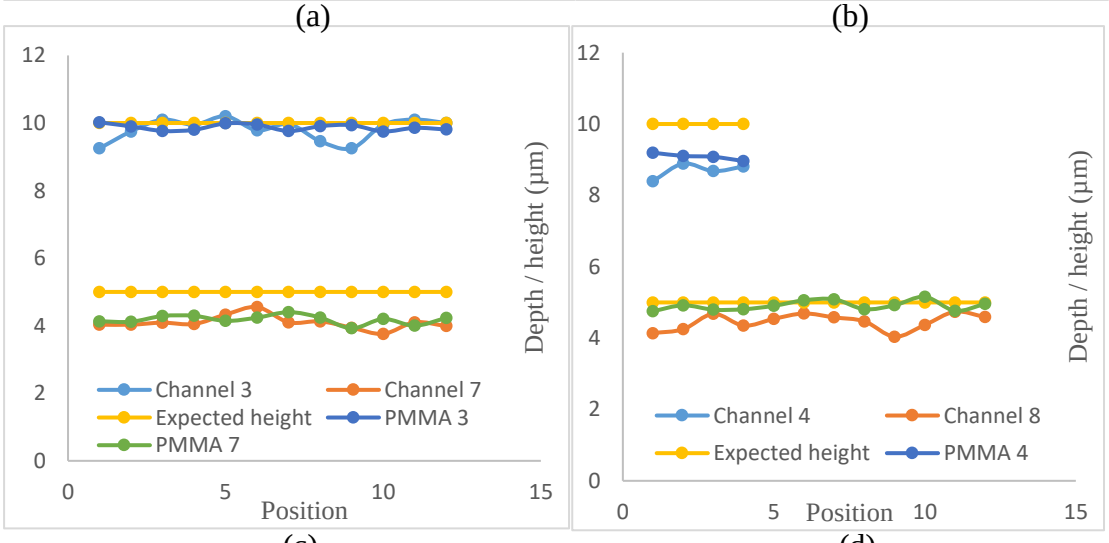

Figure 3.8 Comparison of variation of channel depth to mold height for (a) AR 1:10 (b) AR 1:50 (c) AR 1:100 (d) AR 1:200

3.5 Conclusions

Brass molds were designed, fabricated and verified using the optical profilometer. The variation of the channel heights along the length of the channel is shown and the deviation is within acceptable limits. PMMA samples were by hot embossed and channel depths were measured. Comparison of the channel depths to the mold heights and variation of the mean channel depths along the length of the channel were shown. Replication error values for all the channels ranged from 0.6% to 14% with the maximum error for Channel 5. The dimensions for Channel 5 make it difficult to machine and hot emboss leading to the large deviations.

CHAPTER 4: EXPERIMENTS

4.1 Introduction

A new closed loop control system was developed to automatically control the bonding temperature throughout the PABP process. Hot embossed PMMA samples were cut, cleaned and bonded to the cover slips using thermal fusion bonding with the open loop and closed loop PABP systems. Experiments were conducted to optimize bonding conditions including temperature and pressure for channels with different aspect ratios. To evaluate the bond strength, leak and rupture tests were conducted. Comparison of the maximum rupture pressure of the bonded samples from both the open loop and closed loop systems are presented.

4.2 Sample preparation

Before conducting the bonding experiments, the PMMA substrates containing the microchannels and the cover slips were cleaned and dried to ensure good bonding results. The hot embossed samples were first covered with polyethylene terapthalate (PET) tape to protect the channels before cutting and drilling as shown in Fig. 4.1 (a). The eight channels were cut along the guide structures using a miniature table saw (MicroLux, USA). Holes were drilled at the inlet and the outlet reservoirs using a miniature drill press (MicroLux, USA) using a #71(0.66 mm DIA) size drilling bit (Kemmer Prazision, CA, USA) to connect poly ether ether ketone (PEEK) capillary tubes (0.03125” DIA) (IDEX Corporation, IL, USA). The size of the hole was smaller than the tube to be connected to have an interference fit to prevent leakage of the fluid while testing. Cover slips were cut from 250μm thick PMMA sheets (Plexiglas MC, Goodfellow, Oakdale, PA, USA) to the same size as the channel substrates as shown in Fig. 4.1(b). To protect the downside of the substrate from the sealing bag imprints during bonding, Polycarbonate (PC) sheets were used.

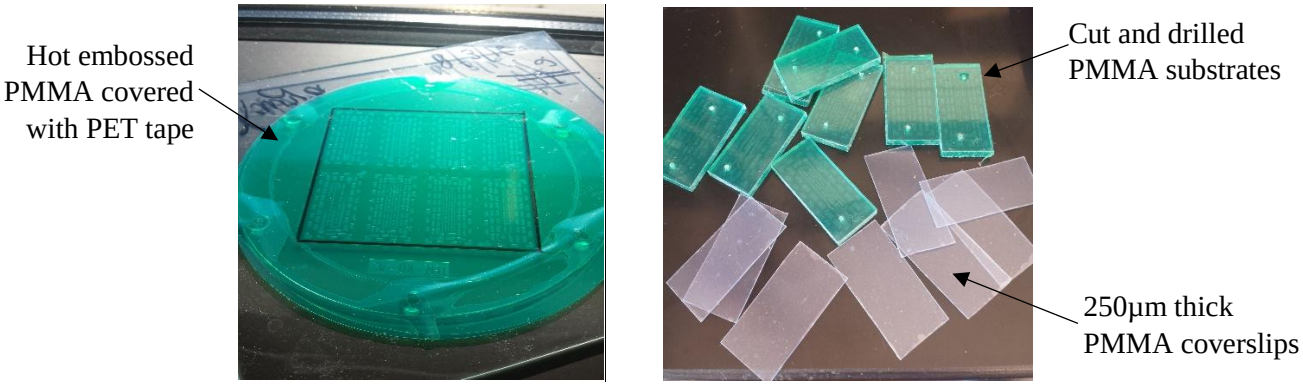

(a) (b)

Figure 4.1 (a) PMMA sample with PET tape to protect the channels (b) Samples and the cover slips after cutting and drilling holes at the inlet and outlet

The substrates, cover slips and the PC sheets were cleaned thoroughly to remove any burrs and residual particles that may have adhered to the surface. The samples were first cleaned in 1% Liqui-Nox soap solution, rinsed with deionized (DI) water, and cleaned in ultrasonic bath (Branson, Danbury, CT, USA) twice for 5 mins in DI water. In ultrasonic cleaning, high frequency sound waves agitate the liquid and help remove particles stuck to the polymer surfaces. The samples were rinsed in DI water and cleaned in an ultrasound bath with 5% isopropyl alcohol solution for 3 mins. The samples were finally rinsed in DI water and dried using ultra high pure compressed nitrogen gas (Airgas, PA, USA). After cleaning and drying, polymer samples were kept in an oven (VWR 1620, West Chester, PA, USA) at 60˚C for about 12 hours to remove any residual moisture.

4.3 Thermal Fusion Bonding Using the PABP system

Affixing the cover plate to the substrate containing microchannels is very important in obtaining well sealed microdevice. In TFB, the substrate and cover slip were heated to near or above the T_g of the polymer along with the application of pressure. Thermoplastic polymers like PMMA soften at temperatures close to T_g and form a bond between the substrate and cover slip by interdiffusion of the surface polymer chains. Constant temperature and even pressure distribution are key factors to

obtain good bonding without channel deformation. In this method of bonding, constant temperature and pressure conditions were achieved by immersing the samples in boiling water.

4.3.1 Working principle

Water boils at its normal boiling point when the pressure is equal to standard atmospheric pressure (101.325 kPa). Once the boiling point is reached, the temperature remains constant with additional heat input. The relationship between the temperature and pressure for boiling water is governed by the Clausius-Claypeyron equation [26]

$$\ln\left(\frac{P_2}{P_1}\right) = \frac{\Delta H}{R}\left(\frac{1}{T_1} - \frac{1}{T_2}\right) \qquad \text{(Equation 2)}$$

where P_1 = standard atmospheric pressure (101.325 kPa), T_1=100˚C (normal boiling point of water), ΔH=enthalpy of vaporization of water (40.65 kJ/mol) and R = universal gas constant (8.314 Jmol/K). Using the above relation, the boiling point of water corresponding to any pressure can be calculated. Fig. 4.2 shows the effect of increasing pressures on the boiling point of water. T_g of PMMA is about 105˚C, it varies depending on the grade, and the corresponding absolute pressure is 120.49kPa which is about 19kPa (2.8 psi) gage pressure. During PABP bonding, the desired temperature was achieved by altering the boiling point of water by increasing the pressure using a pressure vessel.

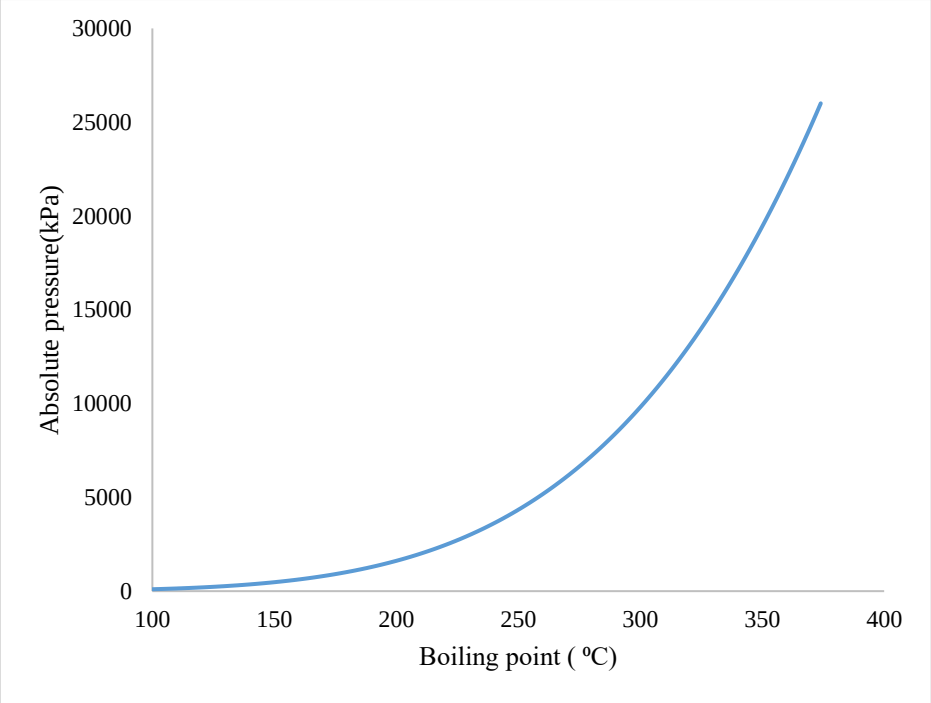

Figure 4.2 Variation of Absolute pressure with increasing temperature for boiling water

4.3.2 Open loop PABP system

A novel TFB method using PABP system with manual control was developed by Park et al. [4, 22] The experimental apparatus and procedure are discussed below. A systematic study was done using this system to determine the optimum pressure and temperature for good bonding.

4.3.2.1 Experimental Apparatus

A modified commercial pressure cooker (8 quarts, Phillipe Richard, China) was used as a pressure vessel. Heat was supplied to the water in the pressure vessel using a portable butane gas burner (Sun Star, Geumsan, Chungeheongnam, South Korea). The polymer samples were inserted in a vacuum bag (Sunbeam Products, Inc., FL, USA) to protect the samples from the boiling water. The bag was connected to a rubber vent tube using a connector (Torr 353444, Torr Technologies, Inc., Auburn, WA, USA) which was open to the ambient air. A Type K thermocouple (OMEGA Engineering,

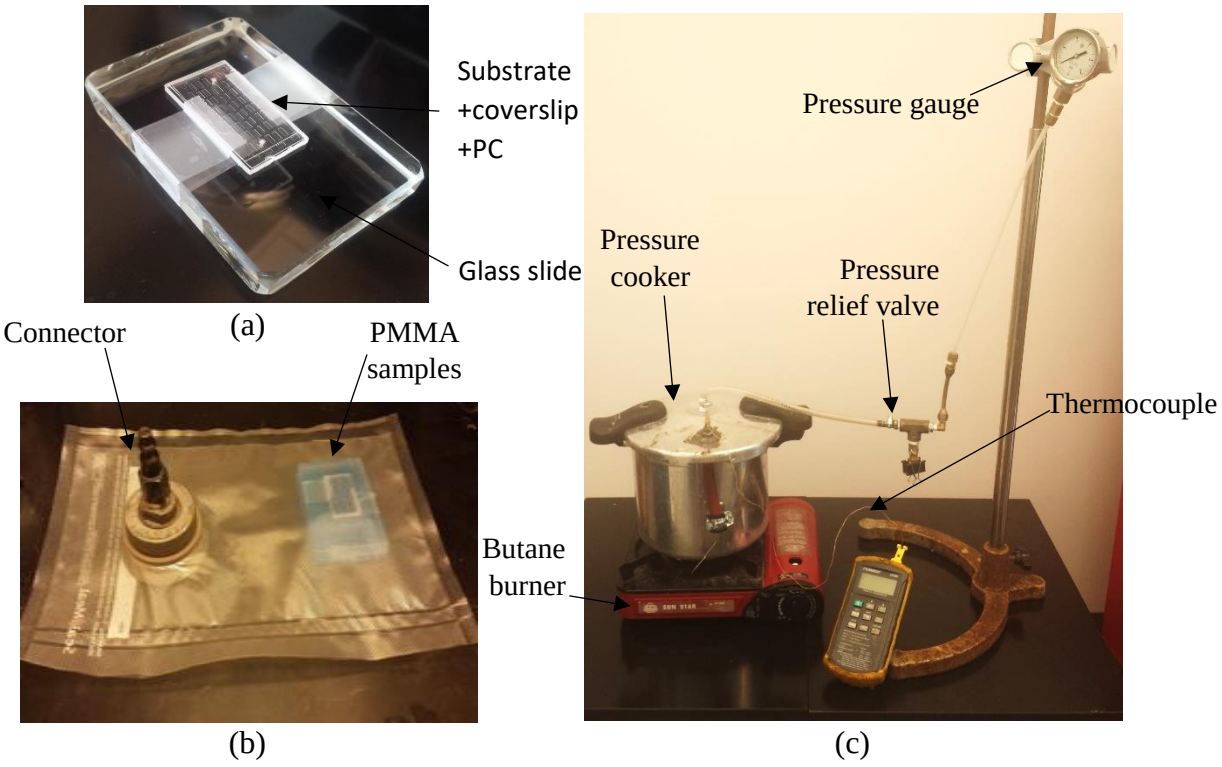

Figure 4.3 (a) Substrate, cover slip and PC sheet fixed against glass slide (b) Sealed bag with the connector containing the PMMA sample to be bonded (c) Open loop PABP system experimental set up

Inc., Connecticut, USA) was inserted into the sealing bag through the vent tube to monitor the temperature throughout the bonding process. A pressure gauge (4088K9, McMaster-Carr, Cleveland, OH, USA) was used to monitor the pressure in the vessel. A brass pressure relief valve (4893K25, McMaster-Carr, Cleveland, OH, USA) was used to maintain constant temperature by manually controlling the release of steam through the vent tube. Fig. 4.3(b) shows the experimental set up with all the components.

4.3.2.2 Procedure

PMMA substrates containing the microchannels were placed with the channels facing upwards on a 5cm x 7.5cm glass plate (McMaster-Carr, IL, USA) of thickness 15 mm (0.625”) that provided a flat reference surface during bonding as shown in Fig. 4.3 (a). The channels were covered with a cover slip and a PC sheet and the entire

assembly was inserted in a sealing bag sealed using a vacuum sealer (Foodsaver V2830, Foodsaver Advanced Design, Sunbeam products, Neosho, MO, USA) as shown in Fig. 4.3(b). The entire bag was immersed in the water in the pressure vessel. The water was heated using a butane burner. Once the temperature reached the desired temperature the heat input was reduced and the temperature was controlled by manually operating the relief valve. The bonding was done for 15 minutes from the time the desired temperature was reached and the samples were removed and checked for deformations. The vapor pressure compressed the bag and the polymer samples creating a bond. This system produces an even pressure distribution over the polymer samples and a constant surface temperature, which are the two essential requirements for good bonding result. [2]

4.3.2.3 Experimental results

4.3.2.3.1 Bonding results for Mold 1

Bonded samples were observed under a microscope (Nikon MM-11, Nikon Corporation, Tokyo, Japan) to inspect the quality of bonding. Bonded samples from Mold 1 (without dummy structures) showed severe channel deformation for AR's greater than 1:50 as shown in Figs. 4.4 (b), (c), (d), (f) and (g). Bonding results were good for lower AR of 1:10 as shown in Fig. 4.4 (a) and (e). Dummy structures are thought to help to eliminate the air trapped during the bonding process and exerts lesser force on the surfaces to be bonded.

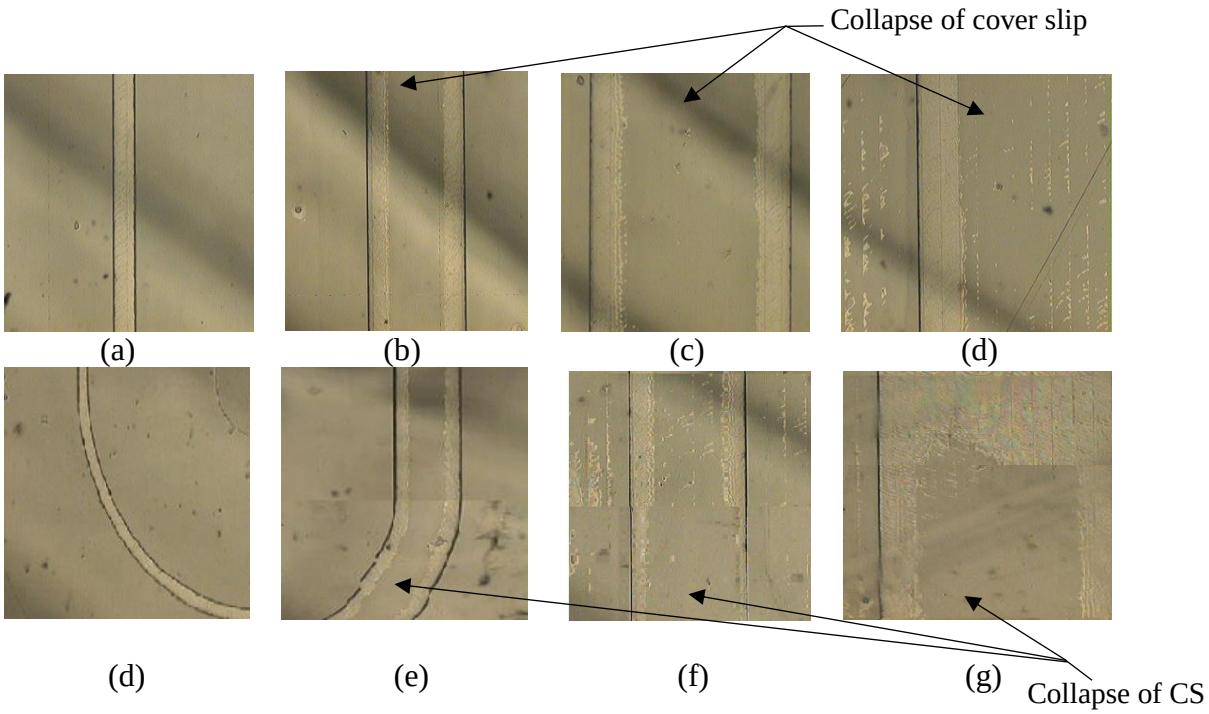

Figure 4.4 Microscopic images after bonding of (a) Channel 1 (b) Channel 2 (c) Channel 3 (d) Channel 4 (e) Channel 5 (f) Channel 6 (g) Channel 7 (h) Channel 8

4.3.2.3.2 Bonding results for Mold 2

Good bonding results and optimized bonding conditions were obtained for samples with AR 1:10, 1:50 and 1:100 without any channel deformation (see Table 4.1). For AR 1:100, bonding of Channel 3 was not repeatable as the width of Channel 3 is twice than that of Channel 7. Channels 4 and 8 with the lowest AR 1:200 had the cover slip collapse into the channel as shown in Figs. 4.5(d) and (h), and optimum conditions were not found.

Table 4.1 Optimized bonding conditions for open loop bonding technique

Channel	Bonding temperature (˚C)	Bonding pressure kPa (psi)
Channel 1	104.8±0.2	3.45 - 4.14 (0.5-0.6)
Channel 2	104.5±0.2	2 - 3.45 (0.3-0.5)
Channel 3	102.8±0.2	1.72 (0.25)
Channel 5	105±0.2	5.17 (0.75)
Channel 6	104.4±0.2	2 - 3.45 (0.3-0.5)
Channel 6	104±0.2	1.72 (0.25)

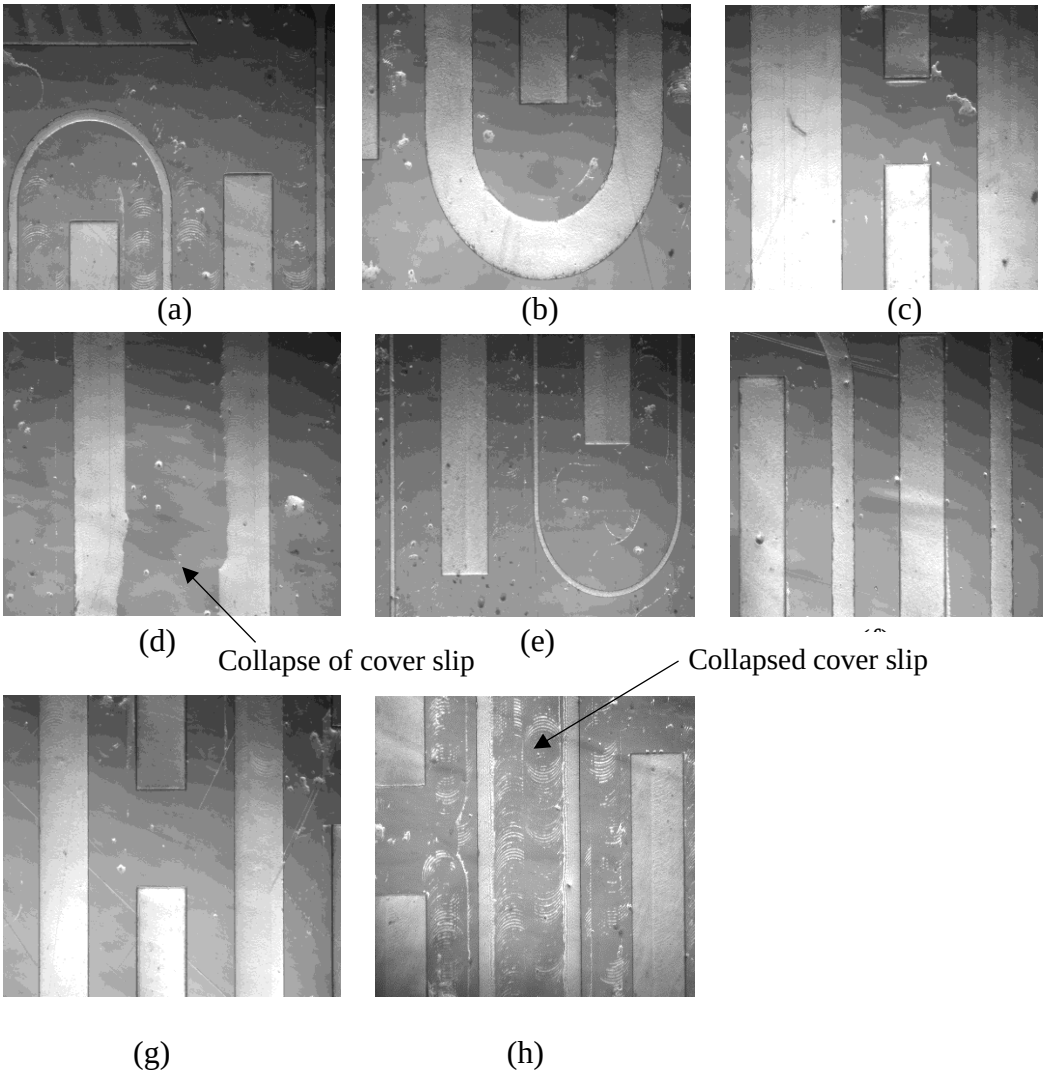

Figure 4.5 Microscopic image using 4x objective lens of bonded samples (a) Channel 1 (b) Channel 2 (c) Channel 3 (d) Channel 4 (e) Channel 5 (f) Channel 6 (g) Channel 7 (h) Channel 8

4.2.3.2.3 Leak test

After the inspection of the samples under the microscope, bonded samples were checked for leaks by passing colored dye through the device. Rhodamine B (Acros Organics, Fisher Scientific, NH, USA) a fluorescent dye of concentration 0.01% by mass was pushed into the microchannels using a syringe pump (New Era Pump Systems Inc., NY, USA) for 15 mins and was observed under a fluorescence microscope, Olympus IX70 (Olympus Corporation, Tokyo, Japan). Flow rate of the dye can be set using the Pump Terminal Emulator software (New Era Pump Systems Inc., NY, USA).

Table 4.2 Flowrates and velocity of the dye tested for different channels

	Cross sectional area (μm^2)	Flow rate (µL/min)	Velocity (mm/sec)
Channel 1	10 x 100 = 1000	5	83
Channel 2	10 x 500 = 5000	4	13
Channel 3	10 x 1000 = 10000	3	5
Channel 5	5 x 50 = 250	5	333
Channel 6	5 x 250 = 1250	4	53
Channel 7	5 x 500 = 2500	3	20

Table 4.2 shows the maximum flow rates and velocity of the dye that the channels withstood without leaking. For higher flow rates, debonding of the cover slip and the substrate was observed. Figs. 4.6(a) – (f) show the images taken from the fluorescence microscope. Leak tests were not conducted for Channel 4 and Channel 8 with AR 1:200 since there were no good bonded samples.

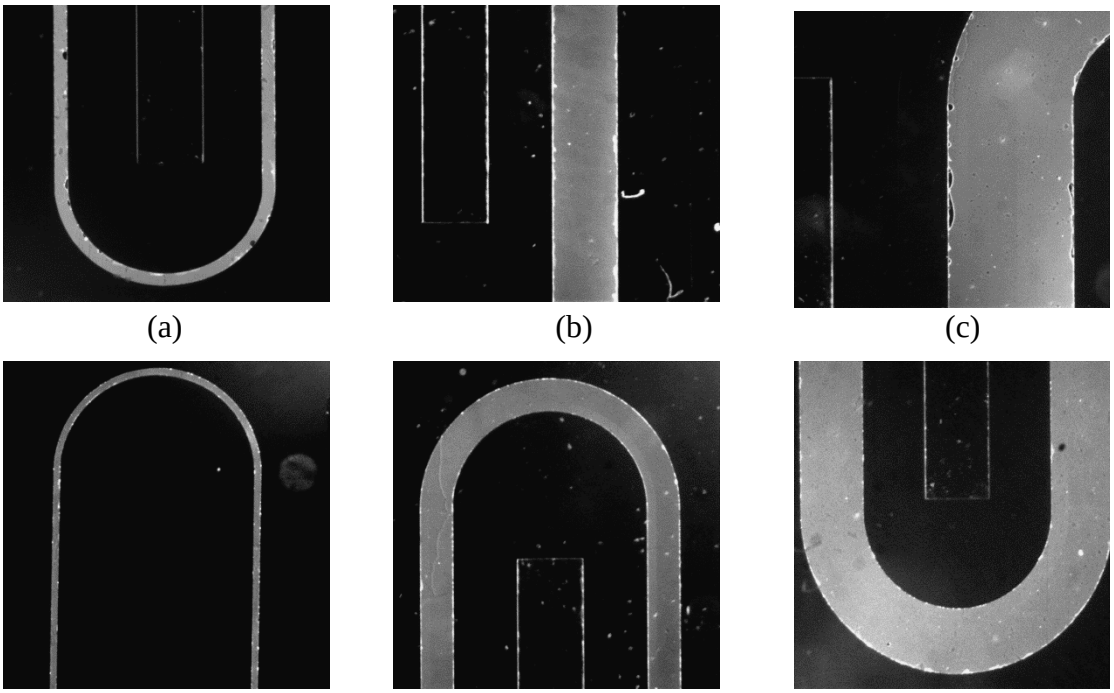

(a) (b) (c)

(d) (e) (f)

Figure 4.6 Microscopic images of leak test using 2x objective lens for (a) (a) Channel 1 (b) Channel 2 (c) Channel 3 (d) Channel 5 (e) Channel 6 (f) Channel 7

4.2.3.2.4Rupture test

A. Experimental set up and procedure

The rupture test was conducted to determine the bond strength of the samples. Fig. 4.7 shows a schematic of the rupture test set up. Compressed nitrogen gas was flowed into the bonded sample through a PEEK micro tube (1/32”OD, IDEX Corporation, IL, USA). A pressure regulator (Harris Product Group, OH, USA) was used to increase the pressure gradually. The pressure reading was recorded continuously in LabVIEW using a pressure transducer (WIKA Instrument, Klingenberg, Germany) connected to a data acquisition board (DAQ) (6212, National Instruments, TX, USA). The pressure transducer needed an input voltage of 1-30V DC and was connected to a power supply (1672, BK Precision Corporation, CA, USA). Two microfluidic shut-off valves (P-732, IDEX Corporation, IL, USA) were used upstream and downstream of the sample to control the entry and exit of the compressed nitrogen.

The inlet and outlet of the bonded sample were connected to the two capillaries of the apparatus. The LabVIEW program was started and the pressure of the compressed nitrogen was gradually increased using the pressure regulator. The sample debonded and ruptured at the maximum pressure, which was recorded. Complete description of experimental apparatus and procedures can be found in Appendix C.

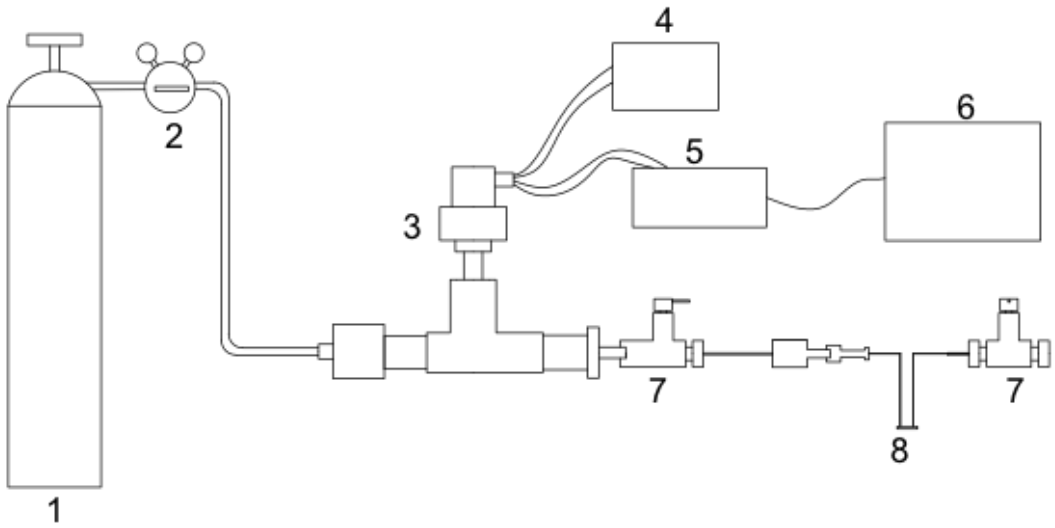

Figure 4.7 Compressed nitrogen, 2. Pressure regulator, 3. Wika Eco-tronic pressure transducer, 4. Power supply, 5. NI 6212 DAQ board, 6. Computer, 7. Shut off valve, 8. Sample to be tested

B. Results

Rupture pressures for six bonded samples for each of the Channels 1, 2, 5, 6 and 7 and three samples of Channel 3 for AR 1:10, 1:50 and 1:100 were measured. The mean rupture pressure was calculated with standard deviation in the range of 75kPa - 165 kPa and represented in Fig. 4.8. The results reveal that the bond strength at higher AR is greater than for a lower AR. For the same AR, bond strength of shallower channels was higher than for the deeper channels. Detailed rupture pressure data for all the samples are included in Appendix D.

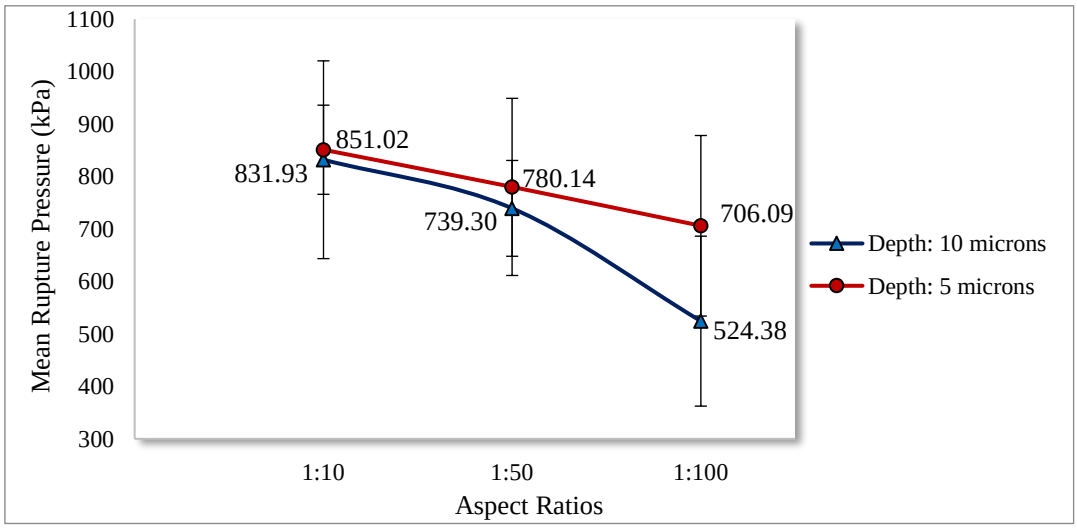

Figure 4.8 Maximum pressure data versus aspect ratio for two depths

4.3.3 Closed loop temperature control system

A closed loop implementation of the TFB method was developed to eliminate human intervention which introduces a time delay in the process, and to maintain the temperature automatically during bonding. This was implemented in LabVIEW where the measured temperature of the boiling water was continuously compared to the set temperature and based on the error a feedback signal was sent to a control valve which opens/closes to maintain the temperature. A schematic of the closed loop system is shown in Fig. 4.9. Lines represent signals in the block diagram.

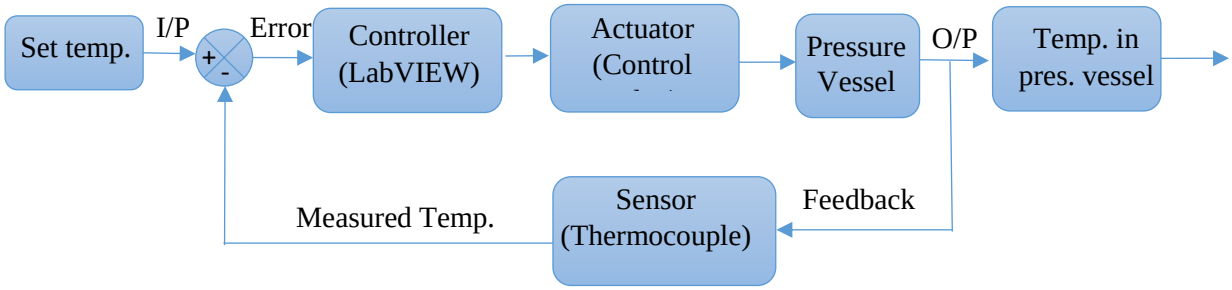

Figure 4.9 Illustration of closed loop system

4.3.3.1 Experimental set up and procedure

The experimental set up for closed loop was similar to the open loop system. It consisted of a pressure cooker (8 quarts, Phillipe Richard, China) used as a pressure vessel. Heat was supplied by a butane gas burner (Iwatani Corporation, NJ, USA). The temperature inside the sealed bag was measured continuously using a Type K thermocouple (Omega Engineering, CT, USA) which was connected to the DAQ board (NI-9211, National Instruments, TX, USA). Pressure was measured using a pressure gauge (WIKA Instrument, Klingenberg, Germany). A proportional type control valve (Belimo, Hinwil, Switzerland) with an electric actuator connected to a NI 6212 DAQ board (National Instruments, TX, USA) was used to maintain the temperature by opening or closing of the valve based on the difference between the measured and set

temperatures. A step-down transformer (Kele, TN, USA) was used to supply 24VAC power to the valve. A schematic of the experimental apparatus is shown in Fig. 4.10.

A sealed bag containing the PMMA samples to be bonded was connected to the vent tube through a connector and immersed in water and a thermocouple was inserted into the bag to measure the temperature. A program was developed using LabVIEW version 2015 (National Instruments, TX, USA) software in which built in proportional-integral-derivative (PID) controller was used to maintain the temperature at the set temperature. The optimal value of the gains for the controller was determined experimentally and the response of the closed loop system is shown in Fig. 4.11. The variation in the temperature was about ±0.15℃. Once the set temperature was reached, a timer was started and bonding was done for 15 minutes. Multiple samples up to four samples can be bonded simultaneously were bonded with good bonding results. Detailed description of the set up and procedure is included in Appendix E.

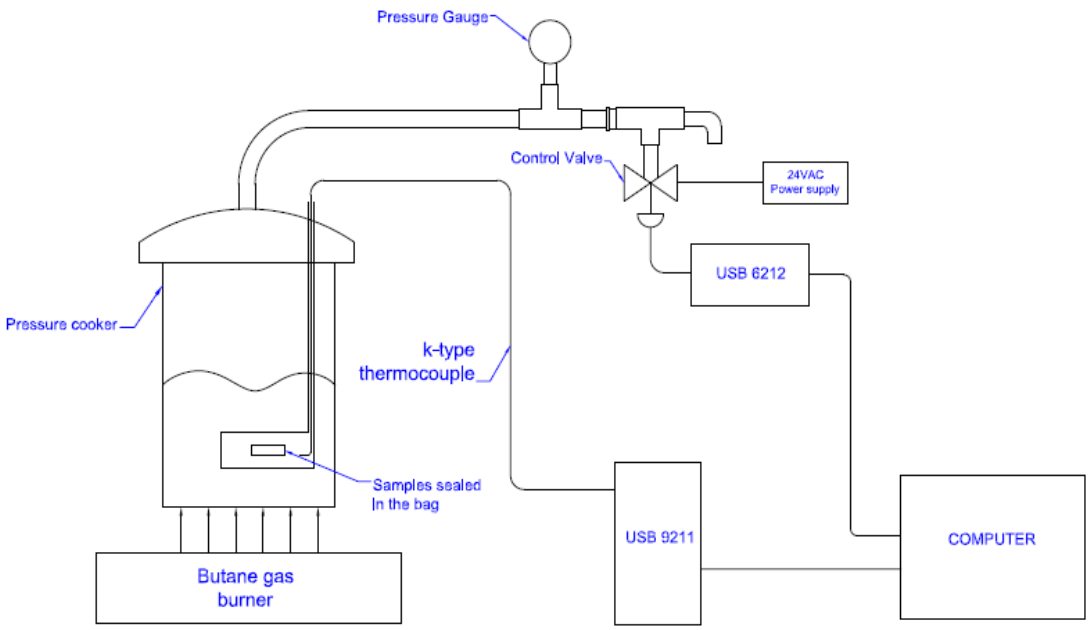

Figure 4.10 Schematic of closed loop experimental set up

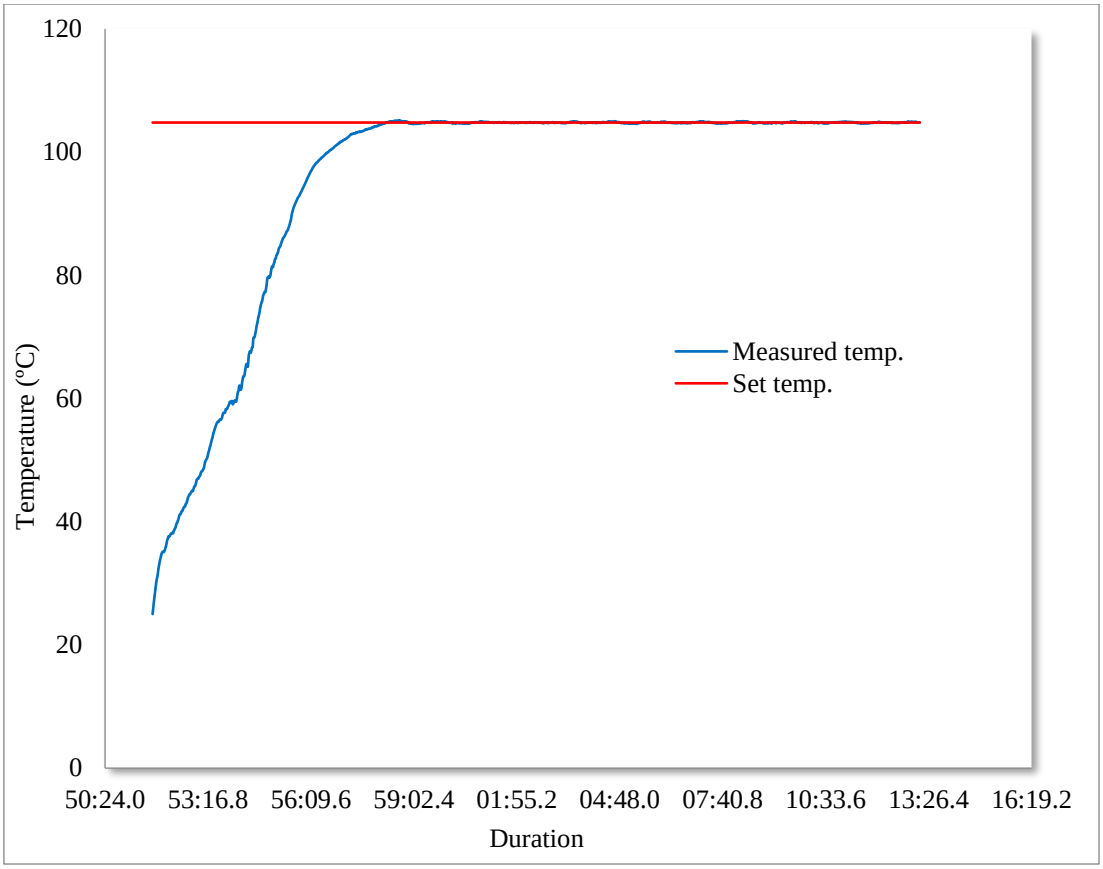

Figure 4.11 Performance of closed loop system

4.3.3.2 Experimental results

A. Bonding results for Mold 2

Upon completion of bonding, the quality of bonded samples was evaluated by observing them under a Nikon microscope. Fig. 4.12 (a) shows a close-up picture of a well bonded Channel 7 chip without any deformation. Channels with higher AR of 1:10, 1:50 and 1:100 were sealed well without any deformation as shown in Figs. 4.12 (b), (c), (d), (f), (g) and (h). For Channel 4 and 8 with lowest AR of 1:200 collapse of the coverslip was observed as shown in Figs. 4.12 (d) and (i), respectively. Bonding was done at different temperatures and optimum conditions were established as given in Table 4.3.

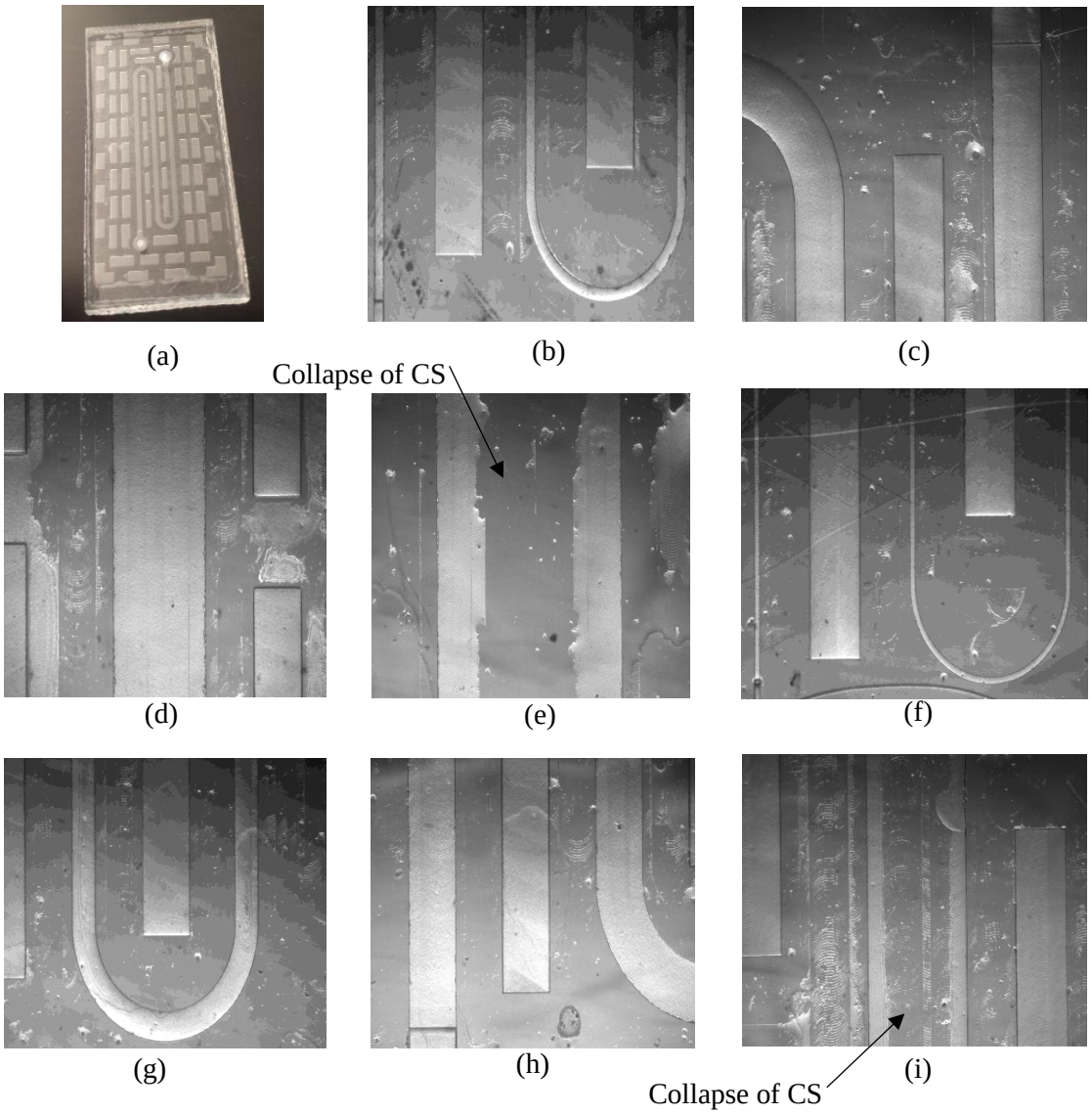

Figure 4.12 (a) Photograph of a bonded Channel 7 chip. Microscopic image of bonded samples using 4x objective lens (b) Channel 1 (c) Channel 2 (d) Channel 3 (e) Channel 4 (f) Channel 5 (g) Channel 6 (h) Channel 7 (i) Channel 8

Table 4.3 Optimum temperature and pressure for all channels using closed loop system

Channel	Bonding temperature (˚C)	Bonding pressure kPa (psi)
Channel 1	104.8±0.15	13.8 – 15.5 (2-2.25)
Channel 2	104.6±0.15	10.3 - 12 (1.5-1.75)
Channel 3	102.6±0.15	1.72 (0.25)
Channel 5	105±0.15	13.8 – 15.5 (2-2.25)
Channel 6	104.6±0.15	10.3 - 12 (1.5-1.75)
Channel 7	103±0.15	3.45 - 5 (0.5-0.75)

B. Leak test

Bonded samples were tested for leaks by sending Rhodamine dye for 15 minutes and observing under a florescence microscope. The microscopic images shown in Figs. 4.13 (a) to (f) confirmed no leakage from the channels. The same flow rates shown in Table 4. 2 were tested for the samples. Channels 4 and 8 were not leak tested since all the samples had collapsed cover slips.

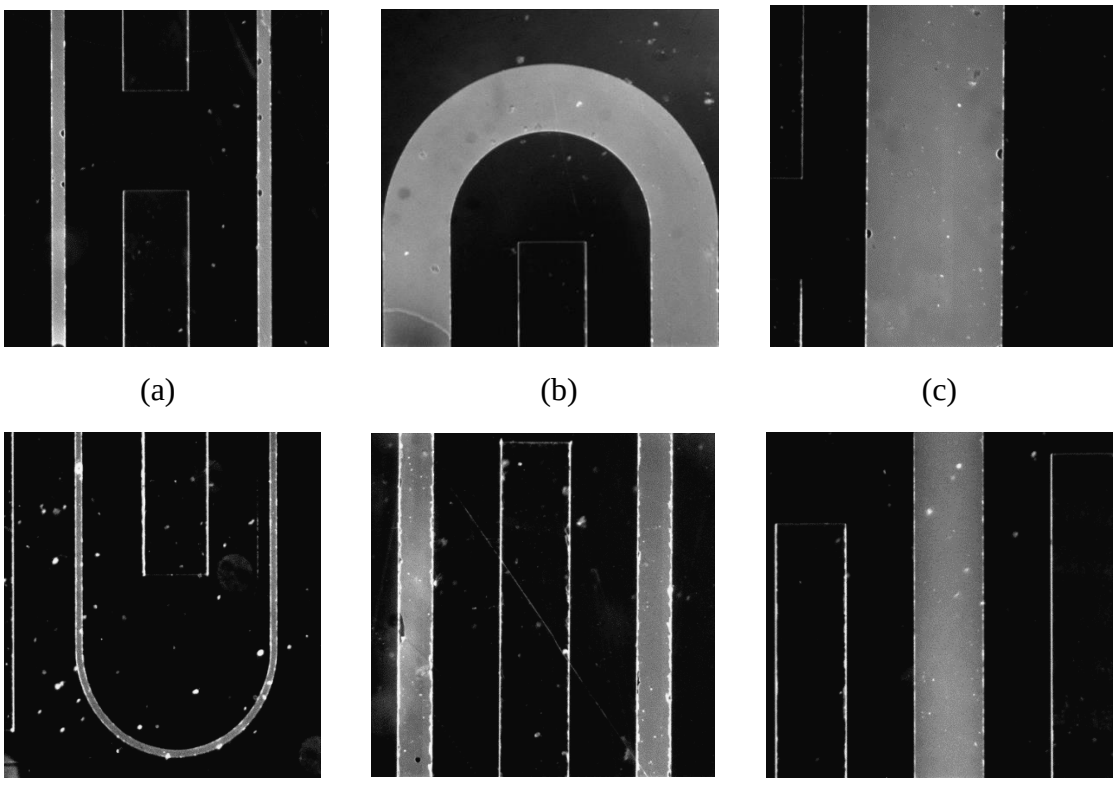

(a) (b) (c)

(d) (e) (f)

Figure 4.13 Florescence images using 2x objective lens for (a) Channel 1 (b) Channel 2 (c) Channel 3 (d) Channel 5 (e) Channel 6 (f) Channel 7

B. Rupture test

Leak tested samples were subjected to a rupture test to evaluate the bond strength. The rupture test was conducted using the apparatus in the Section 4.3.2.3.4. Consolidated data for the mean rupture pressure for different aspect ratios is shown in the Fig. 4.14. It was found that the rupture pressure decreases with the decrease in AR

and was higher for channels with lower depth of 5 µm. Rupture pressure data for each sample tested is included in Appendix D.

Rupture pressures obtained from the open loop and closed loop system were compared and are shown in Fig. 4.15. The rupture pressure behavior was similar for both the systems. The rupture pressure for the samples bonded using the closed loop system was higher compared to that of the open loop system. This may be due to the higher bonding pressure for the same temperature during the bonding process. The error bars in the Fig. 4.15 indicates the 95% confidence interval for the mean rupture pressure calculated using the Student's t distribution with a standard deviation in the range of 55 – 131 kPa. In literature, maximum rupture pressure of 153 kPa has been recorded for PMMA bonded using TFB. [21] Calculations are included in Appendix D. It was revealed that the 95% confidence interval for rupture pressures measured for samples bonded using the closed loop system was smaller compared to open loop system. This indicated that the bond strength of the samples was more consistent and repeatable for closed loop system than the open loop system.

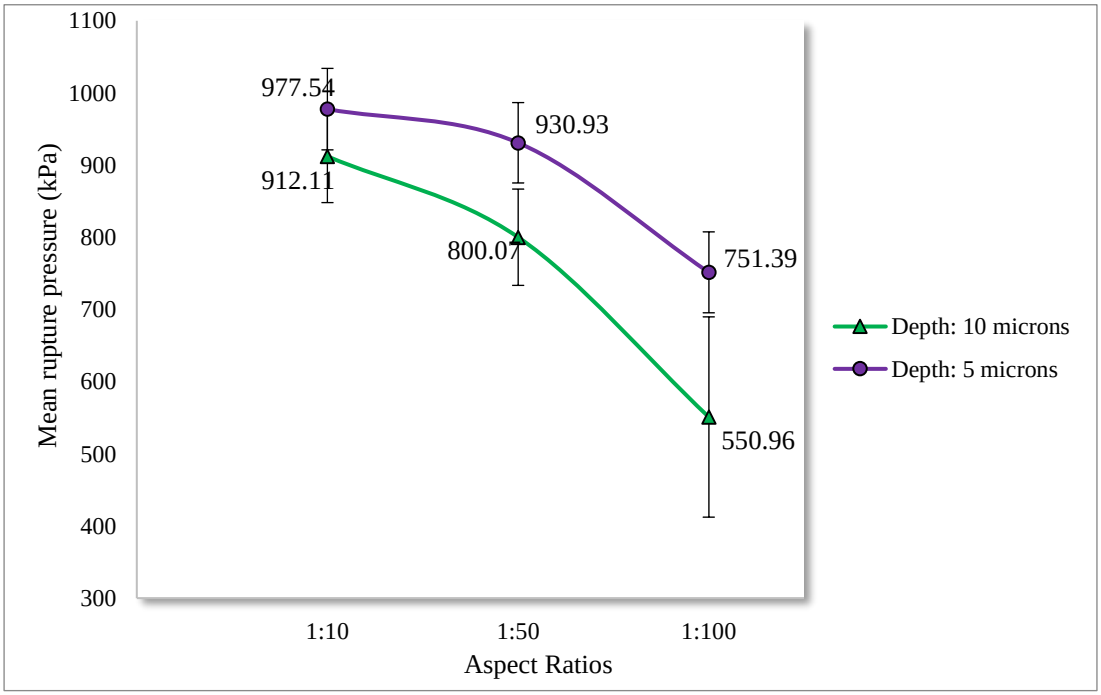

Figure 4.14 Rupture pressure as a function of aspect ratio for closed loop system

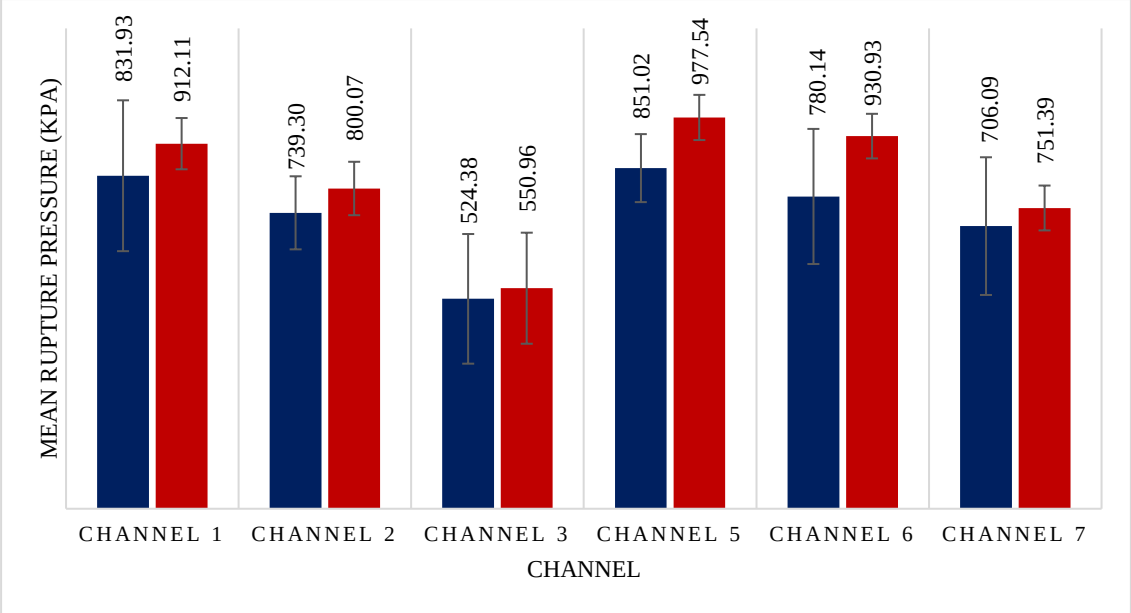

Figure 4.15 Comparison of rupture pressures evaluated for closed loop and open loop system

4.4 Conclusions

Samples of AR 1:10, 1:50 and 1:100 were successfully bonded using an open loop PABP bonding system and optimum temperature and pressure for good bonding were determined. The bonding temperature and pressure decreased for decreasing AR and was in the range of 103-105.5°C. Bonded samples were leak and rupture tested. Maximum rupture pressures of 977 kPa were recorded for Channel 5 with highest AR of 1:10 and depth of 5 µm. Rupture pressures decreased with the decrease in AR and were higher for shallower channels.

A closed loop system for PABP bonding was developed to control the bonding temperature without human intervention. Channels with AR 1:10, 1:50 and 1:100 were sealed without any channel deformation. The optimum bonding temperature were same as that established for open loop system. But the corresponding pressure was higher. Quality of the bonded samples was tested by conduction of leak and rupture tests. Like with the open loop system, rupture pressures decreased with decreasing AR. The rupture pressures obtained for samples bonded using both the systems were compared

and was a 6-20% increase in the rupture pressure for AR of 1:10 and 1:50 and 2-5% increase for AR of 1:100 for samples bonded using the closed loop system. The bonding experiments were more repeatable and bond strength was more consistent than with the open loop system.

CHAPTER 5: CONCLUSIONS AND FUTURE WORK

5.1 Conclusions

A systematic study was done to characterize thermal fusion bonding of PMMA substrates and cover slips using a PABP system with manual control of temperature. PMMA samples with channels of four different aspect ratios 1:10, 1:50, 1:100 and 1:200 were hot embossed using a brass mold insert. The replication error percentage was in the range 0.6 – 14% and was maximum for Channel 5 which had narrowest width of 50 µm and depth of 5 µm and was difficult to achieve both in mold and samples.

Optimum bonding conditions without any channel deformation were determined for the open loop system. It was possible to achieve well bonded samples for AR 1:10, 1:50 and 1:100. Channels with AR of 1:200 had cover slips collapse into the channels and bonding was not possible using this method. The temperature required to achieve good sealing decreased with an decrease in the aspect ratios and was found to be higher for shallower channels. The bonded samples were inspected for leaks using rhodamine dye. A new rupture test experimental apparatus was developed to evaluate the bond strength of sealed chips using compressed nitrogen gas. Rupture tests conducted on the samples revealed that the mean rupture pressure was maximum (851) for Channel 5 with highest AR ratio and shallow depth because of higher bonding temperature. The rupture pressure decreased with the decrease in AR and was least for Channel 3 with largest width and larger depth. Statistical analysis of the mean pressure for all the channels showed that the 95% confidence interval ranged from ±84 – ±188 kPa.

A closed loop system was successfully developed and implemented in LabVIEW to automatically control the bonding temperature, eliminating human intervention and the associated time delay. PMMA samples with same channel design

and AR were bonded using closed loop system. Optimum bonding temperatures remained the same as for the open loop system but the bonding pressure was higher. Good bonding was achieved for channels with AR up to 1:100. Channels with 1:200 AR had collapsed cover slips. It was observed that for 1:100 AR, the bonding result was not consistent for shallower channels compared to the deeper channels. Leak tests ensured good bonding between the substrate and the cover slip and no leaks were detected. Bond strength was determined using the same apparatus. Comparison of bond strength results with that of the open loop system indicated an 8-14% increase in mean rupture pressure for aspect ratios 1:10 and 1:50 and 3-5% increase for 1:100 AR. Statistical analysis revealed less variation of the mean pressure for the closed loop system, which made bonding more consistent and repeatable.

5.2 Future work

This bonding technique has good potential and can be further improved. The current bonding apparatus demonstrated to produce good sealing of PMMA substrates and cover slips. PMMA has a glass transition range of 105-115 °C. In order, to bond PC sheets with higher glass transition temperature of 145°C -148°C, a pressure vessel with a higher temperature range needs to be designed.

Samples of other materials like COC with achievable glass transition temperature can be fabricated and the performance of this bonding technique can be evaluated.

Presently the heat input to the pressure cooker using butane burner is manual and needs to be turned on and off for every bonding experiment. The closed loop system can be completely automated using an electric heater and the heat input can be controlled by a LabVIEW program.

It was found that the PMMA samples with dummy structures around the channels yielded better bonding result with no deformation. A detailed study needs to be done using simulations and experiments to clearly understand the effects of dummy structures on the bonding if any.

The closed loop system was designed to maintain uniform temperature throughout the bonding process and pressure is recorded using a pressure gauge with variation of about 1.7- 2 kPa. The pressure gauge can be replaced with a pressure transducer and the bonding process can be conducted at a required pressure.

REFERENCES

1. Whitesides, George M. "The origins and the future of microfluidics." *Nature* 442, no. 7101 (2006): 368-373.

2. Tsao, Chia-Wen, and Don L. DeVoe. "Bonding of thermoplastic polymer microfluidics." *Microfluidics and Nanofluidics* 6, no. 1 (2009): 1-16.

3. Dimov, Ivan K., Lourdes Basabe-Desmonts, Jose L. Garcia-Cordero, Benjamin M. Ross, Antonio J. Ricco, and Luke P. Lee. "Stand-alone self-powered integrated microfluidic blood analysis system (SIMBAS)." *Lab on a Chip* 11, no. 5 (2011): 845-850.

4. Park, Taehyun, In-Hyouk Song, Daniel S. Park, Byoung Hee You, and Michael C. Murphy. "Thermoplastic fusion bonding using a pressure-assisted boiling point control system." *Lab on a Chip* 12, no. 16 (2012): 2799-2802.

5. Kentsch, Jörg, Stefanie Breisch, and Martin Stelzle. "Low temperature adhesion bonding for BioMEMS." *Journal of Micromechanics and Microengineering* 16, no. 4 (2006): 802.

6. Reyes, Darwin R., Dimitri Iossifidis, Pierre-Alain Auroux, and Andreas Manz. "Micro total analysis systems. 1. Introduction, theory, and technology." *Analytical Chemistry* 74, no. 12 (2002): 2623-2636.

7. Dittrich, Petra S., Kaoru Tachikawa, and Andreas Manz. "Micro total analysis systems. Latest advancements and trends." *Analytical Chemistry* 78, no. 12 (2006): 3887-3908.

8. Harrison, D. Jed, Andreas Manz, Zhonghui Fan, Hans Luedi, and H. Michael Widmer. "Capillary electrophoresis and sample injection systems integrated on a planar glass chip." *Analytical Chemistry* 64, no. 17 (1992): 1926-1932.

9. Harrison, D. Jed, Karl Fluri, Kurt Seiler, Zhonghui Fan, Carlo S. Effenhauser, and Andreas Manz. "Micromachining a miniaturized capillary electrophoresis-based chemical analysis system on a chip." *Science* 261 (1993): 895-895.

10. Becker, Holger, and Laurie E. Locascio. "Polymer microfluidic devices." *Talanta* 56, no. 2 (2002): 267-287.

11. Becker, Holger, and Claudia Gärtner. "Polymer microfabrication technologies for microfluidic systems." *Analytical and Bioanalytical Chemistry* 390, no. 1 (2008): 89-111.

12. Dang, F., S. Shinohara, O. Tabata, Y. Yamaoka, M. Kurokawa, Y. Shinohara, M. Ishikawa, and Y. Baba. "Replica multichannel polymer chips with a network of sacrificial channels sealed by adhesive printing method." *Lab on a Chip* 5, no. 4 (2005): 472-478.

13. Chow, Winnie Wing Yin, Kin Fong Lei, Guangyi Shi, Wen Jung Li, and Qiang Huang. "Microfluidic channel fabrication by PDMS-interface bonding." *Smart materials and structures* 15, no. 1 (2005): S112.

14. Fahrenberg, J., W. Bier, D. Maas, W. Menz, R. Ruprecht, and W. K. Schomburg. "A microvalve system fabricated by thermoplastic molding." *Journal of Micromechanics and Microengineering* 5, no. 2 (1995): 169.

15. Truckenmüller, Roman, Ralf Ahrens, Yue Cheng, Günther Fischer, and Volker Saile. "An ultrasonic welding based process for building up a new class of inert fluidic microsensors and-actuators from polymers." *Sensors and Actuators A: Physical* 132, no. 1 (2006): 385-392.

16. Kim, Joohan, and Xianfan Xu. "Excimer laser fabrication of polymer microfluidic devices." *Journal of Laser Applications* 15, no. 4 (2003): 255-260.

17. Martynova, Larisa, Laurie E. Locascio, Michael Gaitan, Gary W. Kramer, Richard G. Christensen, and William A. MacCrehan. "Fabrication of plastic microfluid channels by imprinting methods." *Analytical chemistry* 69, no. 23 (1997): 4783-4789.

18. Ford, Sean M., Bill Kar, Scott Mcwhorter, Jack Davies, Steven A. Soper, Mike Klopf, Gina Calderon, and Volker Saile. "Microcapillary electrophoresis devices fabricated using polymeric substrates and X-ray lithography." *Journal of Microcolumn Separations* 10, no. 5 (1998): 413-422.

19. Chen, Zhifeng, Yunhua Gao, Jinming Lin, Rongguo Su, and Yu Xie. "Vacuum-assisted thermal bonding of plastic capillary electrophoresis microchip imprinted with stainless steel template." *Journal of Chromatography A* 1038, no. 1 (2004): 239-245.

20. Park, Daniel Sang-Won, Pin-Chuan Chen, Byoung Hee You, Namwon Kim, Taehyun Park, Tae Yoon Lee, Proyag Datta et al. "Titer plate formatted continuous flow thermal reactors for high throughput applications: fabrication and testing." *Journal of Micromechanics and Microengineering* 20, no. 5 (2010): 055003.

21. Kelly, Ryan T., and Adam T. Woolley. "Thermal bonding of polymeric capillary electrophoresis microdevices in water." *Analytical Chemistry* 75, no. 8 (2003): 1941-1945.

22. Park, T. “Small footprint high flowrate microdevice for rare target cell capture (PhD Dissertation).” Louisiana State University (2011).

23. Worgull, M., M. Heckele, and W. K. Schomburg. "Large-scale hot embossing." *Microsystem technologies* 12, no. 1-2 (2005): 110-115.

24. D.C.Montgomery and G.C.Runger. “Applied Statistics and Probability for Engineers.” *John Wiley and Sons, Inc* (2002).

25. Shadpour, Hamed, Harrison Musyimi, Jifeng Chen, and Steven A. Soper. "Physiochemical properties of various polymer substrates and their effects on microchip electrophoresis performance." *Journal of Chromatography A1111*, no. 2 (2006): 238-251.

26. B. Linder. “Thermodynamics and Introductory Statistical Mechanics.” Wiley-Interscience (2004).

27. Park, Taehyun, Thomas J. Zimmerman, Daniel Park, Brooks Lowrey, and Michael C. Murphy. "Thermoplastic fusion bonding of polymer-based micro devices using a pressure cooker." In ASME 2009 International Mechanical Engineering Congress and Exposition, pp. 295-300. American Society of Mechanical Engineers, 2009.

APPENDIX A: PROPERTIES OF PMMA MC GRADE SHEET AS GIVEN BY MANUFACTURER

TYPICAL STANDARD PROPERTIES			
PROPERTIES	**TEST METHOD**	**UNIT**	**VALUE**
PHYSICAL			
Nominal thickness for data unless otherwise noted		in	0.236
Specific Gravity	ASTM D-792	--	1.19
Rockwell Hardness	ASTM D-785	M Scale	90
Poisson's Ratio	N/A	--	0.35
OPTICAL			
Refractive Index (ND @73ºF)	ASTM D-542	--	1.49
Luminous Transmittance[1]	ASTM D-1003	%	92
Haze[1]	ASTM D-1003	%	< 2.0
MECHANICAL			
Tensile Strength, maximum	ASTM D-638	psi	10,200
Tensile Strength, yield	ASTM D-638	psi	10,200
Tensile Elongation	ASTM D-638	%	4.5
Tensile Modulus of Elasticity	ASTM D-638	psi	450,000
Flexural Strength, maximum	ASTM D-790	psi	15,000
Flexural Modulus of Elasticity	ASTM D-790	psi	450,000
Notched Izod Impact @73ºF (23ºC)	ASTM D-256	ft-lb/in	0.3
Un-notched Charpy @73ºF (23ºC)	ASTM D-256	ft-lb/0.5"x1" section	0.7
THERMAL			
Deflection Temperature under Flexural Load @264 psi - unannealed[1]	ASTM D-648	ºF	200
Coefficient of Thermal Expansion @60ºF	ASTM E-831	in/ in/ ºF x 10^{-5}	3.6
Coefficient of Thermal Conductivity	ASTM C-177	BTU / (hr)(ft^2)(ºF /in)	1.3
U-value (summer gain, winter loss)	N/A	BTU / (hr)(ft^2)(ºF /in)	0.89, 0.96
Specific Heat Capacity @77ºF	N/A	BTU / (lb ºF)	0.35
Maximum Recommended Continuous Service Temperature	N/A	ºF	170 - 190
Recommended Thermoforming Temperature	N/A	ºF	275 - 350
CRAZE RESISTANCE			
Constant Stress Craze Resistance, IPA[5]	Modified ARTC Method - Mil P-6997	psi	1,300
Constant Stress Craze Resistance, Aromatic/Alcohol blend[5]	Modified ARTC Method - Mil P-6997	psi	1,200
FLAMMABILITY & SPECIFICATION COMPLIANCE			
Horizontal Burn Rate[1,2]	ASTM D-635	in / min	1.1
Smoke Density	ASTM D-2843	%	1.2
Self Ignition Temperature	ASTM D-1929	ºF	860
Surface Burning Characteristics - Flame Spread	CAN/ULC-S102.2-07 File R16788	--	100 (0.125" - 0.25")
Surface Burning Characteristics - Smoke Developed	CAN/ULC-S102.2-07 File R16788	--	> 500 (0.125" - 0.25")
Plastics Component - QMFZ2.E39437 - Flammability Classification	UL 94	--	94 HB (≥0.060")
Plastics Component - QMFZ2.E39437 - Outdoor Suitability	UL 746C	--	f1 (≥0.060" Colorless) f2 (≥0.060" ALL)
International Building Code	IBC 2606.4	--	CC2 (0.080" - 0.354")
American National Standard for Safety Glazing	ANSI Z97.1	--	PASS (≥0.080")
FMVSS 205 - Federal Motor Vehicles Safety Glazing	ANSI Z26.1	--	AS-5, AS-6, AS-7
Standard Specification for PMMA Acrylic Plastic Sheet	ASTM D-4802	--	Catergory B-1, Finish 1

APPENDIX B: BRASS MOLD DESIGN AND CONSOLIDATED DATA OF HEIGHTS OF THE CHANNELS

B.1 Machining of brass disc for mold insert

A brass disc of 120.6 mm (4.75”) diameter was machined from 12”x24” brass alloy 353 plate of thickness 6.35 mm (0.25”) (8948K7, McMaster Carr,IL, USA) using conventional machining processes. The machine drawings for the top side and bottom sides are shown in Fig.B.1 and Fig. B.2

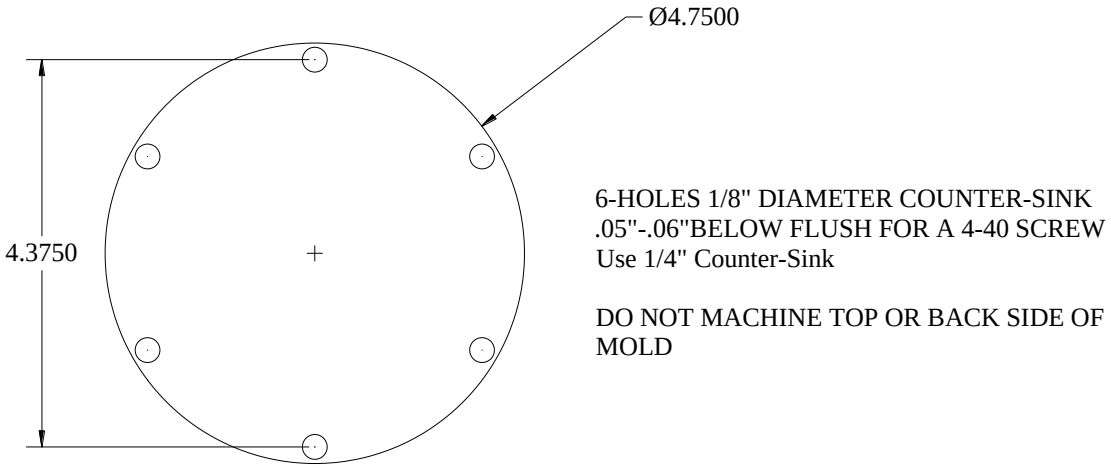

Figure B.1 AutoCAD drawing for top side of brass disc

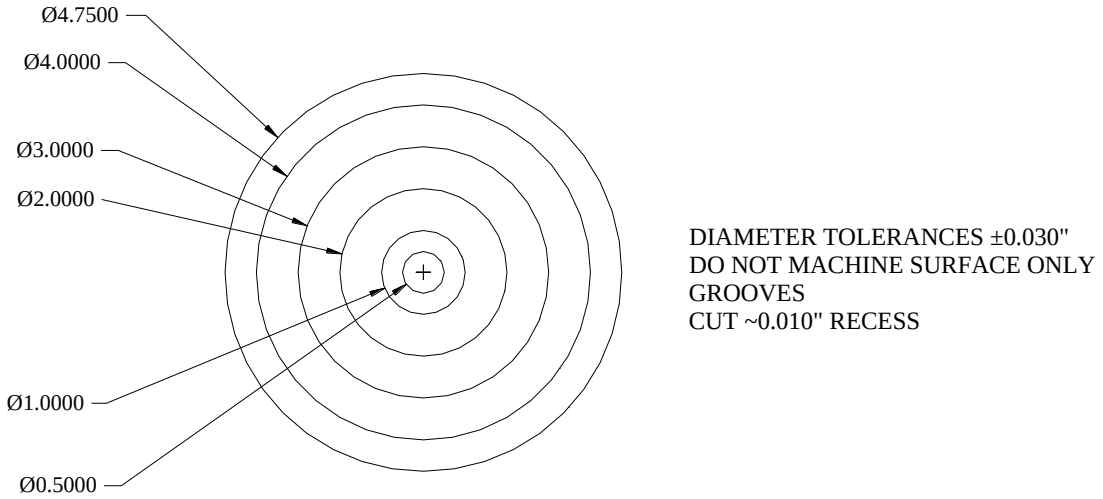

Figure B.2 AutoCAD drawing for bottom side of brass disc

B.2 AutoCAD drawing for micromilling of mold insert

AutoCAD designs along with the dimensions for the micromilling of mold inserts Version 1 and 2 are shown in Fig. B.3 and B.4 respectively. All the structures were drawn using the **polyline** command in AutoCAD to ensure that all polygons were closed. For easy identification of structures, different colors were used for different layers.

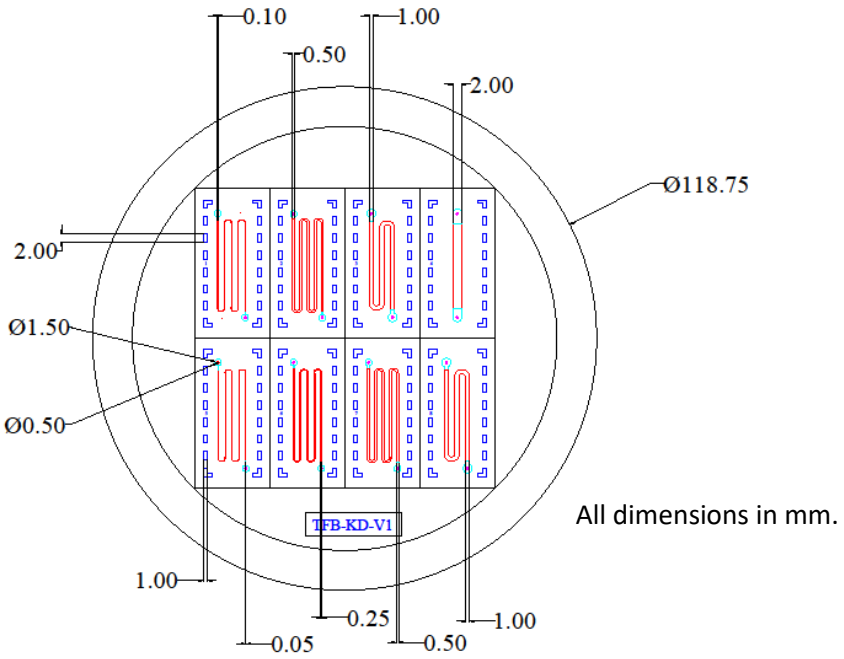

Figure B.3 AutoCAD design of mold Version 1

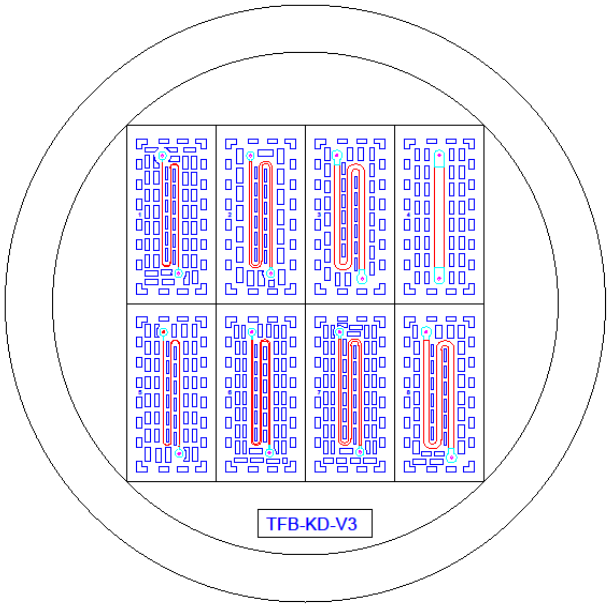

Figure B.4 AutoCAD drawing of mold Version 2 with dummy structures

B.3 Verification of the heights of channels using an optical profilometer

The brass mold was scanned using an optical profilometer and cross sections were taken at 4 different locations along the length of the channel to measure the heights of all the channels. Heights of all the channels and their mean with 95% confidence using Student's t distribution is tabulated below.

Table B.1 Height measured and statistical analysis for mold version 2

	1	2	3	4	5	6	7	8
	9.22	9.4	9.25	8.4	4.8	4.5	4.03	4.14
	10.6	10.1	9.46	8.89	3.8	4.47	4.13	4.47
	9.73	9.45	9.25	8.68	3.6	4.3	3.94	4.04
	8.73	9.69	9.75	8.81	4	4.69	4.03	4.25
	8.25	9.68	9.97		3.4	4.1	4.1	4.58
	8.84	9.7	9.95		4.2	4.4	3.76	4.37
	8.97	9.78	10.1		4.3	4.38	4.09	4.68
	8.87	10.4	9.78		4.2	4.86	4.55	4.69
	8.52	10.4	10.1		3.9	4.8	4.1	4.74
	8.74	9.24	9.95		5	4.28	4.05	4.35
	9.28	10	10.2		4.2	4.7	4.33	4.54
	10.3	10.5	10		4	4.8	3.99	4.59
Mean	9.17	9.86	9.81	8.70	4.12	4.52	4.09	4.45
Std. deviation	0.71	0.42	0.33	0.21	0.45	0.24	0.20	0.23
$t_{95,11}$	2.201	2.201	2.201	3.182	2.201	2.201	2.201	2.201
95% interval	0.47	0.28	0.22	0.20	0.29	0.15	0.12	0.14

APPENDIX C: CONSOLIDATED DATA OF DEPTHS OF PMMA SAMPLES OF ALL CHANNELS

C.1 15 samples for each channel were scanned and mean depth with 95% confidence interval using Student's t distribution were calculated.

Table C.1 Measured depths of 15 samples for Channel 1 and statistical analysis for mean depth

Sample 1	Sample 2	Sample 3	Sample 4	Sample 5	Sample 6	Sample 7	Sample 8	Sample 9	Sample 10	Sample 11	Sample 12	Sample 13	Sample 14	Sample 15
9.39	8.36	7.98	8.14	9.49	9.29	9.82	8.59	8.35	9.11	8.39	8.64	8.7	8.64	8.68
8.35	8.14	8.22	8.95	9.23	9.53	8.23	8.41	8.8	8.75	8.64	8.85	8.79	8.58	8.63
8.9	10.7	9.3	8.07	9.95	9.86	10.5	9.99	10.5	8.14	8.41	8.41	8.25	8.76	8.4
9.16	8.14	8.33	8.46	8.02	8.52	9.43	9.25	8.2	9.92	8.47	8.61	8.51	8.52	8.57
8.28	8.25	8.8	8.96	8.79	8.69	8.85	8.14	8.3	8.45	8.53	8.53	8.23	8.23	8.36
8.59	8.28	7.92	8.19	9.41	9.83	9.17	8.63	8.34	9.72	8.12	8.53	8.51	8.79	8.76
8.85	8.73	8.26	8.73	8.52	8.42	10.2	9.08	8.78	8.62	8.67	8.73	8.89	8.58	8.69
9.23	7.7	8.94	8.67	7.95	8.35	8.66	8.51	8.87	8.51	8.48	8.33	8.48	8.46	8.85
8.76	8.86	9.23	8.09	8.58	9.06	8.66	8.42	8.12	8.8	8.14	8.3	8.24	8.7	8.23
8.91	8.34	8.66	8.51	7.98	8.51	9.19	9.2	9.01	8.51	8.4	8.55	8.52	9.03	8.51
8.91	8.39	8.56	8.67	8.51	7.95	8.73	8.83	8.26	8.74	8.68	8.7	8.51	8.24	8.63
8.55	10.1	7.45	7.78	7.8	7.58	9.05	8.48	9.2	7.79	8.7	8.63	8.66	8.24	8.91
8.8	8.7	8.5	8.4	8.7	8.8	9.2	8.8	8.7	8.8	8.5	8.6	8.5	8.6	8.6
Mean	8.68	Std. dev	0.19	N	15	$t_{95,14}$	2.145							
95% Interval	0.11	Upper limit	8.79	Lower limit	8.57									

C.2 CHANNEL 2

Table C.2 Measured depths of 15 samples for Channel 2 and statistical analysis for mean depth

Sample 1	Sample 2	Sample 3	Sample 4	Sample 5	Sample 6	Sample 7	Sample 8	Sample 9	Sample 10	Sample 11	Sample 12	Sample 13	Sample 14	Sample 15
9.72	9.86	9.36	10.8	9.45	9.49	9.58	9.61	9.51	9.2	9.57	9.53	9.72	9.8	9.72
8.89	9.6	9.61	8.79	9.14	9.41	9.33	9.14	10.4	9.92	9.34	9.01	9.34	9.46	9.3
9.11	9.25	9.01	8.87	9.25	9.11	9.28	9.18	9.4	8.76	9.4	9.02	9.25	9.62	9.3
9.35	9.28	8.94	8.92	8.97	8.96	9.27	9.2	8.95	8.73	9.27	9.01	9.2	9.42	9.14
9.35	9.23	9.51	9.16	8.95	9.66	9.24	9.42	9.78	9.39	9.34	9.19	9.24	9.28	9.49
9.83	10	9.41	9.09	9.69	9.4	9.61	9.6	10.3	9.74	9.58	9.5	9.75	9.83	9.46
9.88	9.61	9.64	9.31	9.13	9.46	9.75	9.57	8.51	9.28	10	9.63	9.61	9.55	9.66
9.23	9.22	9.34	9.51	9.07	9.31	9.24	9.46	9.35	9.36	9.09	9.09	9.38	9.36	9.38
9.58	9.69	9.14	9.25	9.36	9.29	9.51	9.34	9.66	8.73	9.22	9.08	9.29	9.29	9.33
9.63	9.42	9.34	9.28	9.17	9.75	9.39	9.92	8.95	9.11	9.63	9.38	9.61	9.66	9.62
9.22	9.31	9.2	9.52	9.11	9.33	9.33	9.44	9.18	9.42	9.38	9.18	9.13	9.6	9.2
9.61	9.52	9.41	9.28	9.47	9.22	9.35	9.58	9.42	9.24	9.29	9.49	9.68	9.46	9.77
9.5	9.5	9.3	9.3	9.2	9.4	9.4	9.5	9.5	9.2	9.4	9.3	9.4	9.5	9.4

Mean	9.38	Std. dev	0.09	N	15	$t_{95,14}$	2.145
95% Interval	0.05	Upper limit	9.43	Lower limit	9.33		

C.3 CHANNEL 3

Table C.3 Measured depths of 15 samples for Channel 3 and statistical analysis for mean depth

Sample 1	Sample 2	Sample 3	Sample 4	Sample 5	Sample 6	Sample 7	Sample 8	Sample 9	Sample 10	Sample 11	Sample 12	Sample 13	Sample 14	Sample 15
11.5	11	8.94	10.1	9.96	9.84	10.2	9.91	9.31	10.1	10	10.1	9.92	9.69	9.72
9.78	10	10.4	9.97	9.72	9.86	9.69	10.2	10.4	10.4	9.39	9.62	9.81	9.74	9.61
9.88	10.9	10.2	9.9	9.58	9.7	10.2	9.85	9.56	9.67	10.1	10.2	9.81	9.69	9.81
9.67	10.6	9.85	9.67	10.2	10.2	9.45	10	9.46	10	10.2	9.5	9.5	10.1	10.1
9.03	9.41	9.99	9.92	9.84	9.74	9.95	10	10.2	9.83	9.55	9.86	9.86	9.73	9.5
9.58	10.8	9.53	9.73	9.68	9.95	9.62	9.79	9.38	9.62	9.9	9.56	9.56	9.85	9.69
9.73	10.4	9.77	10.2	10.6	9.69	9.83	9.5	8.63	9.3	9.68	9.77	10.3	9.51	9.57
9.83	10.3	9.91	9.67	9.78	9.94	9.74	10.2	9.9	11.2	9.88	9.66	9.6	9.97	9.72
10.2	10.2	9.45	10.4	9.83	9.83	10.2	9.63	9.11	9.5	9.89	10	10.3	9.72	9.58
10	10.3	9.8	9.75	10.6	9.68	9.58	9.63	8.78	9.2	10.2	9.74	9.89	9.85	9.97
9.56	10.5	10.1	10	10	9.95	10.1	10.2	10.1	10.4	9.73	10	9.66	9.84	9.69
10.1	10.3	9.12	9.61	9.16	9.8	9.63	10.1	9.3	10.4	10.1	9.6	10.1	9.92	9.88
9.9	10.4	9.8	9.9	9.9	9.8	9.8	9.9	9.5	10.0	9.9	9.8	9.9	9.8	9.7

Mean	9.87	Std. dev	0.18	N	15	$t_{95,14}$	2.145
95% Interval	0.10	Upper limit	9.97	Lower limit	9.77		

C.4 CHANNEL 4

Table C.4 Measured depths of 15 samples for Channel 4 and statistical analysis for mean depth

Sample 1	Sample 2	Sample 3	Sample 4	Sample 5	Sample 6	Sample 7	Sample 8	Sample 9	Sample 10	Sample 11	Sample 12	Sample 13	Sample 14	Sample 15
9.72	9.57	9.17	9.89	9	8.95	8.92	9.19	9.07	9.36	8.84	9.18	9.02	9.2	8.87
10.1	9.05	9.19	9.07	8.73	8.96	8.62	9.18	9.36	9.19	8.8	9	9.01	9.39	8.94
8.18	9.86	9.9	9.07	8.61	8.98	8.61	9.03	9.3	9.2	8.91	9.06	9.22	9.03	9.24
9.38	9.91	8.9	9.27	8.41	8.79	8.79	8.95	9.13	8.9	8.53	8.69	8.95	9.09	8.76
9.3	9.6	9.3	9.3	8.7	8.9	8.7	9.1	9.2	9.2	8.8	9.0	9.1	9.2	9.0

Mean	9.09	Std. dev	0.25	N	15	$t_{95,14}$	2.145
95% Interval	0.14	Upper limit	9.24	Lower limit	8.96		

C.5 CHANNEL 5

Table C.5 Measured depths of 15 samples for Channel 5 and statistical analysis for mean depth

Sample 1	Sample 2	Sample 3	Sample 4	Sample 5	Sample 6	Sample 7	Sample 8	Sample 9	Sample 10	Sample 11	Sample 12	Sample 13	Sample 14	Sample 15
4	3.8	3.48	3	3.32	3.5	3.36	5.09	3.2	3.23	3.63	3.43	3.67	3.36	3.75
4.2	4.1	3.6	3.8	3.59	3.17	5.05	4.03	3.44	3.74	3.48	3.5	3.56	3.21	3.61
4	3.7	3.86	4.1	2.95	3.2	4.27	3.8	3.33	3.64	3.93	3.7	3.48	3.32	3.47
3	3.9	3.75	3	2.89	3.36	3.09	3.09	3.1	3.06	3.27	3.9	3.4	3.17	3.8
3.2	4.1	3.2	3.1	3.33	3.2	3.2	4	3.2	3.4	3.2	3.7	3.2	4.2	3.3
3.3	3.9	3.47	3.6	3.86	3.4	3.7	3.7	3.3	3.21	3.15	3.4	3.2	4.63	3.4
3.7	3.3	3.41	3.8	2.72	4.6	2.86	4.08	3.08	3.39	3.56	3.55	3.67	3.13	3.87
3.6	3	3.41	4.4	2.54	3.9	2.84	4.59	3.17	4	4.1	3.1	3.36	3.14	3.6
4	4.2	3.41	3.4	2.88	3.8	2.56	3.44	3.31	3.32	4.2	3.6	3.2	3.36	3.5
3.2	3	3.53	3.3	2.95	4.3	4.24	3	3.5	3.03	3.6	3.33	3.5	3.2	3.2
3.3	4.2	3.53	3.2	3.55	4.2	3.87	3.2	4	3.4	3.4	3.34	3.4	3.4	3.31
3.3	5	3.53	3	3.83	4.4	4.61	4	3.16	3.2	3.3	4.32	3.5	3.1	3.59
3.6	3.9	3.5	3.5	3.2	3.8	3.6	3.8	3.3	3.4	3.6	3.6	3.4	3.4	3.5
Mean	3.54	Std. dev	0.19	N	15	$t_{95,14}$	2.145							
95% Interval	0.10	Upper limit	3.64	Lower limit	3.44									

C.6 CHANNEL 6

Table C.6 Measured depths of 15 samples for Channel 6 and statistical analysis for mean depth

Sample 1	Sample 2	Sample 3	Sample 4	Sample 5	Sample 6	Sample 7	Sample 8	Sample 9	Sample 10	Sample 11	Sample 12	Sample 13	Sample 14	Sample 15
4.14	4.24	3.98	4.72	4.33	4.86	4.05	3.85	4.03	4.03	4.31	4.26	4.09	4.43	4.08
4.39	4.24	4.35	4.5	4.52	4.35	4.02	4.15	4.41	4.43	4.17	3.99	4.26	4.28	4.04
4.49	4.17	4	3.83	4.05	3.99	4.04	4.05	3.99	4.16	4.19	4.15	4.27	4.24	4.19
4.72	4.22	4.38	4.69	4.71	5.49	4.61	4.37	4.5	4.3	4.5	4.59	4.74	4.57	4.47
4.02	5.37	4.86	4.54	4.17	4.54	4.07	4.21	3.94	4.66	4.31	4.16	3.89	4.15	4.47
4.28	3.76	4.16	3.94	3.97	3.67	3.86	3.85	4.17	3.97	3.85	4.07	4.15	4.03	3.87
4.59	4.14	4.03	4.37	4.58	4.36	4.59	4.25	4.1	4.22	4.25	4.46	4.22	4.69	4.13
4.17	4.44	4.94	4.65	4.5	4.72	4.3	4.22	4.49	4.55	4.2	4.07	4.14	4.54	4.09
4.17	4.33	3.59	4.08	4.2	4.88	4.21	4.13	4.37	4.03	3.93	4.13	4.2	4.13	4.03
3.94	4.5	3.69	4.55	4.15	4.16	4.66	4.52	3.94	4.19	4.03	4.42	4.1	4.53	4.5
4.16	3.49	4.47	4.75	4.22	4.35	4.22	4.1	4.42	4.37	4.1	4.33	3.86	4.11	4.61
4.74	3.71	3.89	3.97	4.05	3.93	3.99	3.82	3.97	3.66	4.15	3.83	4.46	3.8	3.98
4.3	4.2	4.2	4.4	4.3	4.4	4.2	4.1	4.2	4.2	4.2	4.2	4.2	4.3	4.2
Mean	4.25	Std. dev	0.08	N	15	$t_{95,14}$	2.145							
95% Interval	0.05	Upper limit	4.30	Lower limit	4.20									

C.7 CHANNEL 7

Table C.7 Measured depths of 15 samples for Channel 7 and statistical analysis for mean depth

Sample 1	Sample 2	Sample 3	Sample 4	Sample 5	Sample 6	Sample 7	Sample 8	Sample 9	Sample 10	Sample 11	Sample 12	Sample 13	Sample 14	Sample 15
4.15	4.17	3.89	4.15	4.09	4.15	4.1	3.96	3.98	4.11	4.03	4.43	4.47	4.1	4.19
3.94	4.37	4.41	4.21	3.94	4.19	4.22	4.43	4.71	4.42	4.17	3.94	4.27	4.35	4.05
4.19	3.66	3.77	3.81	3.86	3.91	4.14	3.88	3.74	3.83	4.1	4.04	4.07	4.03	3.82
4.03	4.02	4.1	4.17	4.2	4.14	3.89	4.11	3.92	3.88	4.19	4.75	4.38	3.99	3.99
4.05	4.52	4.83	4.37	4.32	4.3	4.37	4.27	4.66	4.52	4.26	4.31	4.25	4.49	4.49
4.39	4	4.32	4.36	4.22	3.96	4.05	4.35	3.85	3.93	4.32	4.27	4.36	4.3	4.3
4.21	4.25	4.3	4.27	4.48	4.3	4.3	4.33	3.93	4.19	4.31	4.47	4.37	4.14	4.47
3.91	3.98	4.15	4.3	4.05	4.43	4.44	4.37	4.49	4.17	4.35	4.36	4.26	4.11	4.22
4.28	3.94	3.6	3.71	3.76	4.35	4.22	4.15	3.64	3.48	4.27	4.24	3.98	4.2	4.2
4.25	4.44	4.41	4.27	4.65	4.2	4.32	4.6	3.7	4.07	4.3	4.47	4.14	4.37	4.2
3.94	3.99	3.93	3.94	4.42	4.14	3.88	4.15	4.16	4.7	4.46	3.89	4.24	4.38	3.92
4.25	4.16	4.04	4.36	3.94	4.43	4.39	4.24	4.3	3.92	4.2	4.33	4.48	3.99	4.42
4.1	4.1	4.1	4.2	4.2	4.2	4.2	4.2	4.1	4.1	4.2	4.3	4.3	4.2	4.2
Mean	4.18	Std. dev	0.06	N	15	$t_{95,14}$	2.145							
95% Interval	0.03	Upper limit	4.19	Lower limit	4.13									

C.8 CHANNEL 8

Table C.8 Measured depths of 15 samples for Channel 8 and statistical analysis for mean depth

Sample 1	Sample 2	Sample 3	Sample 4	Sample 5	Sample 6	Sample 7	Sample 8	Sample 9	Sample 10	Sample 11	Sample 12	Sample 13	Sample 14	Sample 15
4.96	5	4.72	4.9	5.11	5.1	5.64	4.2	4.55	4.07	4.75	4.5	4.63	4.6	4.59
4.02	4	5.16	5.36	4.43	5.05	4.81	4.6	5.27	5.85	4.69	4.83	4.5	4.48	5.11
4.66	5.5	3.93	4.35	6.63	6.87	5.8	4.92	3.98	4.17	4.75	4.27	4.63	4.74	4.63
5.24	5.68	4.27	4.71	5.6	5.46	4.5	5.31	5.08	4.2	4.72	4.65	5.02	4.53	4.82
4.47	5.37	5.35	5.25	4.91	5.33	5.2	5.8	6.14	5.8	4.25	4.6	4.58	4.69	4.59
4.8	6	4.11	4.91	7.08	4.24	6	5.97	4.63	4.75	4.97	4.91	4.92	4.85	5.22
5.11	4.2	4.17	4.42	5.97	6.01	5	5.01	4.5	4.04	4.65	4.74	4.46	4.87	4.79
4.39	5	5.73	5.14	4.76	4.77	4.94	6.46	5.79	5.82	4.66	4.7	4.61	4.87	4.24
4.87	5.2	3.86	4.41	5.64	5.27	6.5	4.08	4.46	4.26	4.54	4.48	4.68	4.61	4.63
4.86	5.4	4.48	4.43	5.58	5.69	4.5	5.44	3.66	4.11	4.63	4.66	5.04	4.75	4.91
4.48	4.8	5.01	5.22	4.65	4.86	5.31	5.5	5.46	5.73	4.47	4.85	4.37	4.38	4.49
5.09	5.5	4.15	4.21	5.05	6.51	6	5	4.25	4.53	4.8	4.66	4.88	4.88	4.87
4.7	5.1	4.6	4.8	5.5	5.4	5.4	5.2	4.8	4.8	4.7	4.7	4.7	4.7	4.7
Mean	4.92	Std. dev	0.30	N	15	$t_{95,14}$	2.145							
95% Interval	0.17	Upper limit	5.09	Lower limit	4.750									

APPENDIX D: COMPLETE DESCRIPTION OF RUPTURE TEST SET UP

D.1 Experimental apparatus

All of the components of the rupture test set up is shown in the Fig. D.1. More details about the components and vendors are listed in Table D.1

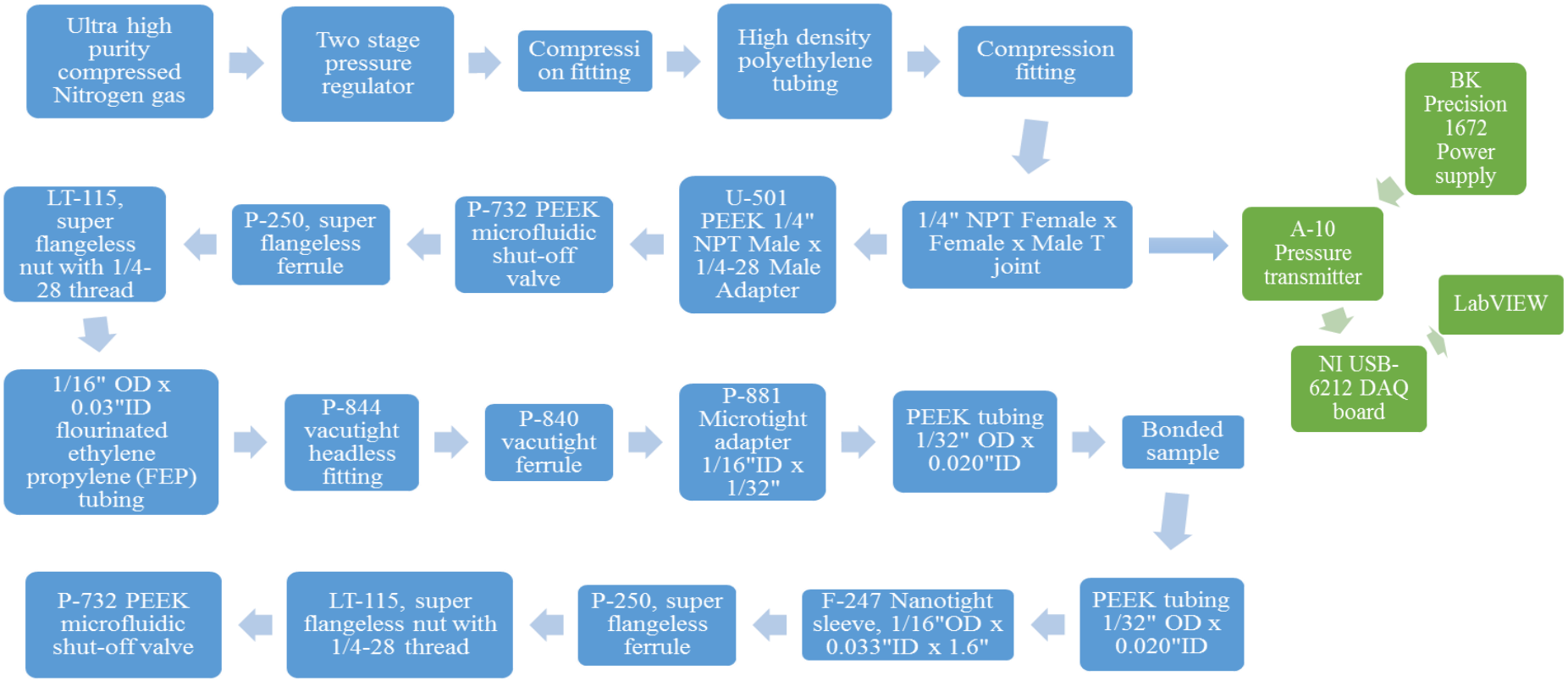

Figure D.1 Illustration of all the components of apparatus in order.

Table D.1 Parts list for rupture test set up

Part name and number	Quantity	Company	Location
Compressed Nitrogen gas	1	Airgas	PA, USA
¼” NPT Female x Female x Male T joint P/N- 9171k32	1	McMaster Carr	IL, USA
PEEK 1/4" NPT Male x 1/4-28 Male Adapter P/N-U501	1	IDEX Corporation	IL, USA
PEEK microfluidic shut-off valve P/N – P-732	2	IDEX Corporation	IL, USA
Super flangeless ferrule P/N – P-250	2	IDEX Corporation	IL, USA
Super flangeless nut with ¼-28 thread P/N – LT-115	2	IDEX Corporation	IL, USA
1/16” OD x 0.03”ID FEP tubing	1	IDEX Corporation	IL, USA
Vacutight headless fitting P/N – P-844	1	IDEX Corporation	IL, USA
Vacutight ferrule P/N- P-840	1	IDEX Corporation	IL, USA
Microtight adapter 1/16” OD x 1/32” ID P/N – P-881	1	IDEX Corporation	IL, USA
PEEK tubing 1/32” OD x 0.02” ID	2	IDEX Corporation	IL, USA
A-10 pressure transmitter P/N - 50426834	1	WIKA Instrument	Klingenberg, Germany
DC Power supply Model - 1672	1	BK Precision Corporation	CA, USA
DAQ board Model – NI USB 6212	1	National Instruments	TX, USA

D.2 Rupture test procedure

The pressure transducer requires an input voltage of 0-30V DC power supply. Two of the variable outputs of the power supply were set to “Independent” mode. The positive terminal of the master was connected to the negative terminal of the slave and to the ground terminal using jumper wires. Both of the ground terminals of the slave were connected to the ground terminal of the master and the negative terminal of the slave.

Switch on the power supply and set the voltage of both the channels to 15V so that the lead wire from the negative terminal of the slave provides -15V and the positive terminal supplies +15V. Connect the “red” wire of the transducer to the positive terminal of the power supply, the “black” wire to the negative terminal of the power supply, and the “white” wire to the ground terminal of the power supply. This completes the power supply connection to the transducer.

The output voltage from transducer is 0-10V and is compatible with the DAQ board NI USB-6212 which accepts output analog voltage in the range ±10V. DAQ board has input ports which receives signals from external sensor and output ports which sends signals to the actuators and instruments for control engineering. The pinout configuration of the screw terminal is shown in Fig. D.2. The “black” wire from the transducer is connected to the channel AI 8 (screw terminal 16) and “blue” wire from the transducer is connected to the channel AI 0 (screw terminal 15) of the DAQ board using lead wire and alligator adapter.

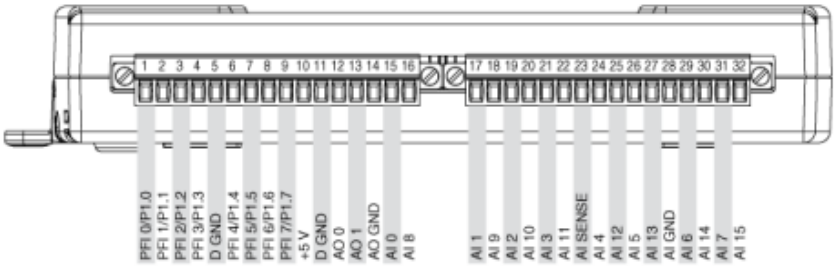

Figure D.2 Pinout configuration of screw terminals of NI USB-6212

A program was developed using LabVIEW software version 2015 to record the rupture pressure of the bonded samples. There are two windows displayed, “Block diagram” and “Front panel”. Code for the program was developed in the block diagram window and the result of the code was displayed in the front panel which served as a user interface. The front panel and the code for the rupture test are shown in Figs. D.3 (a) and (b) respectively.

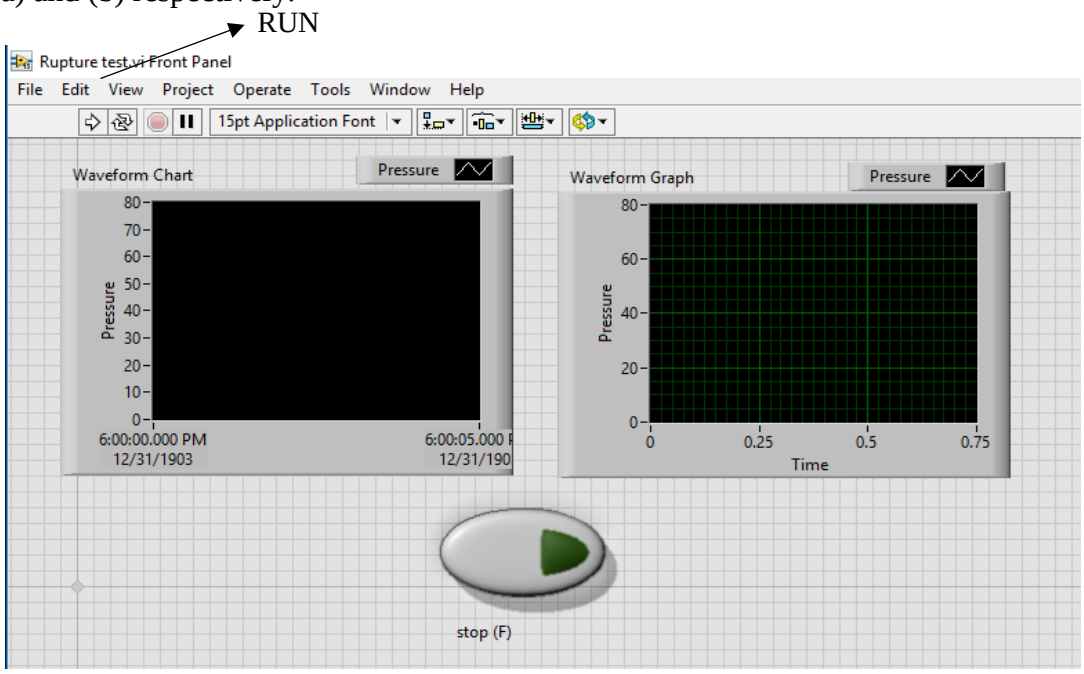

Figure D.3 (a) Front panel of rupture test program

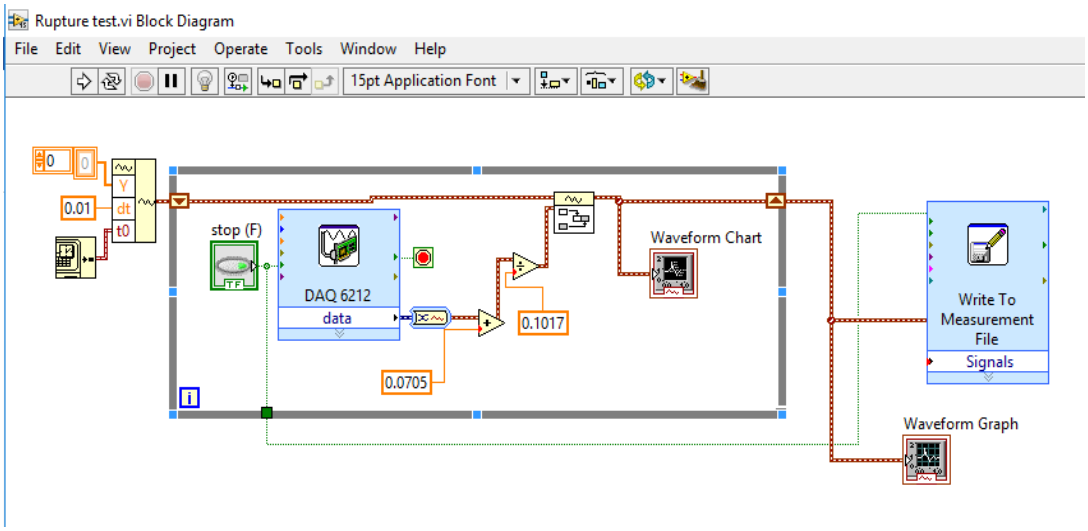

Figure D.3 (b) Block diagram of rupture test program

The bonded sample to be tested was connected to the micro capillaries and the program is executed by clicking the RUN button in the front panel. The pressure of the compressed nitrogen is increased gradually and updated continuously in the Front panel. When the sample ruptures, the pressure starts decreasing and at this point the program is stopped by clicking the "Stop" button. The user is prompted to save the pressure readings from the start until the end in ".lvm" format to the desired location which can be later converted to an Excel file.

D.3 Experimental results

A. Open loop system

Consolidated graphs of the rupture pressure data for all of the samples as obtained from the LabVIEW program are shown in Figs. D.4 (a) – (f). Maximum value in the exported data is considered as the rupture pressure.

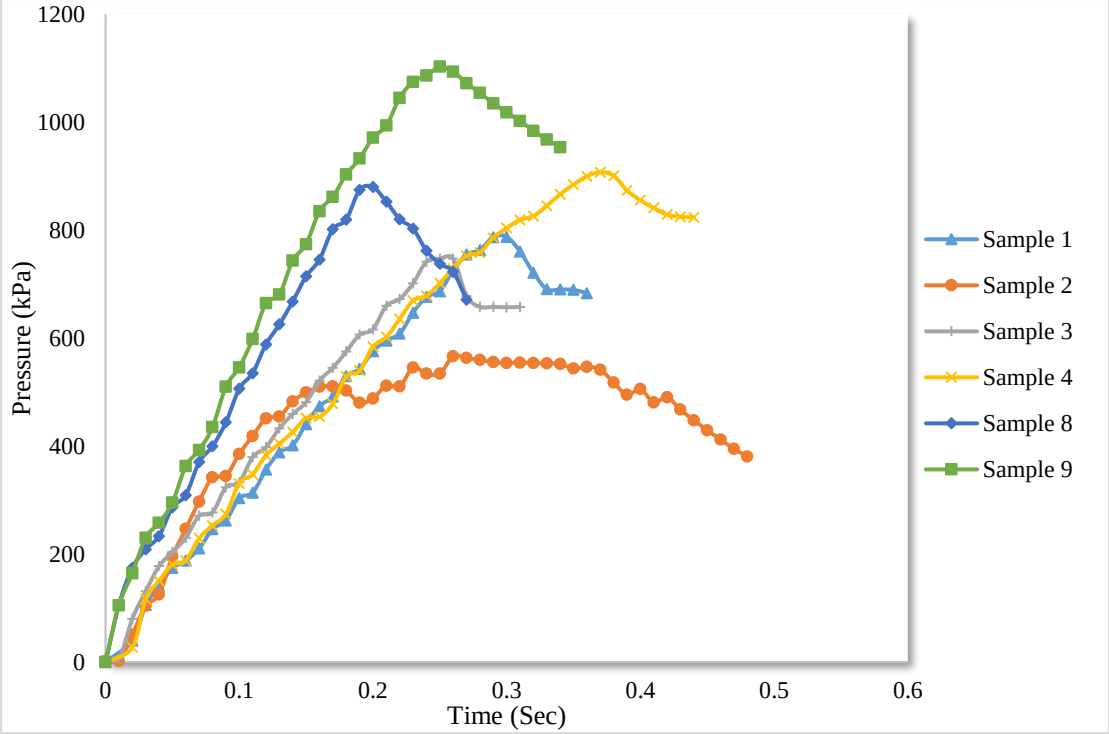

Figure D.4 (a) Rupture pressure data of all samples for Channel 1 of AR 1:10 with depth 10µm

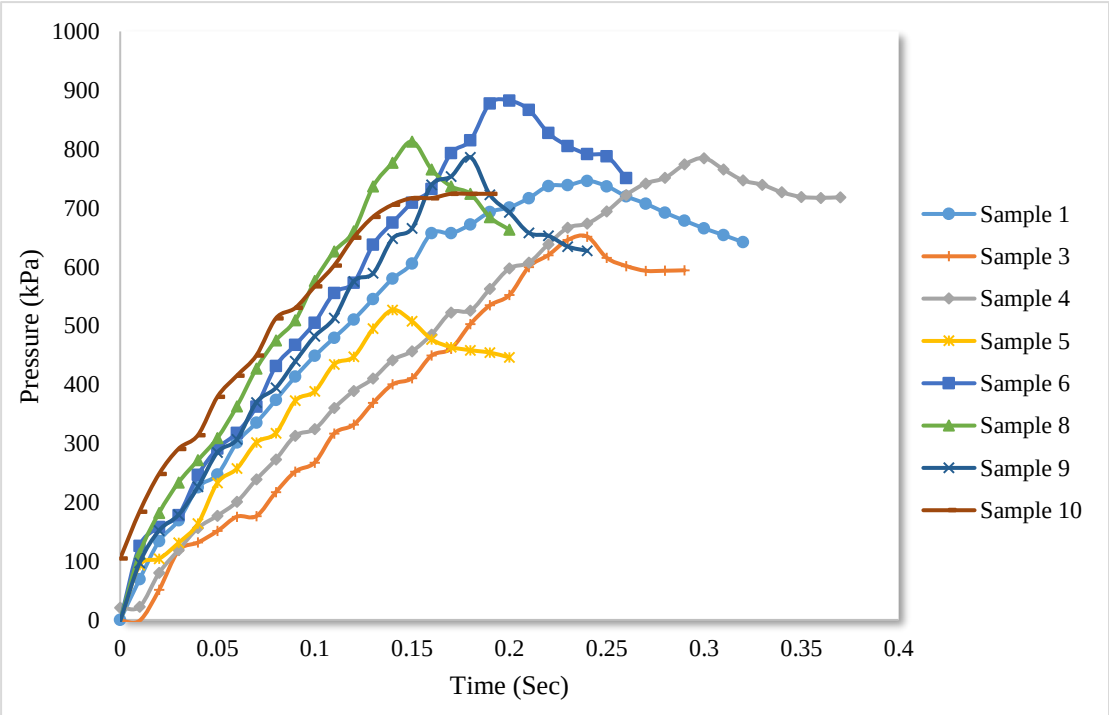

Figure D.4 (b) Rupture pressure data of all samples for Channel 2 of AR 1:50 with depth 10µm

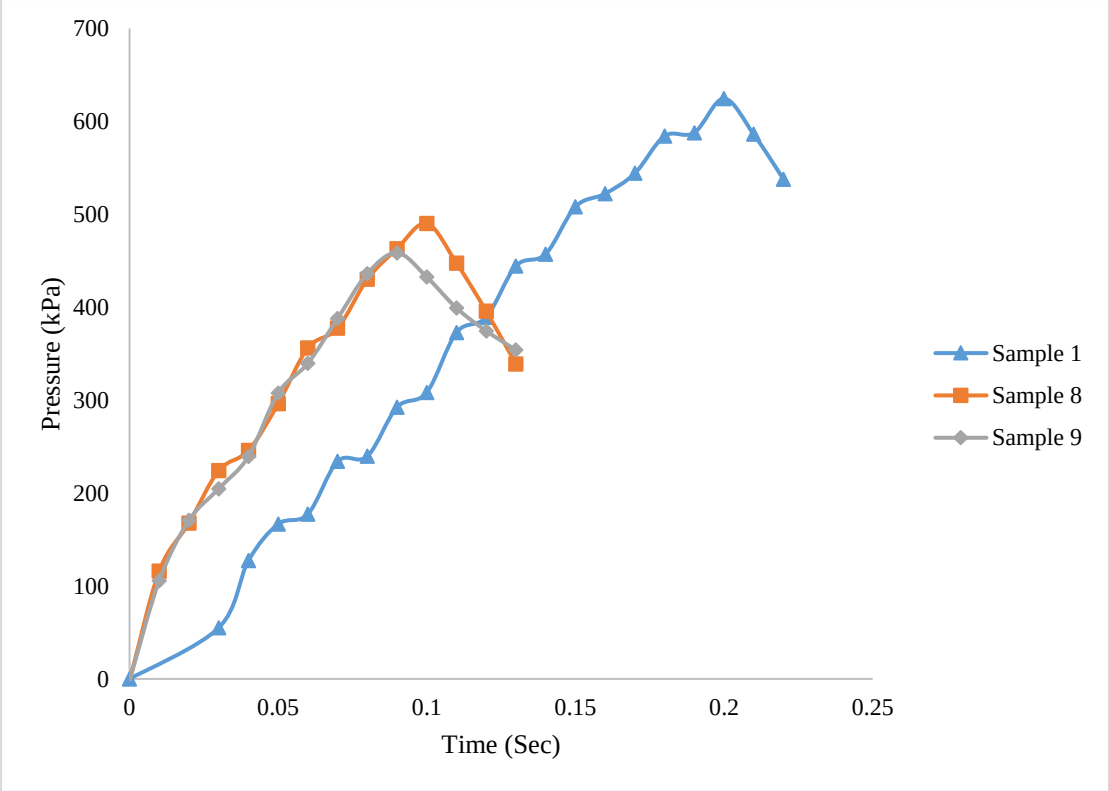

Figure D.4 (c) Rupture pressure data of all samples for Channel 3 of AR 1:100 with depth 10µm

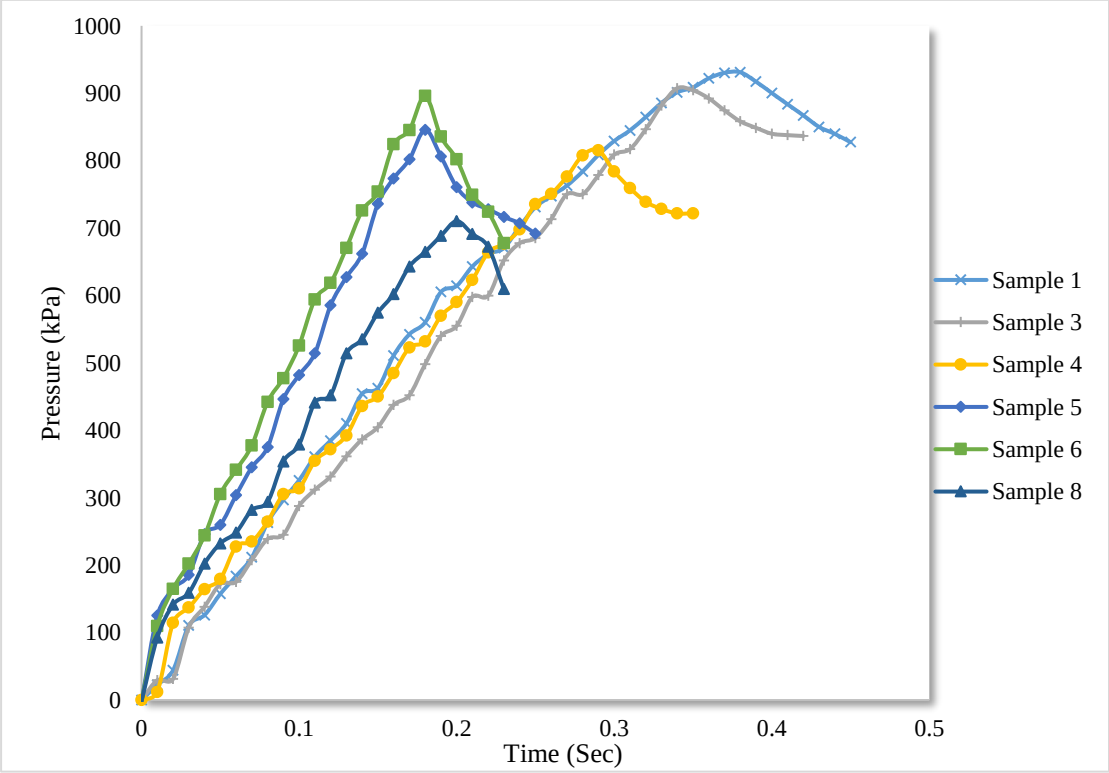

Figure D.4 (d) Rupture pressure data of all samples for Channel 5 of AR 1:10 with depth 5µm

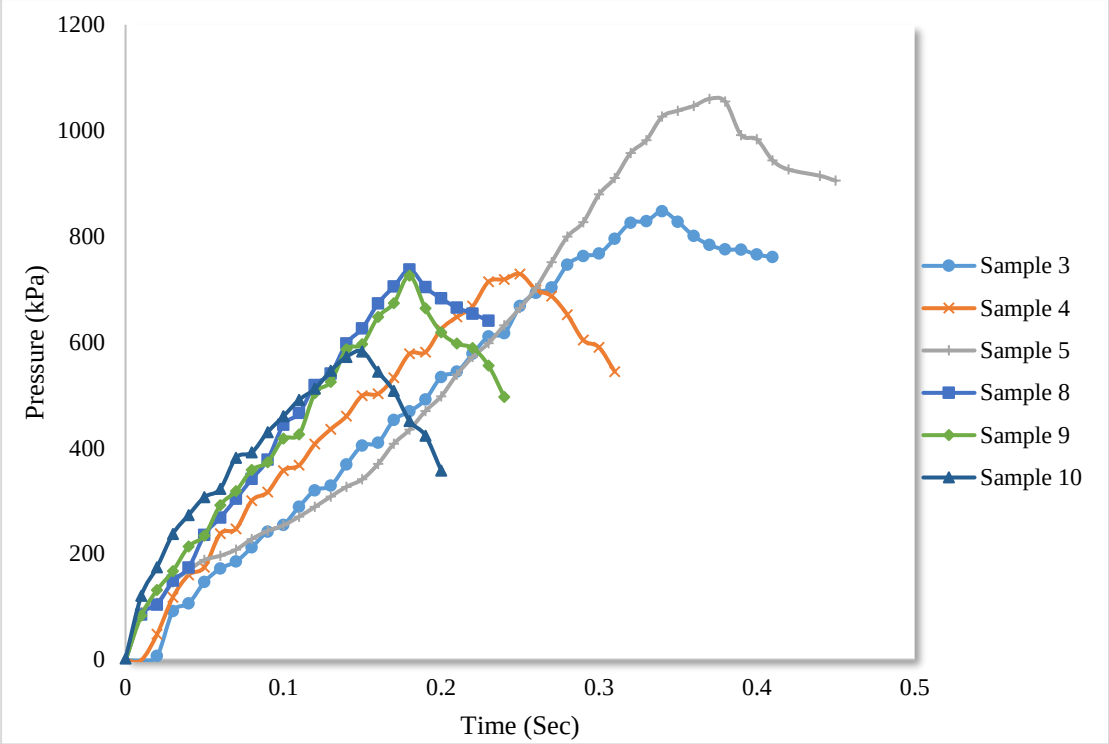

Figure D.4 (e) Rupture pressure data of all samples for Channel 6 of AR 1:50 with depth 5µm

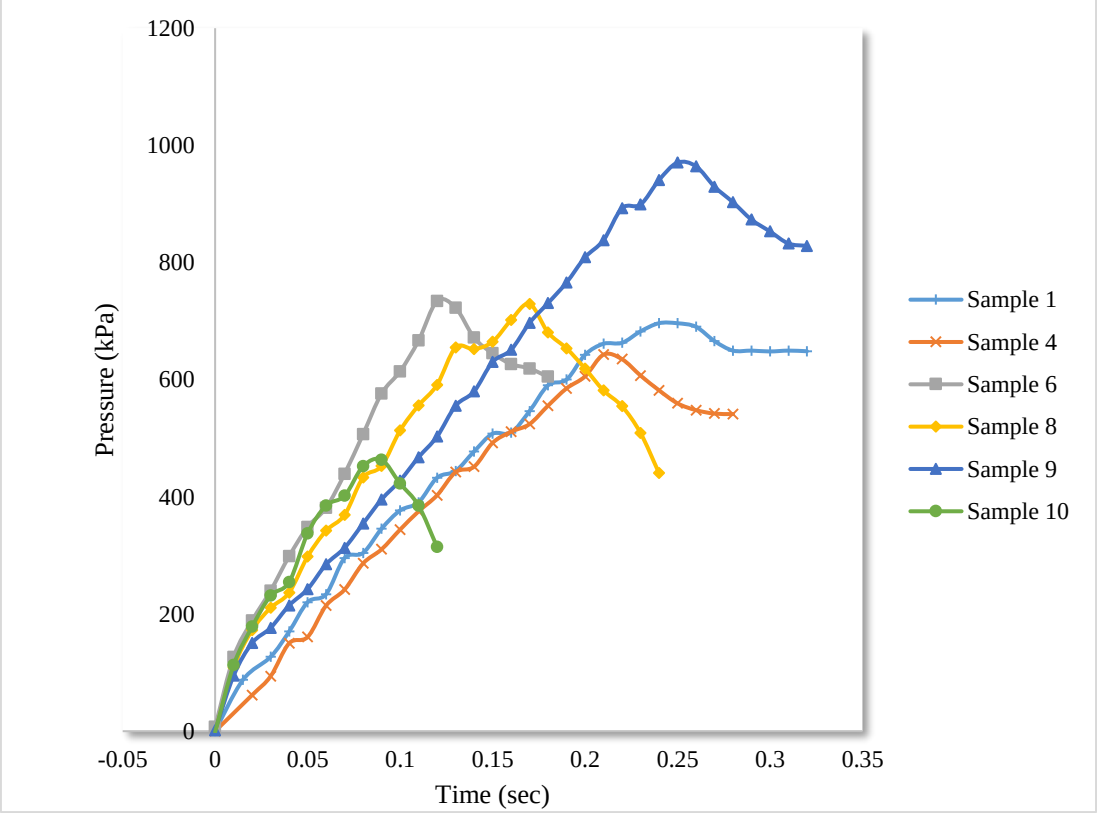

Figure D.4 (f) Rupture pressure data of all samples for Channel 7 of AR 1:100 with depth 5µm

Table D.2: Calculation of mean rupture pressures for samples bonded using open loop system.

CHANNEL 1		CHANNEL 2		CHANNEL 3		CHANNEL 5		CHANNEL 6		CHANNEL 7	
Samples	Max.Pressure (Psi)	Samples	Max.Pressure (Psi)	Samples	Max.Pressure (Psi)	Samples	Max.Pressure (Psi)	Samples	Max.Pressure (Psi)	Samples	Max.Pressure (Psi)
Sample 1	787.77	Sample 1	746.20	Sample 1	624.53	Sample 1	931.20	Sample 3	847.19	Sample 1	696.43
Sample 2	566.16	Sample 3	651.39	Sample 8	490.16	Sample 3	907.53	Sample 4	728.85	Sample 4	642.79
Sample 3	747.52	Sample 4	784.76	Sample 9	458.46	Sample 4	815.36	Sample 5	1059.89	Sample 6	734.17
Sample 4	907.57	Sample 5	526.58	Mean	524.38	Sample 5	845.78	Sample 8	737.00	Sample 8	729.44
Sample 8	879.98	Sample 6	882.30	Std. dev. (s_x)	88.16	Sample 6	896.05	Sample 9	725.66	Sample 9	970.55
Sample 9	1102.78	Sample 8	812.90	N	3	Sample 8	710.31	Sample 10	582.54	Sample 10	463.34
Mean	831.96	Sample 9	786.17	$t_{95,2}$	3.182	Mean	851.04	Mean	780.19	Mean	706.12
Std. dev. (s_x)	179.50	Sample 10	724.11	Interval	161.97	Std. dev. (s_x)	80.93	Std. dev. (s_x)	160.78	Std. dev. (s_x)	163.89
$t_{95,5}$	2.571	Mean	739.30	Upper limit	686.35	N	6	N	6	N	6
Interval	188.40	Std. dev. (s_x)	109.14	Lower limit	362.41	$t_{95,5}$	2.571	$t_{95,5}$	2.571	$t_{95,5}$	2.571
Upper limit	1020.36	N	8			Interval	84.94	Interval	168.76	Interval	172.02
Lower limit	643.56	$t_{95,7}$	2.37			Upper limit	935.98	Upper limit	948.95	Upper limit	878.14
		Interval	91.26			Lower limit	766.10	Lower limit	611.43	Lower limit	534.10
		Upper limit	830.56								
		Lower limit	648.04								

B. Closed loop system

Rupture pressure data of all samples bonded using the closed loop system are shown in Figs. D.5 (a) to (f).

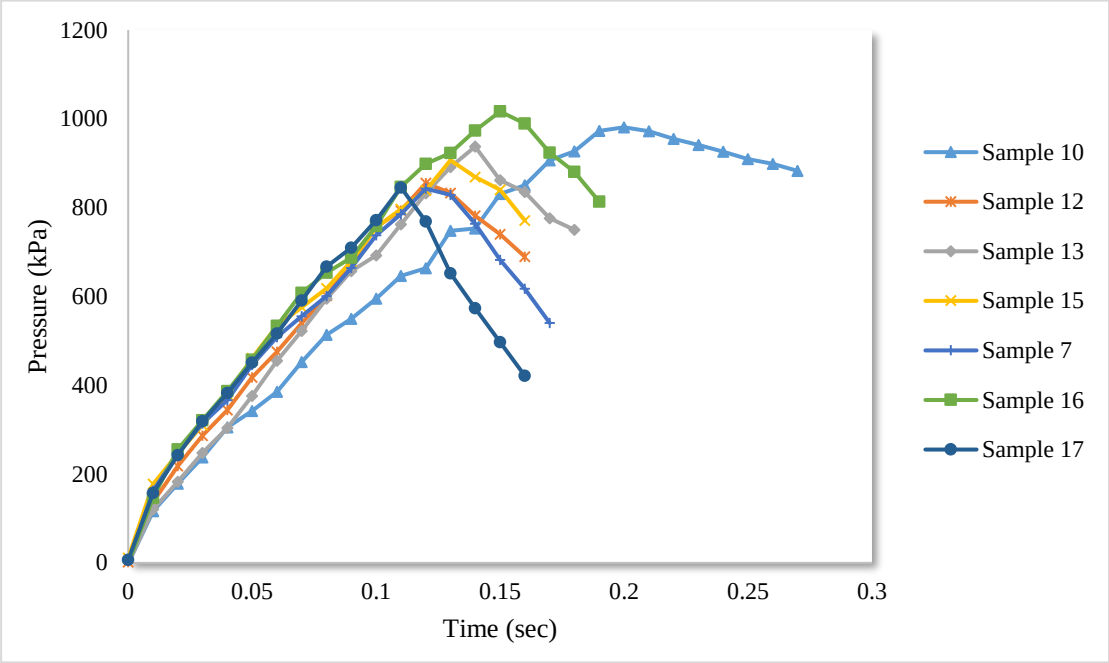

Figure D.5 (a) Rupture pressure data of all samples for Channel 1 of AR 1:10 with depth 10µm

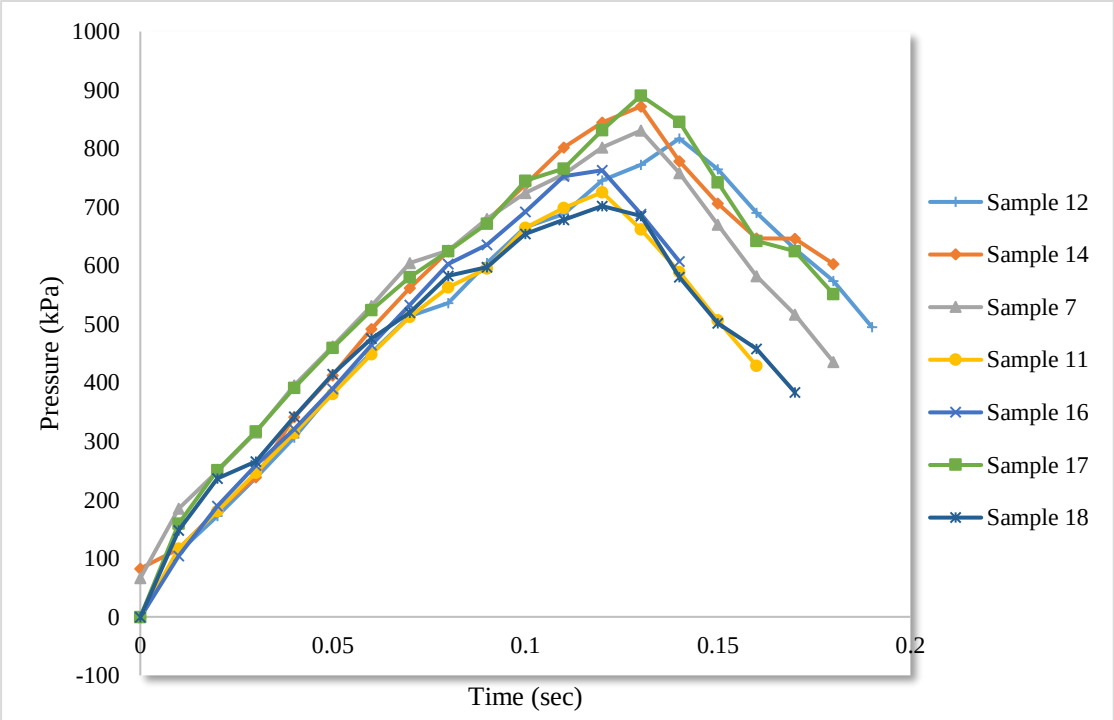

Figure D.5 (b) Rupture pressure data of all samples for Channel 2 of AR 1:50 with depth 10µm

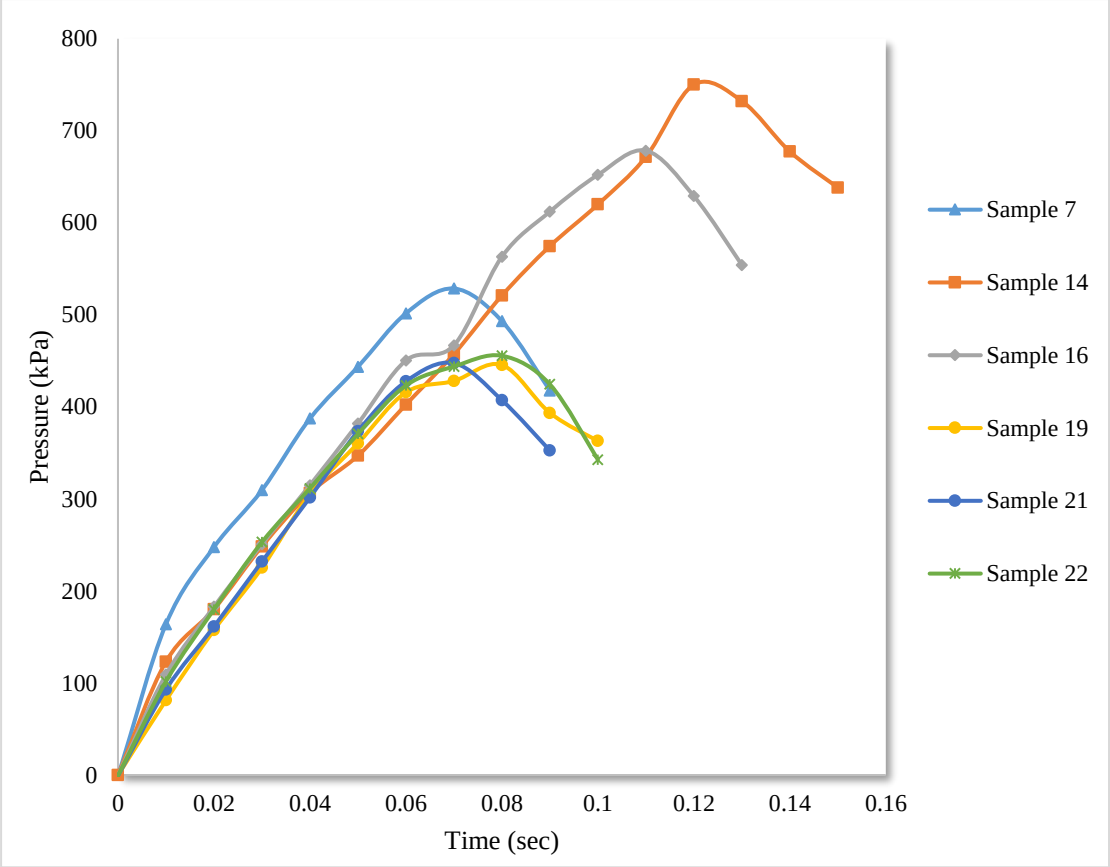

Figure D.5 (c) Rupture pressure data of all samples for Channel 3 of AR 1:100 with depth 10µm

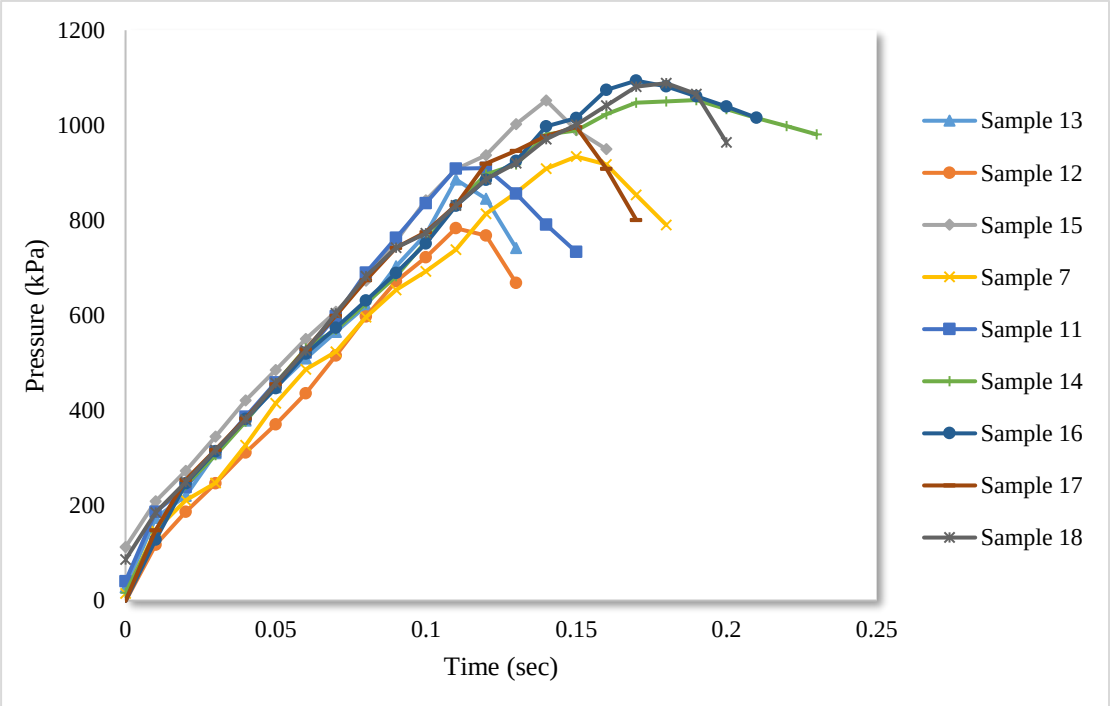

Figure D.5 (d) Rupture pressure data of all samples for Channel 5 of AR 1:10 with depth 5 µm

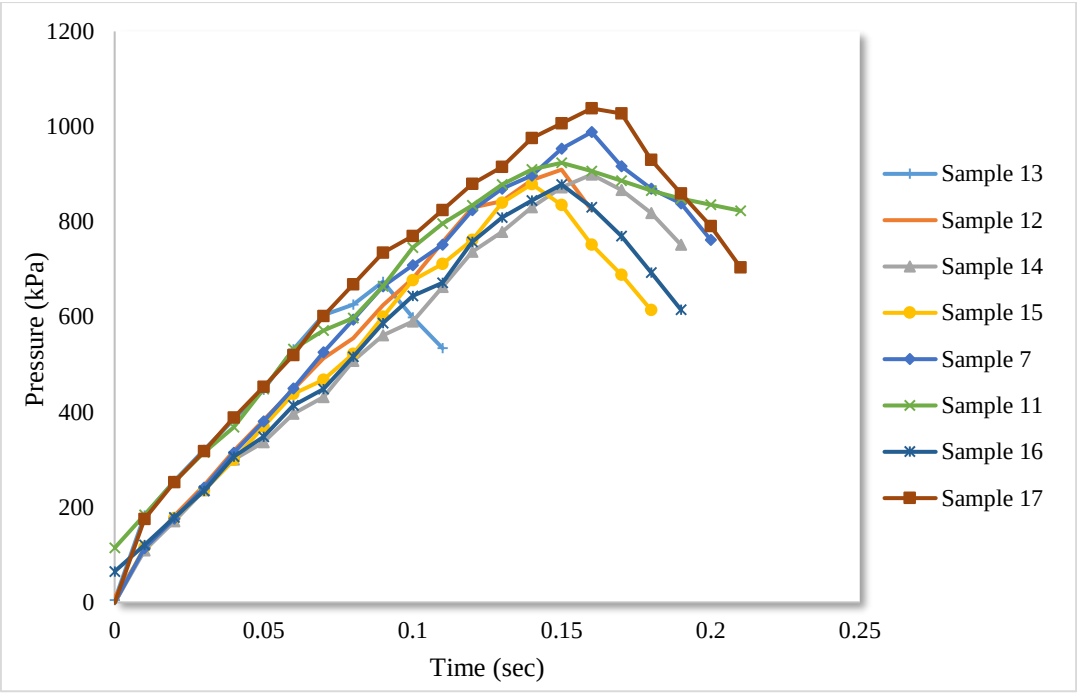

Figure D.5 (e) Rupture pressure data of all samples for Channel 6 of AR 1:50 with depth 5 µm

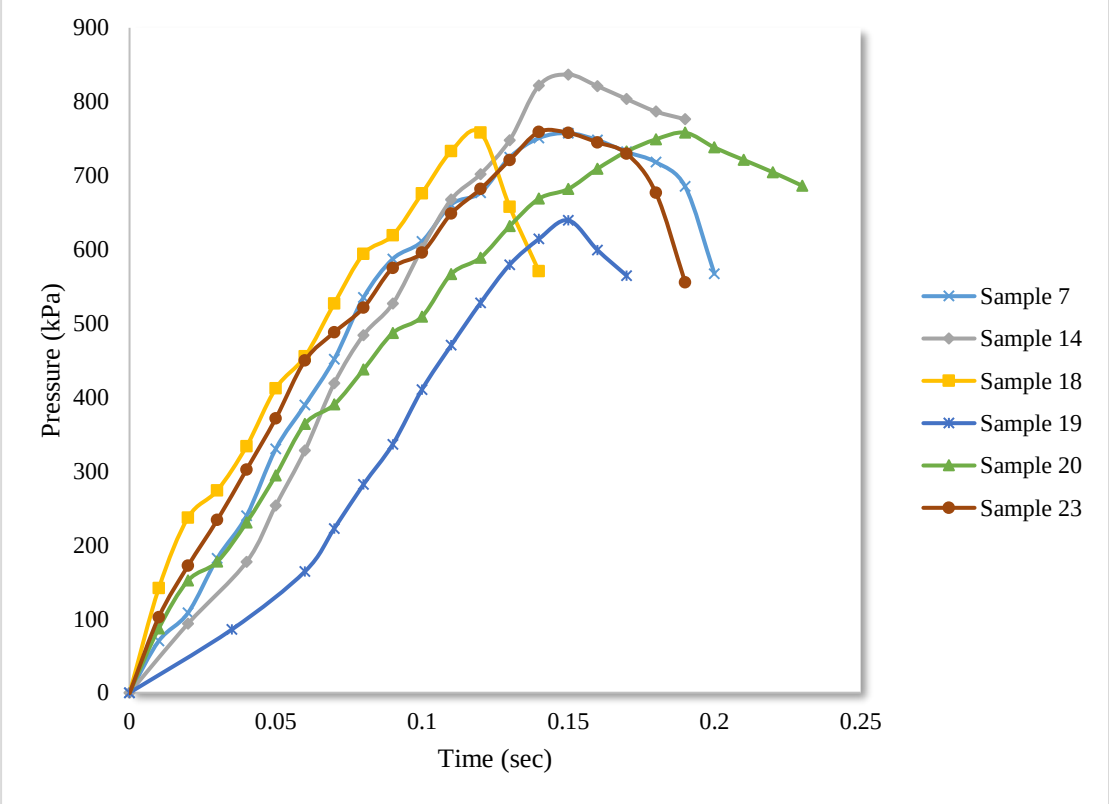

Figure D.5 (f) Rupture pressure data of all samples for Channel 7 of AR 1:100 with depth 5 µm

Table D.3: Calculation of mean rupture pressures for samples bonded using closed loop system

CHANNEL 1		CHANNEL 2		CHANNEL 3		CHANNEL 5		CHANNEL 6		CHANNEL 7	
Samples	Max.Pr. (psi)	Samples	Max.Pr. (psi)	Samples	Max.Pr. (psi)	Samples	Max. Pr . (psi)	Samples	Max. Pr. (psi)	Samples	Max. Pr. (psi)
Sample 10	980.88	Sample 12	817.18	Sample 7	528.59	Sample 12	783.31	Sample 12	909.48	Sample 7	757.44
Sample 12	855.07	Sample 14	872.24	Sample 14	750.11	Sample 13	885.85	Sample 14	899.28	Sample 14	836.72
Sample 13	937.31	Sample 7	830.80	Sample 16	678.39	Sample 15	1052.28	Sample 15	879.07	Sample 18	757.90
Sample 15	906.84	Sample 11	725.25	Sample 19	445.53	Sample 7	934.07	Sample 7	988.40	Sample 19	639.51
Sample 7	842.73	Sample 16	762.95	Sample 21	447.54	Sample 11	909.94	Sample 11	923.83	Sample 20	757.99
Sample 16	1016.49	Sample 17	890.54	Sample 22	455.55	Sample 14	1053.10	Sample 16	878.16	Sample 23	758.99
Sample 17	845.46	Sample 18	701.80	Mean	550.95	Sample 16	1093.90	Sample 17	1038.12	Mean	751.42
Mean	912.11	Mean	800.11	Std. Dev.	132.15	Sample 17	996.50	Mean	930.90	Std. Dev.	57.70
Std. dev.	69.28	Std. dev.	72.18	N	6	Sample 18	1088.66	Std. dev.	60.25	N	7
N	7	N	7	$t_{95,6}$	2.571	Mean	977.51	N	7	$t_{95,3}$	2.571
$t_{95,6}$	2.447	$t_{95,6}$	2.447	Interval	138.70	Std. dev.	73.42	$t_{95,3}$	2.447	Interval	56.07
Interval	64.07	Interval	66.76	Upper limit	689.66	N	9	Interval	55.72	Upper limit	807.50
Upper limit	976.19	Upper limit	866.87	Lower limit	412.25	$t_{95,6}$	2.306	Upper limit	986.63	Lower limit	695.35
Lower limit	848.04	Lower limit	733.35			Interval	56.44	Lower limit	875.18		
						Upper limit	1109.54				
						Lower limit	996.66				

APPENDIX E: COMPLETE DESCRIPTION OF CLOSED LOOP SYSTEM

E1 Experimental apparatus

All the components used for the experimental set up is shown in Fig. E.1. More details about the parts are given in Table E.1.

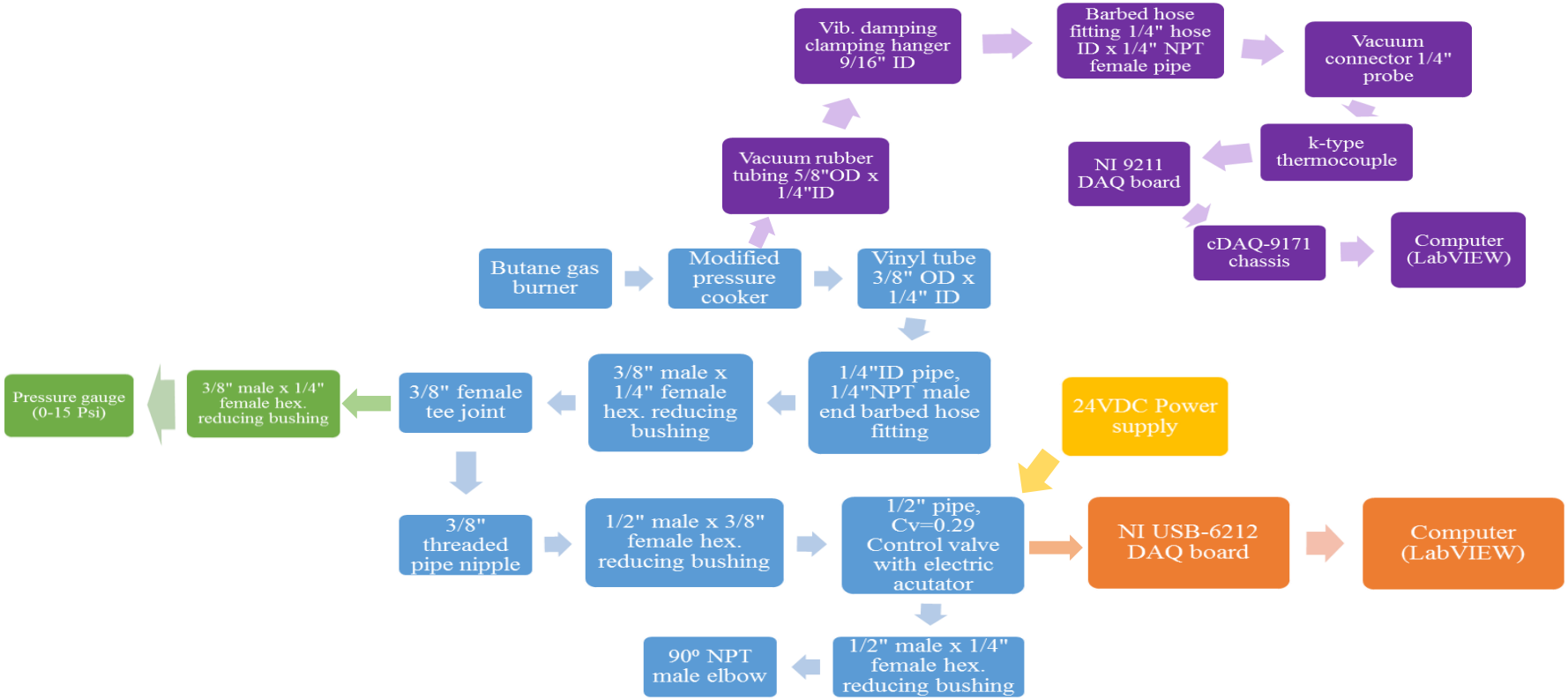

Figure E.1 Illustration of all the components of closed loop system in order

Table E.1 Parts list for the closed loop bonding system

Component Name	Part number	Company	Location
Butane gas burner	ZA 3HP	Iwatani Corporation of America	NJ, USA
8 quart pressure cooker	-	Philippe Richard	CA, USA
Vinyl tube 3/8"OD x 1/4"ID	652395	Louwes	NC, USA
1/4" pipe dia, 1/4" NPT male end barbed hose fitting	5346K27	McMaster	IL, USA
3/8" x 1/4" bushing	4429K471	McMaster	IL, USA
tee joint	4429K252	McMaster	IL, USA
3/8" threaded pipe nipple	4568K151	McMaster	IL, USA
1/2" x 3/8" bushing	4429K413	McMaster	IL, USA
Control Valve with electric actuator	B215HT046/T FRB24-SR-NC	Belimo	Switzerland
1/2" x 1/4" bushing	645891	Louwes	NC, USA
90º NPT male elbow	50925K111	McMaster	IL, USA
k-type thermocouple	5TC-GG-K-30-72	Omega Engineering	CT, USA
24VDC power supply	DCP-250-P	Kele	TN, USA
NI USB 6212	780107-01	National Instruments	TX, USA
NI 9211	779001-01	National Instruments	TX, USA
Cdaq-9171	781425-01	National Instruments	TX, USA
Vacuum rubber tubing	62996-335	VWR International	PA, USA
Vib. Damping clamping hangers	2615T11	McMaster	IL, USA
Barbed hose fitting 1/4" hose ID x 1/4" NPT female pipe	5361K52	McMaster	IL, USA
Vacuum connector 1/4" probe	353444	Torr Technologies, Inc.	WA, USA

E.2 Experimental procedure

The Type K thermocouple with lead wires is connected to the DAQ board NI 9211 which can receive voltage in the range of ±80mV. The positive wire (yellow color) was connected to screw terminal "0" and the negative lead wire (red color) was connected to screw terminal "1" of the DAQ board NI 9211 and was connected to the computer. A proportional type of control valve with an electric actuator was used to maintain even temperature during the bonding process. The valve requires 24VDC input power and generates output voltage in the range of 2-10V, which is compatible with the USB 6212 DAQ board. A step-down transformer that converts 110VAC to 24VDC was used to supply power to the control valve. A program was developed in LabVIEW using the built-in PID module, which continuously compared the measured temperature from the thermocouple with the set temperature, and a signal corresponding to the error was sent to the control valve. The temperature at the boiling point was maintained at the set point temperature with $<\pm 0.15$℃ deviation. Figures E.1 and E.2 show the front panel and block diagram of the LabVIEW program.

The polymer samples were inserted inside a sealing bag and sealed using a food sealer. The bag was connected to the rubber tube using the connector and the thermocouple was inserted into the bag via rubber tube. The entire assembly was then immersed in DI water in the pressure cooker. The user should enter the desired bonding temperature on the front panel as the set temperature. Output high should be 6 and low should be 3 in the output range in front panel. The PID gains were determined experimentally and good response was observed for values of K_c=1 min^{-1}, T_i=0.2 min and T_d=0.2 minute. After entering all the values, the water was heated by switching on the butane burner and the program was started. The plot shows the temperature variation of the bonding process and the temperature value and the input voltage to the

control valve is continuously indicated in the indicator in front panel. The burner is kept on high flame until the temperature was about 5°C lower than the set temperature and then the flame was reduced to its minimum setting. Once the set temperature was reached, a timer was started and bonding was done for 15mins. After 15 mins, the burner was turned off and the program was stopped by pressing the "Stop" button on the front panel.

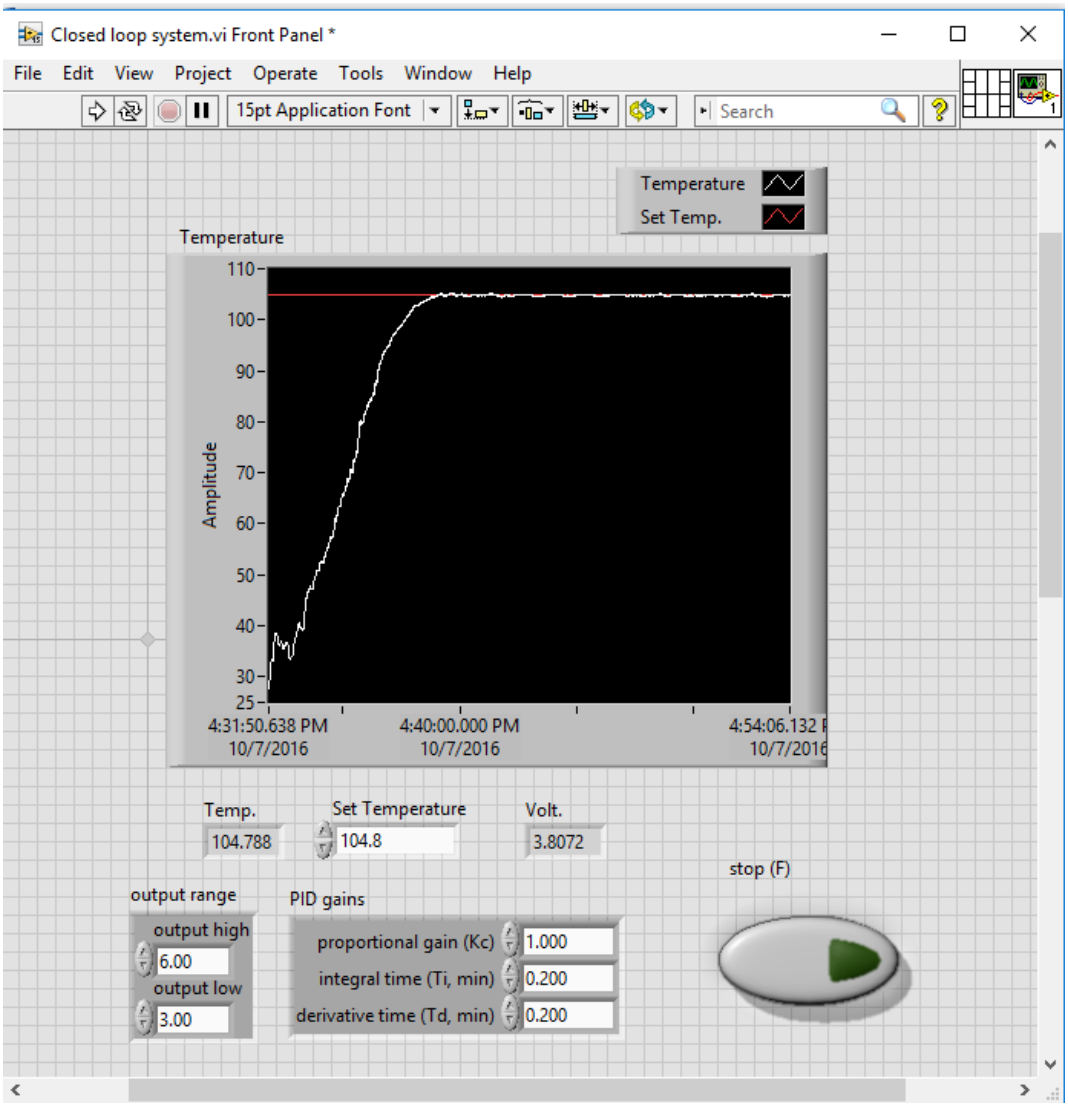

Figure E.1 Front panel (user interface) of LabVIEW program for closed loop system

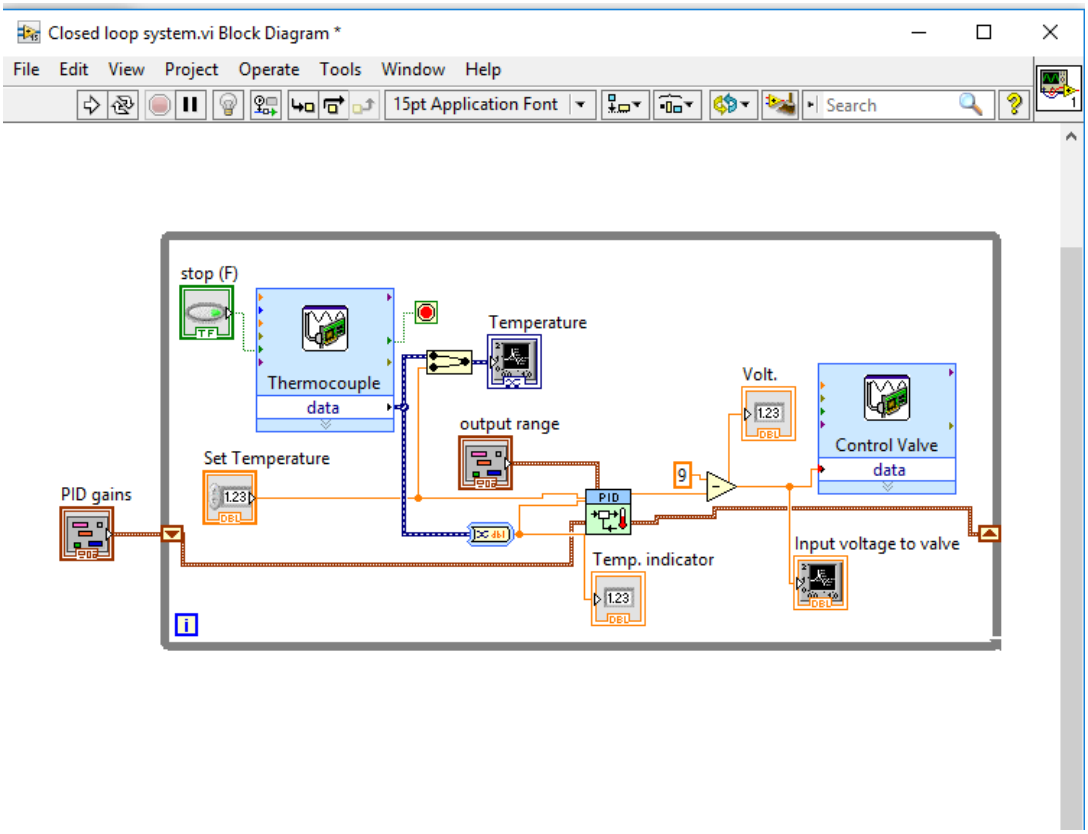

Figure E.2 Block diagram of closed loop system for bonding process

Vita

Kavya Dathathreya received her bachelor's degree in department of Mechanical Engineering in 2009 at PES Institute of Technology, Bangalore, India. Upon completion, she worked in industry for four years and joined Department of Mechanical Engineering at Louisiana State University in January 2013 to pursue master's degree. She began her research in microfluidics under the supervision of Dr. Michael C. Murphy and expects to receive her master's degree in December 2016.